

Dissertation

zum Thema

Synthesis of Metallic Nanowires Using Integrated DNA Molecules as Templates

der Fakultät Maschinenwesen
der Technischen Universität Dresden
vorgelegt von

Dipl.-Ing. Christiane Erler

geboren am 04. 11. 1982 in Freiberg

und

zur Erlangung des akademischen Grades
Doktoringenieur
(Dr.-Ing.)
begutachtet durch

Prof. (em.) Dr. rer. nat. habil. Wolfgang Pompe
Prof. Dr.-Ing. habil. Gerald Gerlach

Verteidigt am 23. 03. 2010

The projects that are part of this thesis were conducted between 12/2006 and 11/2009 in the group “BioNanotechnology and Structure Formation” at Max Bergman Center for Biomaterials at Technische Universität Dresden. The thesis supervisor was PD Dr. rer. nat. et Ing. habil. Michael Mertig.

Abstract

The DNA double helix is inherently a nanoscale wire-like object, possessing a 2 nm diameter as well as a remarkable capability for molecular recognition and the interaction with other chemical compounds, thus making it an attractive material for biologically driven assembly of artificial nanostructures. In this work methods for the construction of functional electronic networks from single DNA molecules are presented. For this, (i) the generation of patterns of distinct interconnects between micro-fabricated contact pads are explored by stretching end-specifically thiol-functionalized, single-tethered DNA molecules using hydrodynamic flow as well as an electric field-induced thermal flow. (ii) These networks then serve as a template for a selective *in-situ* photoinduced nucleation and growth of platinum clusters of ~ 4 nm diameter along the DNA molecules. In the synthesis exclusively platinum ions from an aqueous $\text{Pt}(\text{NO}_3)_2$ solution bonded electrostatically to the backbone of the immobilized DNA can be reduced upon irradiation with UV light, while background metallization is inhibited. Furthermore, the metallization scheme is applied to DNA nanotubes and another photochemical deposition process is used to tune the interparticle gap space in a discontinuous platinum cluster chain to form conducting nanowires.

The “process toolbox” presented in this work offers a versatile alternative for the hierarchical patterning and incorporation of biotemplated nanomaterials into micro-/nanofabrication schemes.

Kurzfassung

Ein doppelhelikaler DNA-Strang besitzt mit seinem hohen Aspektverhältnis von Natur aus Ähnlichkeit mit einem Kabel. Zusammen mit seinen einzigartigen Selbstassemblierungseigenschaften sowie der Fähigkeit, mit einer Vielzahl von chemischen Stoffen eine Verbindung einzugehen, macht dies ihn zu einem aussichtsreichen Baumaterial für den Aufbau von künstlichen Nanostrukturen. In dieser Arbeit werden deshalb verschiedene Methoden für den Bau von elektronischen Schaltkreisen aus einzelnen DNA-Strängen demonstriert. Dazu wird (i) die Herstellung von Verdrahtungsmustern zwischen lithographisch gefertigten Kontaktstrukturen untersucht. Endständig mit Thiolgruppen funktionalisierte DNA-Moleküle, die an nur einem Ende mit der Oberfläche verknüpft sind, werden mittels Strömung oder eines elektrothermisch induzierten Flusses zwischen Elektroden gespannt. (ii) Diese Netzwerke dienen im Weiteren als Vorlage für ein selektives, lichtinduziertes Wachstum von Platinpartikeln mit Durchmessern von ~ 4 nm lokal entlang der DNA-Moleküle. Dabei werden unter UV-Bestrahlung nur solche Platinionen reduziert, die aus einer $\text{Pt}(\text{NO}_3)_2$ -Lösung elektrostatisch an die immobilisierte DNA angebunden haben. Partikelwachstum in der umgebenden Lösung wird weitgehend verhindert. Darüber hinaus wird dieses Verfahren auch auf DNA-Nanoröhren angewendet und ein weiterer photochemischer Abscheideprozess eingesetzt, um unterbrochene Clusterkettern zusammenzuwachsen, mit dem Ziel, elektrisch leitfähige Nanodrähte zu erhalten.

Die vorgestellten Verfahren stellen eine vielseitige Alternative zu herkömmlichen, hierarchischen Fabrikationsschemen der Mikro- und Nanotechnologie dar.

Contents

Introduction	1
1 DNA-Based Nanowire and Network Fabrication	5
1.1 State of the Electronic Packaging Technology	6
1.2 General Aspects on DNA	9
1.2.1 DNA Structure	9
1.2.2 DNA Mechanics	10
1.3 End-Specific DNA Functionalization and Site-Specific Immobilization . .	12
1.4 Stretching DNA	15
1.4.1 Mechanically Induced Stretching	15
1.4.2 Electric Field Induced Stretching	18
1.5 Deriving Relevant Tasks for the Integration of DNA into Microelectrode Structures	25
1.6 Bottom-up Nanofabrication with DNA	26
1.7 DNA Metallization	30
1.8 Deriving Relevant Tasks for the Metallization of Integrated DNA	36
2 Integration of DNA into Microelectrode Structures	37
2.1 Tethering DNA Ends to Electrodes	37
2.2 Stretching DNA by Hydrodynamic Flow	39
2.2.1 Experimental Setup	39
2.2.2 Stretching DNA Between Interdigital Electrodes	41
2.2.3 Determination of Anchoring Sites	44
2.3 Stretching DNA by Electric Field Induced Flow	48
2.3.1 Stretching DNA in Heterogeneous Electric Fields	49
2.3.2 Construction of Interconnect Patterns	57
2.4 Conclusion	59
3 Photoinduced Platinum Deposition on DNA Templates	61
3.1 Formation of Platinum Cluster Chains on Double-Stranded DNA	62
3.1.1 Metal Salt Concentration Dependence During Activation/Reduction	63
3.1.2 Influence of Other Control Parameters	71
3.1.3 UV/VIS Spectroscopy	73
3.1.4 Discussion of the Cluster Formation and Growth Mechanism	76
3.2 Investigation of Continuity of Cluster Chains	78
3.2.1 Analysis by Transmission Electron Microscopy	79
3.2.2 Correlated AFM/TEM Study	82

Contents

3.3	Conclusion on Photoinduced Platinum Deposition on DNA Immobilized on a Surface	85
3.4	Metallization of DNA Tubes	85
3.4.1	Verification by Transmission Electron Microscopy	86
3.4.2	UV/VIS Investigation of Metal Salt-Tube Interaction	87
3.5	Conclusion on Photoinduced Metallization of DNA Tubes	88
4	DNA Nanowire Fabrication	89
4.1	Photoinduced Metallization of Integrated DNA Molecules	90
4.2	Towards Electric Conductivity Measurements	91
4.2.1	Influence of the Substrate Surface	91
4.2.2	Photochemical Tuning of Platinum Cluster Chains Using Their Surface Plasmon Resonances	95
4.3	Conclusion on DNA Nanowire Fabrication	99
	Summary	100
A	Appendix	103
A.1	Experimental Methods	103
A.1.1	Integration of DNA into Microstructures	103
A.1.2	UV-Induced Preparation of Cluster Chains Along DNA	105
A.1.3	Preparation of TEM Samples	106
A.2	Matlab Based Image Processing	107
	Bibliography	109
	Publications	123
	Acknowledgement	125

Introduction

In 1956 W. B. Shockley, J. Bardeen and W. H. Brattain were honored with the Nobel Prize in Physics for their researches on semiconductors and their discovery of the transistor effect. The development of the transistor was the decisive step marking the start of microelectronics as what it means for us today. The feasibility for integration into circuits together with other electronic components constitutes the transistor's significant advantage. For the large-scale production of such integrated circuits the silicon-based semiconductor technology developed. Therein inclosed manufacturing steps are predominantly of top-down lithographical nature. That is, a fabrication where from a large block of material the more elaborate structure is carved out and which relies on macroscale manufacturing operations, high-precision equipment and controlled environments to achieve micrometer or sub-micrometer resolution in patterning and processing steps.

For half a century now, with each new technology generation the trend has been to create ever-smaller products using fewer chips of greater complexity implemented in microelectronics technologies that allow smaller and smaller feature sizes of the transistors. This continuing miniaturization is not a fundamental physical principle, but is destined by the empirical MOORE's Law¹ and nowadays assessed by the "International Technology Roadmap for Semiconductors" [1], arranged by international semiconductor industry associations. With an enormous effort again and again the limits of what is technically feasible are pushed to new limits. The results of this tremendous endeavor are complex. Nowadays also three-dimensional chip architectures with features considerably below 100 nm in size are available. And although the end of lithographical techniques has been predicted already for years, at the moment there is no alternative method, which can compete with them—especially considering that by 2010, the number of world-wide built transistors will be around one billion transistors per person per year!

In contrast to the linear decrease of structure sizes the development of the technologies of the second manufacturing phase in semiconductor industries—the assembly and packaging of the silicon chips—takes place batch-wise. At the moment, those two trends disperse. The next packaging technology wave to close the "packaging gap" on MOORE's Law is still to come. And the present situation will even intensify in the near future with structure sizes falling below 10 nm in the year 2020.² Up to now, there is no paradigm or concept for large-scale integration in "nanoelectronics" analogous to integrated circuits in microelectronics.

¹A historical observation by Intel co-founder Gordon Moore in 1965, that the market demand (and semiconductor industry response) for functionality per chip (bits, transistors) doubles every 1.5 to 2 years.

²according to the 2008 ITRS update—technology trends versus actuals and survey

Introduction

Besides the driving force from top to bottom, there is also a category of devices emerging from the other end of the scale: new nanomaterials may display distinct mechanical, optical, electronic or chemical properties resulting from their size, shape, composition or structure. They may incorporate functionalities that do not necessarily scale according to MOORE's Law, but provide additional—"More than MOORE"—value. But the key feature of these materials is, that they are not carved from a large block, but assemble upward from building blocks that are exactly in the size range, which is desired in future top-down approaches. This bottom-up method allows in principle a very precise positioning of collections of atoms, hence functionalities. However, among others, also here a lack of packaging solutions matching the dimensions and requirements of these nanoscale devices prevents their large-scale technical utilization.

But to expand on the building block concept omnipresent in nature, one can further state, that the over millions of years evolutionary refined, intelligent biomolecular structures could not only serve as building blocks but also provide new routes to assembly and packaging. Because the formation of biological structures is based on the two fundamental principles of molecular recognition and self-assembly, biomolecules can attach to each other at highly specific binding sites and thus, do not only allow for the assembly from small subunits into well-defined larger superstructures, but also for guiding functional elements other than biological (for example, tiny particles of insulators, semiconductors and metals) into complex networks and moreover, for the positioning in space. Assuming a well designed set of linker elements one could think of programmed, but autonomous bottom-up self-assembly under comparatively simple process conditions—near room temperature in aqueous solutions, whereas the availability of a large quantity of different binding sites enables flexibility and diversity like in biological structures.

Thus at present, biomolecules are exploited as building blocks to fabricate completely artificial constructs [2], which are only composed of biomolecules. Furthermore, as recognition properties are better developed for organic materials than for inorganic ones, biomolecules are used as "glue" for inorganic objects. This strategy, which initially utilized the simple base-pairing interactions of DNA to assemble inorganic nanoparticles into periodic macroscopic structures [3] has grown to include interactions between antibodies and antigens [4], and between protein receptors and their ligands [5], among the list of highly specific biomolecules. In contrast, properties like electric conductivity are much better understood for inorganic material. But, the biomolecules can also serve as templates, i.e. as model patterns, which promote the selective deposition of inorganic material [6–8]. It is therefore envisaged that especially the combination of the different material types will lead to fruitful new approaches. It may be the case that assembly will take place via recognition of organic parts followed by derivatization with inorganic materials, or that small inorganic units modified with organic anchoring points are assembled into circuits in a single process.

Although in comparison to the semiconductor technology this non-lithographical work is at a preliminary stage and competing practical applications are some way off, this approach gains increasing interest as a promising alternative to conventional top-down lithography.

In this context, a future realization of integrated (molecular) electronics relies on the two fundamental steps:

- interconnection and arrangement of an immense number of (molecular) devices into a functional circuit, requiring specific recognition between device, interconnector and a larger interface
- carrying out operations on a broad range of length scales (from tens of micrometers down to one nanometer) to *in-situ* prepare the interconnector for a certain kind of transport, e.g. electric current.

Among certain well-characterized biomolecules conceivable for that tasks, deoxyribonucleic acid (DNA) constitutes a particularly promising candidate to be used as building block and structure determining component with precise control of length scales in the nanometer range and below.

The self-assembly of complex systems requires coding of tremendous amounts of information into the molecular ingredients and assemblers that utilize that information. Despite of its simplicity the enormous specificity of the A-T- and G-C-WATSON-CRICK base pairing is meant for that job as it enables programming of not only artificial receptors but also complete architectures aside from the natural double strand. Using the four-letters alphabet DNA mediated assembly and immobilization of non-nucleic acid components was shown: Either as a linker element the DNA promotes assembly of inorganic phases or the biomolecule serves as a template, i.e. molding guide, for the organization of proteins, small molecules or inorganic material like metallic or semiconducting nanoparticles, which are tagged with the complementary base sequence. In the early 1980s NADRIAN SEEMAN and coworkers laid the foundation for an extension of the concept of hybridization of complementary sequences by their pioneering work on the fabrication of artificial nucleic acid structures made from synthetic DNA motifs [9]. Following and extending this idea, diverse building blocks with tailored designs, functional sites, flexibility or stiffness were made through the intelligent combination of certain single- and double-stranded DNA components.

But it is not only the self-assembling capability via the specific base pair recognition that makes DNA an interesting construction material. Further advantages of DNA are its mechanical, chemical and thermal stability. And besides the above mentioned DNA-directed immobilization of non-nucleic acid material by sticky-end cohesion the aromatic rings of the nucleic bases as well as the phosphate backbone themselves provide a large number of binding sites for organic and inorganic molecules. Especially the latter is helpful if one wants to use DNA in a new packaging concept not only as guide for assembly but also to build up electric circuitry. A DNA molecule with a diameter of 2 nm and a practically unlimited length is exceptionally suited for the fabrication of wire objects. But, as native DNA molecules longer than 100 nm have a high electric resistance, conductivity has to be induced by site-specific deposition of metal along the molecule. However, as the molecular recognition properties of a DNA molecule are no longer accessible after the decoration with metal, the metallization of the molecules integrated at well-defined positions in the electric circuit has to be the last process step.

Introduction

In this framework, also the present work is settled. Instead of developing a precise and controllable manipulation technique to troublesome integrate a precasted connector for the designated transport into circuitry, it is thought to appear more advantageous to use the remarkable molecular recognition capabilities of DNA for the purpose of integration and afterwards tune the electric properties of an assembled interconnection. Therefore, in this thesis methods are described which allow (i) the integration of DNA molecules into microelectrode structures and (ii) lead to the *in-situ* formation of metal particles on the biomolecules by means of a photoinduced platinum nucleation.

Serving this course of practical workflow, also this thesis is structured as follows. The first chapter focuses on the fundamentals and basic principles which are important for the understanding of the subsequent investigations. For the sake of completeness, the state of the conventional packaging technology is briefly reviewed at the beginning. Then, the structure as well as the mechanical properties of DNA are discussed, thus introducing the construction material of choice and its important features. Subsequently, different strategies are explained which have been applied for the site-specific anchoring of DNA ends to surfaces. This step constitutes the prerequisite for the formation of DNA networks and their integration into micro-fabricated electrode structures. As conductor track patterns can be either defined by precasted patches of artificial DNA network structures or by “track by track knitting” through stretching of single DNA molecules one section briefly reviews nanostructure formation with DNA and another section gives an overview on published methods for DNA stretching comprising methods based on mechanical forces and the phenomenon called dielectrophoresis. Finally, the basics of DNA metallization are summarized.

After this introduction, the construction of interconnect patterns by stretching DNA using hydrodynamic or electric field-induced flow, respectively is investigated in Chapter 2. In Chapter 3 the metallization of DNA molecules is studied. In particular, the photoinduced selective growth of metal clusters on DNA adsorbed to substrates is investigated. Additionally findings on the metallization of DNA tubes are shown. Finally, in Chapter 4 the metallization of DNA molecules integrated into electrode structures is demonstrated, followed by the first results on their electrical characterization. The work is summarized in the last chapter.

1 DNA-Based Nanowire and Network Fabrication

DNA has emerged over recent years as the molecule of choice for nanodesigners. There are two reasons for this. First, in the more than 50 years since the description and proof of evidence for the double helix being the structure of DNA in the “annus mirabilis” 1953 [10–12], a detailed understanding of its properties and formation has developed. This allows one to predict the shapes into which a DNA molecule of a given sequence will fold in solution and in reverse, to therefore design DNA sequences to fold into certain artificial structures.

Second, the development of a sophisticated chemical synthesis and automated parallel synthesizers have nowadays made it possible to easily obtain DNA molecules of any desired sequence, of lengths up to 100 nucleotides (the monomer unit of DNA, refer to subsequent text). Using biological methods, also longer molecules may be obtained through exponential DNA amplification in a polymerase chain reaction (PCR) or molecular cloning approaches.

The molecular engineer is thus armed with two of the basic elements needed to build structures of interest: the material for building and an understanding of their properties. The barrier he has to surmount next is to deploy his knowledge to develop structures and devices that are “really useful”.

As it is the intention of the present work to use DNA in an engineering context, in particular for DNA-templated electric circuit construction, understanding the structural and chemical properties of DNA herein also builds the basis to establish the further construction steps. They comprise (i) bottom-up controlled interconnection of microfabricated gold contact arrays by stretching single-tethered DNA molecules into a wire-like conformation, (ii) fixation of this configuration by site-specific attachment and finally (iii) the DNA metallization. Thus, subjects of the following sections are first, a brief review of the state of the packaging technology to show the engineering context the DNA-based assembly has to be seen in conjunction with. Second, in order to understand the construction material of this work, DNA structure and mechanics are described. After the introduction of methods for an end-specific functionalization of the molecule to allow a locally controlled attachment of the both ends, techniques are demonstrated to stretch long DNA molecules against the acting entropic forces. Fourth, strategies follow to realize the functionality of a conductive nanowire on unmodified DNA of low conductivity. To complete, work which has previously been done on nanofabrication with DNA as well as construction, is briefly reviewed.

1.1 State of the Electronic Packaging Technology

On the one hand, the development of electronic packaging is significantly determined by miniaturization and increase in integration density in semiconductor industry (“more MOORE geometrical scaling”). Because of their character as mass-produced articles with the biggest market share, memories (Dynamic Random Access Memories, DRAMs) and logic circuits (microprocessor units, MPUs) are at the forefront of this progress and therefore the evolution of their characteristic feature size is shown as an example in Figure 1.1. According to this predictions, by 2022, the year when the current ITRS

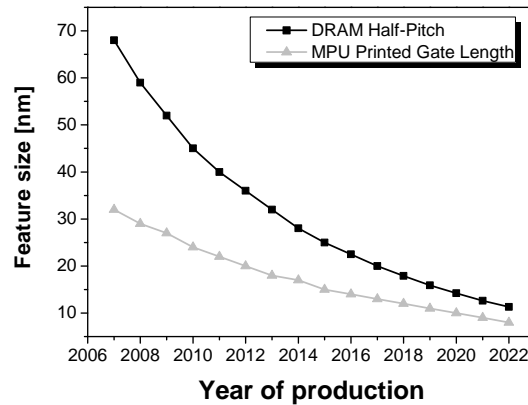


Figure 1.1: Evolution of minimum feature size in semiconductor industry using the examples of DRAMs and MPUs (Source: ITRS-2007/update 2008, [1]). For DRAM the minimum feature size is represented by the half pitch of first level interconnect dense lines, while for MPU it is the gate length of the transistor

forecast ends, the minimum feature size goes below the limit of 10 nm and will thus be comparable to (bio-)molecular dimensions! This size is also close to physical limits (quantum effects and non-deterministic behavior of small currents) and technological limits (such as power dissipation, design complexity and tunneling currents) and may hinder the progress of microelectronics on the basis of conventional MOORE’s Law circuit scaling. Already today, technological problems, together with exponentially increasing investment costs, slow the speed of progress for conventional CMOS technology. Concerning in particular the packaging, the wiring required to interconnect transistors must scale at the same rate as the transistor size to take advantage of improvement in size and speed. Taking also into consideration the simultaneously increasing signal frequencies on the chip as well as the cost pressure (increased device complexity requires higher cost packaging solutions, so that the package cost does not follow the die cost reduction curve), it becomes clear, that the geometrical requirements on the packaging, in this case especially on the wiring, will rise extremely.

On the other hand, the development of electronic packaging is driven by the increasing needs on the part of the product’s functionality (“more than MOORE functional diversification”). Changes in system design would allow the system performance to continue to increase, thus reducing the cost per function on a chip. There is therefore great scope for

1.1 State of the Electronic Packaging Technology

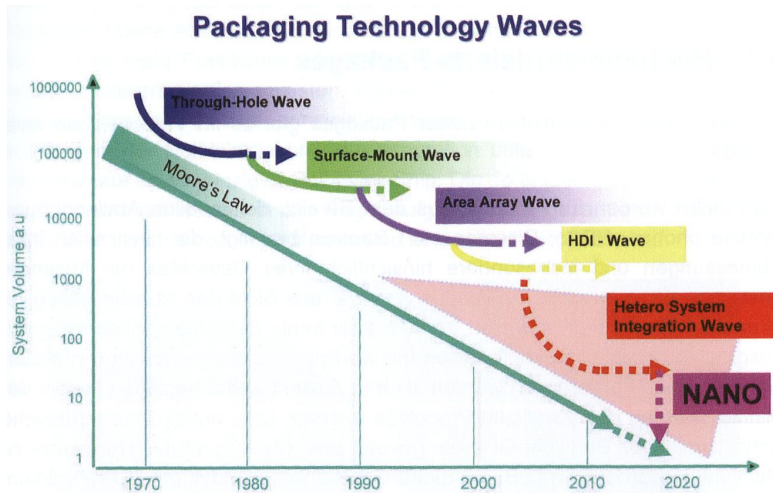


Figure 1.2: Packaging Technology Waves (source: [13])

technologies which may be integrated on a CMOS chip and enhance the functionality of the CMOS chip.

As a result of both development directions, a significant trend consists in system integration. This development took place batch-wise throughout the last 40 years (Figure 1.2): Through-hole mounting was displaced in the 1980s by surface-mount technology (SMT). In the 1990s area array packages enhanced the number of connections per unit area by consistently using the SMT. In the late 1990s high density interconnect (HDI) packages kept up with structure miniaturization. Today, the image has to be viewed differently as there are three main trends: highly miniaturized components and packages, highly integrated single-chip packages as well as integrated packages combining multiple technologies. The second technique describes the integration of as many different functional Si-based (or perhaps other) units on one single silicon chip as possible (system-on-a-chip, Figure 1.3a) leading to an enormous number of external connections of decreasing size but shortest interfunctional unit connections on the chip. In contrast, the third technique comprises the flexible (vertical) stacking of chips with different functions (multi-chip module, system-in-package, Figure 1.3b). The latter approach may be preferable, as it is easier to test smaller systems and development costs are reduced. However, these available approaches in today's form are not considered to provide the solutions to packaging aspects for a continued miniaturization beyond 2020. The gap opening between the producible feature size and the size of obtainable packages is closed by the trend "nano" in Figure 1.2, but is also termed "packaging gap" as concrete solutions are far from existing.

The forecast of the semiconductor industry, namely ITRS, predicts that CMOS miniaturization described up to here will continue until 2022 (the horizon of the current ITRS). After that, new technologies based on nanoelectronic devices should be envisaged and new architectures are required to overcome fatal bottlenecks in interconnects. Thereby, industrially applicable nanofabrication techniques have to have the following minimal

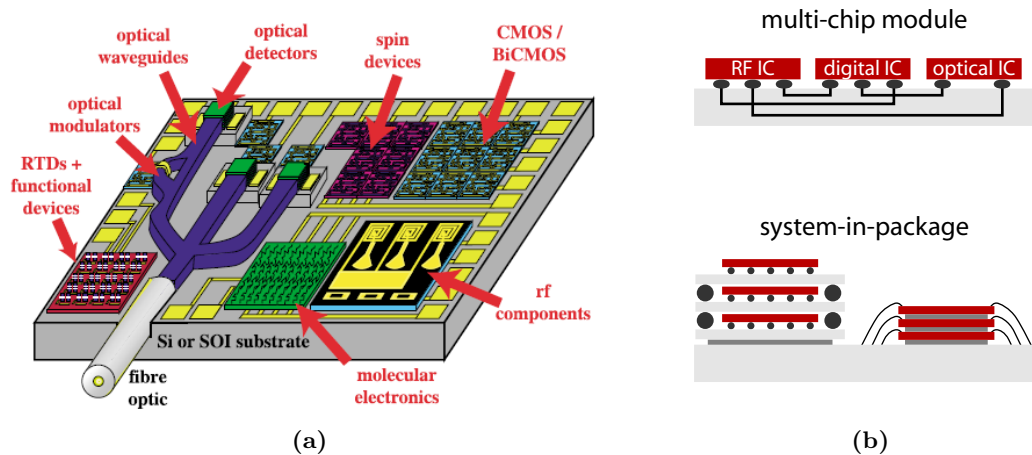


Figure 1.3: Schematic diagram of current packaging concepts. Full compatibility of new technologies with CMOS is desirable, but (a) a complete integration as in systems-on-a-chip [14] may be too expensive or suffer from severe technological drawbacks such as crosstalk or radio frequency incompatibility. (b) Multi-chip modules or systems-in-package may therefore be a more adequate solution for specific applications (adapted from [13]).

requirements: they must be able to produce millions or billions of these small structures in a quick, reliable and cost-effective way and the techniques must be able to connect these structures in a predefined manner. ITRS identifies these important technological challenges, but for most of them no solutions are outlined.

This lack of solutions offers a window of opportunity for alternative approaches like bottom-up assembly and “beyond CMOS” technologies which are proposed to scale information processing for decades beyond the 2022 time horizon projected for CMOS scaling [14]. The candidate technologies chosen for evaluation in the ITRS are nanoelectromechanical switches and FETs, spin transfer torque logic, collective strongly correlated many-electron spin devices, carbon-based nanoelectronics, atomic/electrochemical metallization switches, single electron transistors and CMOL/FPNI (Field Programmable Nanowire Interconnect). A general property of many of the nanoscale devices outlined above is, that they can be scaled down to the order of tenths of a nanometer. This is their main advantage over CMOS devices and makes them attractive as possible building blocks of electronic circuits. Being able to downscale, however, is only one problem facing the development of nano-scale integrated circuits. Solutions also need to be found for the interconnect bandwidth problem, the testing effort, which gets extraordinary large as integration densities increase and might make self-testing architectures a necessity and most important, the nanoscale functional elements have to be positioned in space. Here, the information should be present in the assembly that allows their own confinement at the desired place—an approach pursued in this thesis.

1.2 General Aspects on DNA

1.2.1 DNA Structure

DNA from all organisms is made up of the same chemical and physical components. It is a linear polymer composed of repeating monomer units called nucleotides. Each nucleotide comprises three parts: the pentose 2-deoxyribose, a phosphate and one of the heterocyclic nucleobases adenine (A), cytosine (C), guanine (G) and thymine (T), respectively (Figure 1.4).

The bases are coupled to the pentose via its 1'-carbon atom, forming together a nucleoside. The phosphate rest is attached to the fifth carbon of the sugar residue. At its 3'-position an OH group is existing. By a phosphodiester bond it allows concatenation

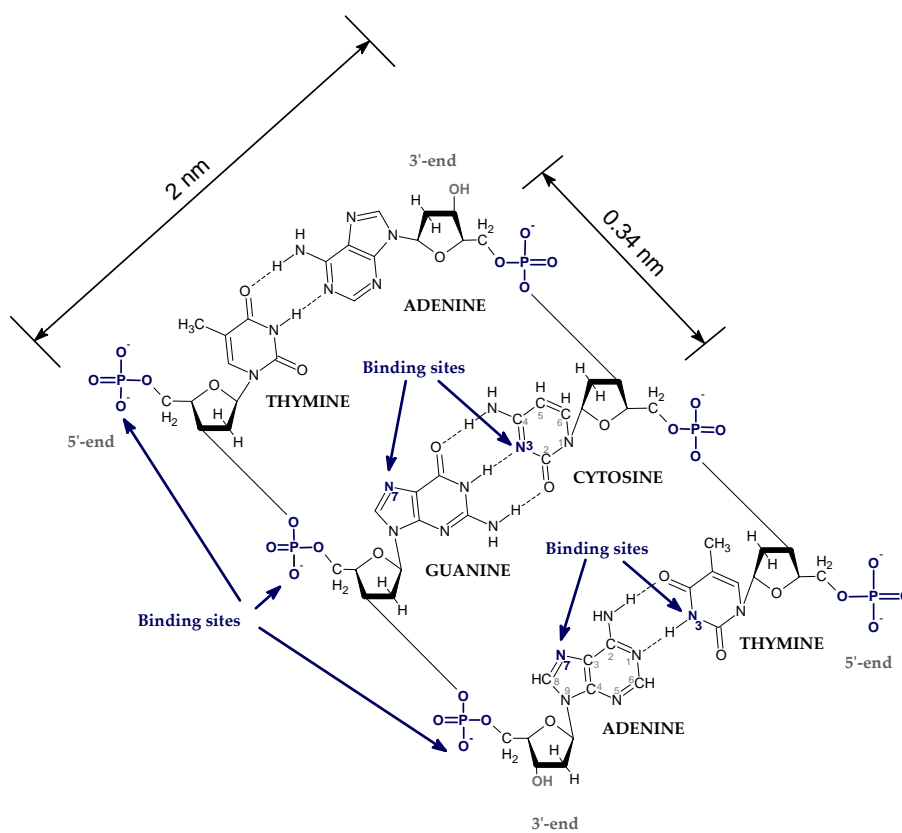


Figure 1.4: Chemical structure of the DNA double helix. The backbone of the DNA strand is made from alternating phosphate and the sugar residue 2-deoxyribose. Molecular recognition by WATSON-CRICK base pairing means that the purine adenine pairs with the pyrimide thymine and the purine guanine pairs with the pyrimide cytosine, respectively. The non-covalent hydrogen bonds between them are shown as dashed lines. Additionally, two classes of binding sites for DNA-templated nanowire fabrication are shown: negatively charged phosphate groups in the backbone, and N7 atoms of bases G and A and N3 atoms of bases C and T. Morphological data is included as well.

1 DNA-Based Nanowire and Network Fabrication

of the deoxyribose with the fifth carbon of the adjacent nucleotide via its phosphate (Figure 1.4), thus forming the DNA backbone. Moreover, the alternating sugar-phosphate backbone of a DNA strand thereby has a directed chemical structure: from a free hydroxyl (in case of dephosphorylation) or phosphate group at the 5'-carbon of a pentose (5'-end) to a free hydroxyl group at the 3'-carbon of its terminal sugar (3'-end). Additionally, as a result of the negative charge of the phosphate group at neutral pH, the DNA backbone in total is charged with $1 e^-$ per nucleotide and has a hydrophilic as well as an acidic character.

Naturally, DNA appears as two nucleic-acid polymer chains that are wound around one another to form a regular, right-handed helix called B-DNA, as WATSON and CRICK discovered in 1953, putting together pieces of the chemical puzzle that researchers had been collecting for more than 80 years. The orientation of the two strands is antiparallel: at each end of the double helix one strand has its 3'-end, whereas the other has its 5'-end. Through the association of the two strands in the center of the double helix certain bases face each other, they are paired. Caused by size, shape and chemical composition of the bases, A is always (apart from the occasional erroneously synthesized, missing, or damaged nucleotide) paired with T through two hydrogen bonds and C is always paired with G through 3 hydrogen bonds. Thus, the DNA molecule is composed of two complementary strands of DNA. The hydrogen bonds account for the high specificity of the base pairing whereas stacking interactions between the large number of base pairs stacked on top of one another provide stability of the helix structure.

As a purin always binds to a pyrimidine, the distance between the parallel base planes is always the same, namely 0.34 nm in B-DNA. The whole B-DNA helix has a diameter of 2 nm and winds 36° with each base pair. Consequently, one complete turn is (idealised) reached every 10 bases (10.5 bases average in solution). In single-stranded DNA (ssDNA) the mean distance between two bases of 0.43 nm is slightly greater than in double-stranded DNA (dsDNA).

1.2.2 DNA Mechanics

The basic features of the DNA molecule were elucidated above. Now in this section, more focus will be put on the mechanical properties of this molecules in order to get quantitative values for the work that has to be done in the subsequently described DNA manipulating steps.

Although mechanical properties vary according to local sequence and helical structure, DNA in many biological contexts is usefully represented as a flexible chain, that is a line that bends smoothly under the influence of random thermal fluctuations. To describe this type of semiflexible molecules, in 1949 KRATKY and POROD introduced the worm-like chain (WLC) model [15], which characterizes a polymer using a single parameter, the persistence length a . The value of a defines the distance over which the direction of the deflected line persists, or in other words: over contour lengths shorter than a the double helix is essentially straight. The persistence length depends very much on the ionic strength of the solution. As under low salt concentrations the backbone charge shielding is reduced, the repulsion of the chain segments is increased and the persistence

1.2 General Aspects on DNA

length is raised. For dsDNA in physiological buffer, $a \approx 50$ nm [16]. Single-stranded DNA is much more flexible and has persistence lengths of smaller than 10 nm [17].

In solution, DNA segments, that are much longer than one persistence length, are crumpled into random coils by thermal bending, resulting in an average end-to-end distance much shorter than its contour length. When no external forces are applied, according to the WLC model the end-to-end distance $\langle r^2 \rangle$ of a molecule of contour length L averages to $2aL$. That is, a $16.2 \mu\text{m}$ long λ -DNA, which is used in the following experiments, has a mean end-to-end distance of $1.3 \mu\text{m}$ only. Pulling the molecule into a more extended chain is entropically unfavorable, as there are fewer possible conformations at longer extensions, with only the one single possible conformation of a perfectly straight line for maximum extension. The resulting entropic force increases as a random coil is pulled from the ends. Such direct measurements of force and extension on single molecules for example can be performed by fixing one DNA end to a surface and attaching a microscopic “handle” such as a bead to the second end. Forces can then be applied to the DNA molecule by moving the bead with an optical or magnetic tweezer (Figure 1.5a) [18, 19]. The resulting extension of the DNA molecule can be measured by

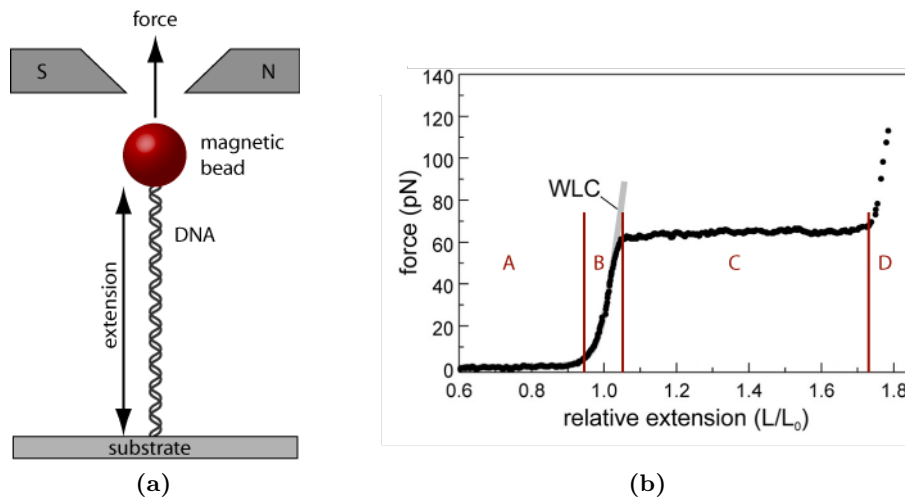


Figure 1.5: DNA mechanics. (a) The mechanics of DNA can be studied by measuring the extent to which a single DNA molecule stretches relative to its normal B-form contour length when e.g. in a magnetic tweezer a force is applied to a magnetic bead attached to the surface-tethered DNA. (b) Force versus relative extension for dsDNA molecules (adapted from [20]).

monitoring the position of the bead with a microscope leading to force-extension curves as shown in Figure 1.5b. Double-stranded DNA requires about 0.1 pN to be extended significantly to about 50% of its contour length. To stretch the double helix from 50% to about 95% of its total B-form length, the force rises drastically from 0.1 to about 10 pN (region A in Figure 1.5b). This reflects the increasing amount of work that must be done to suppress thermal bending fluctuations at successively shorter length scales. Subjected to a force of more than 10 pN the double helix starts to stretch linearly (region B) until near a force of about 65 pN a sharp transition occurs (region C). The double

helix changes from about 107% to nearly 170% of the contour length over just a few pN. However, the extend of this over-stretching is less than one might expect as the distance between two bases in a fully stretched-out single strand is about 0.7 nm, which is more than 200% of the 0.34 nm in B-DNA. The question about the molecular mechanism behind this overstretching transition has been a matter of discussion [21, 22] until only recently it was concluded from convincing experiments directly visualizing the structure of DNA during overstretching, that the generic process governing the transition is the melting of bases [20].

In conclusion, to keep a stretched, straight DNA molecule with the ends attached to a surface, one needs anchors, which at least last a few pN. From this perspective, in the following, different methods for the attachment of DNA to surfaces will be considered.

1.3 End-Specific DNA Functionalization and Site-Specific Immobilization

During DNA replication, the basis for biological inheritance, the DNA double helix is unwound and each strand acts as a template where nucleotides are matched to synthesize the new complementary strand. This process, which nature provides a large number of efficient tools, enzymes, for, can also be performed outside a cell (*in vitro*) to modify DNA molecules, namely to incorporate additional functional groups at particular sites in a DNA strand to cross-link the duplexes to surfaces.

A common strategy for DNA end functionalization is the polymerization of nucleotides against single-stranded overhangs at the end of DNA duplexes. These so called sticky ends are filled in by a reaction using DNA polymerase, isolated from cells, and deoxynucleotide triphosphates (dNTP). The technique relies on the incorporation of nucleotides modified to include the desired functional group (Figure 1.6a). This way, for example the Large Fragment of Polymerase I (*Klenow polymerase*) fills in 5'-overhangs, thus creating blunt ends (Figure 1.6a) or in other words one can prepare DNA duplexes which are end-specifically functionalized with a certain reactive site. The most prominent examples used to allow site-specific binding of DNA to other materials are thiols (R-SH), the coenzyme biotin [17, 21] and digoxigenin [23, 24]. All of these functionalities can also be incorporated into short single-stranded DNA parts—so called oligomers—where then longer double strands with a complementary sticky end can reassociate by hybridization (Figure 1.6b). These kinds of binding assays make use of the possibility, that during chemical oligonucleotide synthesis functional groups can easily be attached to either the 3'- or the 5'-end or any other position of the synthesized strand.

The end-specific functionalization of DNA is an important first step for the site-specific anchoring of the molecules to surfaces. As explained before, such tethered DNA molecules are a prerequisite to measure their mechanical properties, but in their single-stranded form they are for example also the origin of customized oligonucleotide synthesis and hybridization sensors. In the context of this work, the end-specific coupling of a DNA molecule to a surface is necessary for the application of a stretching force. Thereby, the aim is the combination of an *end-specific* attachment with a *locally controlled* positioning

1.3 DNA Functionalization and Immobilization

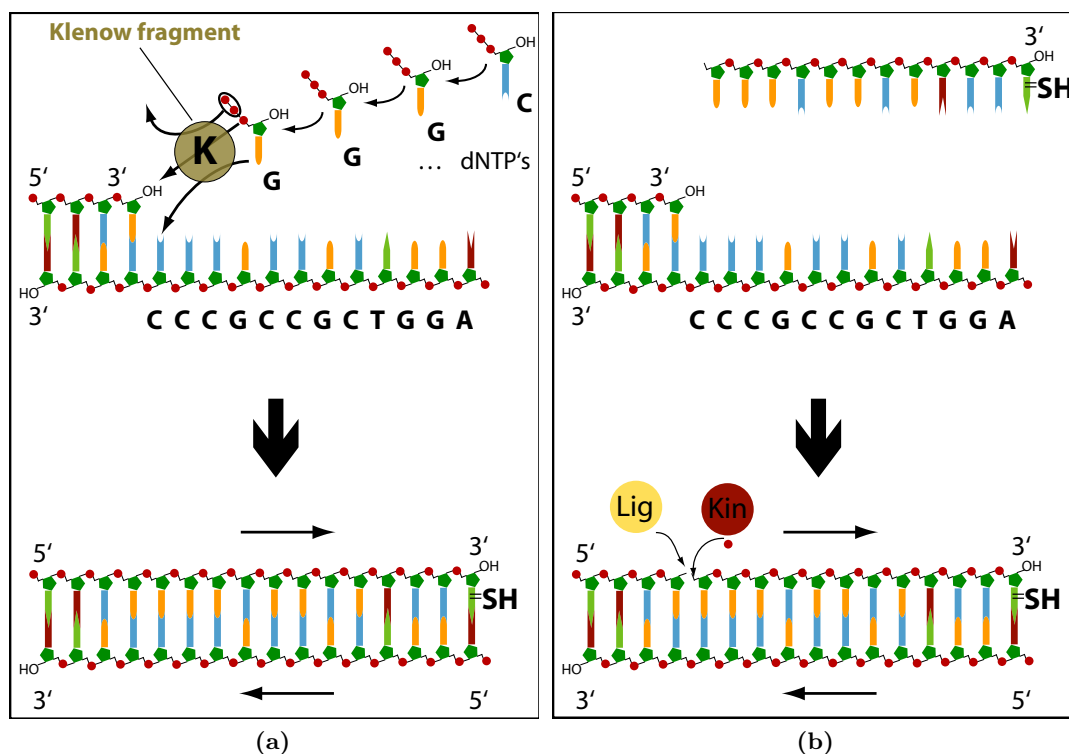


Figure 1.6: Sticky end functionalization. (a) Filling-in recessed 3' ends: The exonuclease-free Klenow fragment of DNA polymerase incorporates the deoxynucleotide triphosphates dATP, dCTP, dGTP and the thiol-modified S^4 -TTP, resulting in a functionalized blunt end. (b) Hybridization of a thiol-modified oligomer to the sticky end of λ -DNA. The single stranded nick can be closed by phosphorylation of the OH-terminated 5'-end of the oligomer before hybridization using T4 kinase (Kin) and ligation after hybridization using T4 ligase (Lig).

of the both molecule ends at electric conducting contact pads, so that stable DNA interconnects can be formed.

In general, besides artificially introduced functional sites, DNA offers many possibilities for coupling purposes: the amines in the bases, the negatively charged backbone, the phosphodiester within the backbone, and the phosphates at the 5'-end as well as the hydroxyl group at the 3'-end are potential candidates.¹ The most common techniques for the immobilization of DNA on surfaces make use of them for covalent binding, affinity reactions or adsorptive interactions, respectively.

DNA can be coupled covalently to reactive surface sites by a large number of suitable coupling compounds and reactions. Besides the NH_2 -groups further reactive groups on the DNA can be derived by activation reactions like for example by the carbodiimide- or the activated ester method [25]. The introduction of the binding partner on the surface is facilitated by the use of linker molecules. A very attractive method for the activation

¹It should be noted that in the double strands the bases themselves are engaged in hydrogen bonds and thus, are not accessible for coupling reactions.

1 DNA-Based Nanowire and Network Fabrication

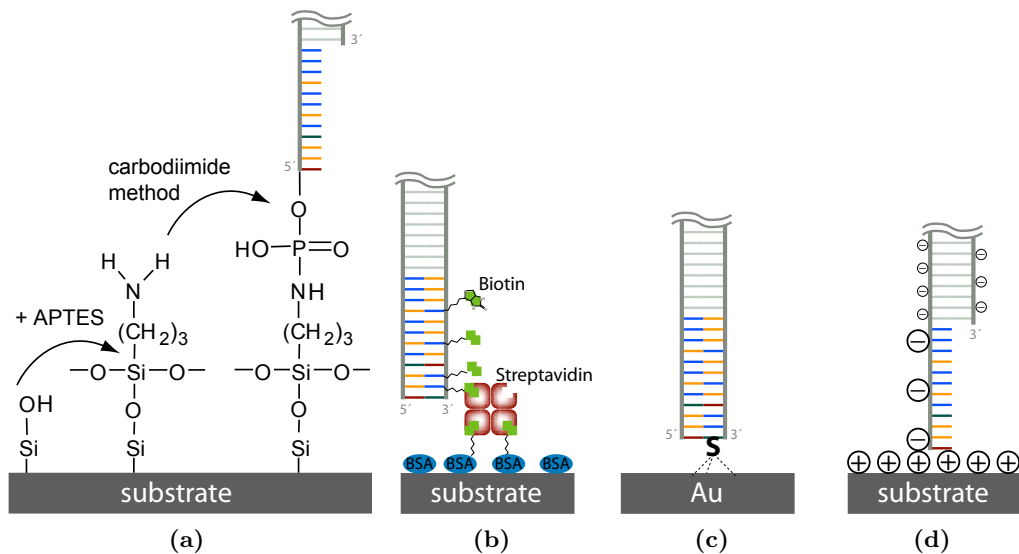


Figure 1.7: Schematic of four different methods for end-specific anchoring of DNA to surfaces: (a) At the DNA end an activated phosphorester—introduced by the carbodiimide method—is attacked by nucleophilic agents such as through silanization formed amines to form a stable covalent bond. (b) Affinity reaction forming a streptavidin bridge between the biotinylated DNA end and a BSA-biotinylated surface. (c) Specific binding of thiol-functionalized DNA to a gold surface. (d) Electrostatic bonding between amino groups and negatively charged DNA ends.

of hydroxyl-terminated substrates such as silica or glass is silanization with reactive silanes. A commonly applied silane is 3-aminopropyltriethoxysilane (APTES), shown in Figure 1.7a, providing an amino group for a chemical reaction with a functional group on DNA.

Besides covalent bonds, the interaction between the protein avidin (streptavidin respectively) and the coenzyme biotin is one of nature's strongest. Avidin and streptavidin are closely related tetrameric proteins that have the unique characteristic of binding four biotins with extremely high affinity [26, 27]. Therefore, this combination is also a suitable method for the firm attachment of biotinylated DNA (or more general any biotinylated object) onto (strept-) avidin coated surfaces (Figure 1.7b). The bond strength between biotin and streptavidin strongly depends on the force loading rate and thus rises from 5 pN to values as high as 170 pN for increasing loading rates [28].

Another bond of high strength but noncovalent nature is the one between thiols and gold surfaces (typical bond energy 126 kJ/mol [29]). The use of thiols is one of the best established solutions for the adsorption of biomolecules on metal surfaces like gold (Figure 1.7c), silver, platinum, or copper [30]. Gold is usually the substrate of choice because of its inert properties and the formation of a well-defined novel crystal structure in which each sulfur atom is bonded coordinatively with three gold atoms. Experiments showed, that the sulfur-gold anchor ruptures at forces of 1.4 nN (at force-loading rates of 10 nN/s) [31]. Furthermore, by means of photolithography gold surfaces can easily be

patterned with sub-micrometer precision, thus providing a possibility to confine binding events to well-defined sites at the surface.

Immobilization of DNA on surfaces is also possible by electrostatic interactions, as the negatively charged backbone of the DNA itself benefits the coupling to charged surfaces. Besides naturally charged surfaces like mica, most suitable for doing so are supports which are modified to exhibit amino (Figure 1.7d) or carboxyl groups. Two factors have critical impact on the resulting binding quality and specificity. (i) The addition of positively charged cations like Mg^{2+} to the buffer fine tunes the adhesion of negatively charged DNA molecules to initially negatively charged and therefore DNA repelling surfaces. Otherwise, at too low cation concentrations (< 0.05 mM) DNA cannot bind tightly and will be swept away during the alignment procedure or random DNA networks will be formed, thus hindering the alignment at high cation concentrations (> 1 mM), respectively [32]. (ii) To ensure the tethering of the molecule at one or both extremities only, thus avoiding multi-site attachment by binding of the molecule along its length, the pH has to be adjusted to a range where the DNA's extremities still bind, whereas its inner parts no longer adhere [33].

A DNA molecule, specifically end-tethered by one of the methods presented above, can then be stretched. The following section focuses on different principles of DNA stretching and their applicability for nanowire fabrication, where individual DNA molecules must be separated and stretched to serve as templates for the formation of nanowires.

1.4 Stretching DNA

Controlled fabrication of DNA-templated nanostructures requires the ability to manipulate DNA molecules on a surface prior to further processing, e.g. before DNA loses thereby its biological functionality and steps such as site-specific assembly are not possible any more. Since at equilibrium long native DNA molecules in aqueous solution have the conformation of a random coil, for a use as linear connection between two points they have to be stretched against the acting entropic forces which shorten the end-to-end distance to a much smaller size than the contour length.

To gain a linear, "wire-like" shape, many approaches have been used to stretch individual DNA molecules, including atomic force microscopes, optical and magnetic tweezers and techniques which are preferably suitable not only for the stretching of individual DNA molecules but at the same time for their alignment on surfaces, like molecular combing, electrophoretic stretching and hydrodynamic flow. As the latter is the purpose of this work, the following two subsections will focus on these last named principles of DNA stretching and their applicability for nanowire fabrication.

1.4.1 Mechanically Induced Stretching

Molecular Combing

One of the least complicated techniques of stretching and aligning DNA molecules on surfaces and thus the most widely employed one is molecular combing. Individual,

1 DNA-Based Nanowire and Network Fabrication

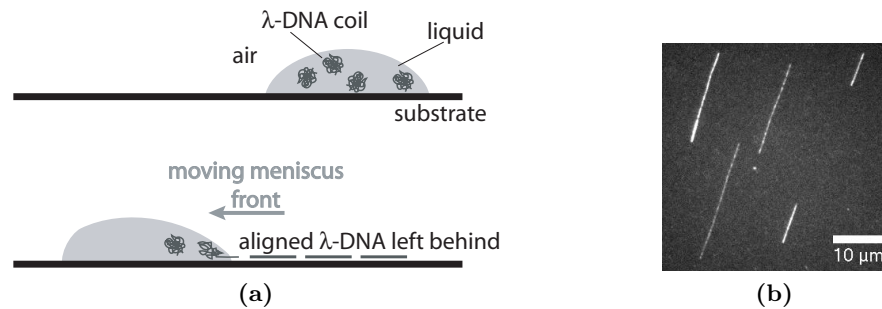


Figure 1.8: Molecular combing. (a) Schematic diagram of the mechanism. The receding meniscus generates a surface tension which stretches DNA. (b) Fluorescent micrograph of λ -DNA stained with the fluorescent dye YOYO-1 and combed on polydimethylsiloxane (PDMS).

adsorbed DNA molecules are stretched by a so-called receding meniscus, a moving air-buffer liquid interface and left to dry on the surface in an aligned manner (Figure 1.8). The surface tension, acting perpendicular to the direction of motion of the meniscus, extends the DNA during movement, provided that this force is greater than the entropic force but smaller than the force needed to break covalent bonds. The relative movement between the liquid front and a multitude of substrates can be achieved by a variety of approaches, each case being characterized by different physico-chemical parameters optimized to allow a specific anchoring of the molecules by their extremities only. For example, a droplet of DNA solution can be left for evaporation between a surface and a coverslip, as in the first report of molecular combing by BENSIMON *et al.* [34]. To gain a unidirectional alignment of DNA molecules, the receding meniscus can be guided by sucking up the droplet with absorbent paper [35] or a pipet [36] or compressed gases like air or nitrogen were used to drive the DNA solution to flow away along one direction on the substrate [32]. And molecular combing can also be done in a controlled way by passing the liquid-air interface with the substrate, e.g. by dipping the substrate into a basin of DNA solution and pulling it out again at constant speed [37, 38]. All this techniques where the direction of stretching is controlled also allow for the creation of 2D DNA arrays by a second alignment along another direction [39].

Despite its technical simplicity and parallel manipulation character, direct molecular combing onto solid substrates solely is not suitable for controlled deposition—meaning that the location of each end of the DNA molecule is predefined. The inherent lack of control over the location of the first anchoring point of a DNA molecule can only be overcome by a combination of surface-energy [40] or -topography [39] modification prior to molecular combing and subsequent transfer printing of the pattern of elongated and aligned DNA to desired surface areas. With this approach DNA strands bridging gold electrode gaps on silicon chips could be achieved [41]. However, in spite of the outlook in [41] that by means of molecular combing and transfer printing produced structures should

then enable DNA to be used in practical nanodevice fabrications, the functionality of the printed structures as templates for a selective metal deposition was never published.²

Hydrodynamic Flow

In order to improve the control over the tension on a DNA molecule a hydrodynamic flow can be created by pumping a buffer solution through a defined microfluidic channel [42]. In this way DNA tethered at one end to the channel bottom wall is stretched by the shear force acting on the different sides of the initial DNA coil in a parabolic POISEUILLE velocity profile near the substrate surface³ [46].

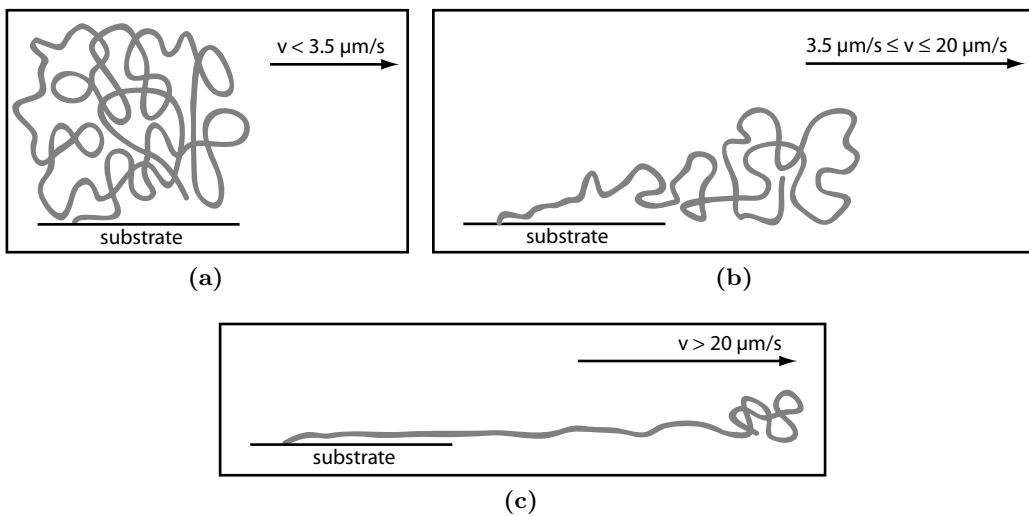


Figure 1.9: Sketch of the fluctuations of a single-end tethered DNA molecule subjected to an increasing flow velocity (force). One representative conformation each is shown for (a) the small-velocity regime: the chain is almost unperturbed; (b) the intermediate regime: the molecule is extended in the force direction and adopts a *trumpet* shape; (c) the high-velocity regime: the *trumpet* disappears and the molecule adopts the *stem and flower* conformation.

Under an increasing flow velocity, a single-end tethered flexible polymer like DNA is expected to display three types of conformation [47–49]: in the small-velocity regime—equivalent to small friction forces—the molecule is relatively unperturbed, that is like in the quasi-equilibrated entropic coil shape (Figure 1.9a). For increasing applied forces, that is at flow velocities $v > 3.5 \mu\text{m/s}$, the DNA molecule’s conformation crosses over to the so-called *trumpet* shape [47]. Figure 1.9b displays a narrow section of the molecule close to its tethered head and a widening section close to its free end. This shape is the

²The probably also transferred monolayer of stamp material laying on top of the transfer printed DNA pattern might be a reason for that.

³This scenario of interest for the integration of stretched DNA strands into specific surface-sites has to be distinguished from the cases where the extension (and relaxation) of DNA attached to beads was investigated in (steady) flow by means of optical or magnetic tweezers in the absence of unwanted interaction with the surface [43–45].

result of a nonuniform friction force acting on the molecule, whereas the largest forces affect the tethered end to extend this molecule section in the direction of flow. At higher velocities ($v > 20 \mu\text{m/s}$), the tethered DNA end is subjected to even increased tension so that the trumpet disappears and the molecule adopts the *stem and flower* conformation where the fully stretched part is demoninated *stem* and the remaining small coil at the free end is termed *flower* (Figure 1.9c).⁴

Besides the supply of the stretching force, the flow also defines the orientation of the elongated DNA molecules [50] which becomes especially obvious in the case of flow spinning, where viscous force generated by rotational flow extends the polymer [51, 52].

Like molecular combing, the approach of stretching surface-tethered DNA by hydrodynamic flow has one key advantage over other DNA manipulation methods: it can (but does not necessarily need to) be performed using many DNA molecules in parallel. However, flow manipulation and combing methods do not allow for the independent manipulation of molecules within the fluid flow. What is needed is the achievement of high throughput and yet individual manipulation at the same time.

1.4.2 Electric Field Induced Stretching

A method to cope with the quandary between high throughput, in the sense of fast processing, and yet high resolution, meaning single molecule precision, is the application of an electric field to induce stretching of DNA molecules between electrodes. With the switching-on of the electric field between two contacts also the stretching operation is triggered, so that an interconnection is selectively established—“switched on”—only between those gaps, where the electric field was applied. Then, an effective switching algorithm together with a permanent anchoring of the DNA molecules in contact with the electrodes could provide an automated wiring procedure. Further, no additional parts like e.g. microfluidic channels need to be assembled because the electrodes necessary for the setup of the electric field are mandatory anyway if the purpose of the stretched molecule is the electric interconnection between them.

Several groups have studied the application of a uniform electric field, causing polyanionic chains like DNA to migrate toward the anode [24, 53, 54]. Like in gel electrophoresis this experiments are carried out in agarose gels and might therefore not be very useful for preparing nanowire templates.

Therefore, another widely used electric field-based method to stretch DNA is dielectrophoresis. Its basic principle as well as important findings for the application to DNA stretching will be presented in the following.

Dielectrophoresis

Dielectrophoresis (DEP) is the translation of neutral matter caused by polarization effects in a nonuniform electric field (Figure 1.10). The dielectrophoretic force is given by [55]

$$\vec{F}_{DEP} = (\vec{p} \cdot \nabla) \vec{E}, \quad (1.1)$$

⁴Eventually, past a velocity of $65 \mu\text{m/s}$, the coil-shaped subsection itself vanishes at the expense of the disentangled section and the tethered chain approaches complete extension [46].

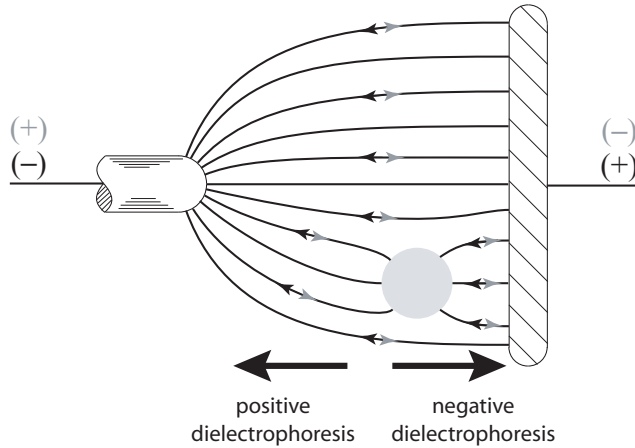


Figure 1.10: Sketch of the dielectrophoretic motion of a polarized particle in an inhomogeneous, oscillating electric field.

where \vec{E} is the electric field and \vec{p} the induced dipole, which can be calculated according to

$$\vec{p} = \alpha(\omega)\vec{E}, \quad (1.2)$$

where $\alpha(\omega)$ is the frequency dependent polarizability of the moving object. In the case of simple geometrical particles like a sphere, the DEP force can be calculated with several assumptions: (i) The particle is a homogeneous dielectric particle with ohmic conductance but no dielectric loss. (ii) This particle is suspended in a dielectric solvent, which also only shows ohmic loss. (iii) Additionally, the electric field must be applied much longer than the time constant associated with the accumulation of free charge at the surface of the sphere. Then, the basic formula describing the time averaged dielectrophoretic force $\langle F_{DEP}(t) \rangle$ acting on a spherical, isotropic particle of radius R , permittivity ε_2 and conductivity σ_2 which moves under the influence of an inhomogeneous, sinusoidal oscillating electric field of frequency ω and average strength E_{rms} in a medium with ε_1 and σ_1 reads [56]

$$\langle F_{DEP}(t) \rangle = 2\pi\varepsilon_1 R^3 \text{Re}[K(\omega)] \nabla E_{rms}^2, \quad (1.3)$$

with the complex CLAUDIUS-MOSSOTTI function given by

$$K(\omega) = \frac{\varepsilon_2 - \varepsilon_1 - j(\sigma_2 - \sigma_1)/\omega}{\varepsilon_2 + 2\varepsilon_1 - j(\sigma_2 + 2\sigma_1)/\omega}. \quad (1.4)$$

From Eq. 1.3 it becomes apparent, that the dielectrophoretic force vector is aligned with the gradient of the electric field squared. Its magnitude and direction linearly depend on the quantity and the sign of the CLAUDIUS-MOSSOTTI factor K as a function of the complex permittivities. For DNA—except for one publication [57]—only positive dielectrophoresis ($K(\omega) > 0$) is reported, i.e. molecules are attracted into regions of highest field strength.

A Survey of Findings on Dielectrophoretic Stretching of DNA

In contrast to the previous explanation, DNA is not a homogeneous dielectric sphere and the assumptions made above do not apply, making Equations 1.1 and 1.2 the origin of the subsequent discussion.

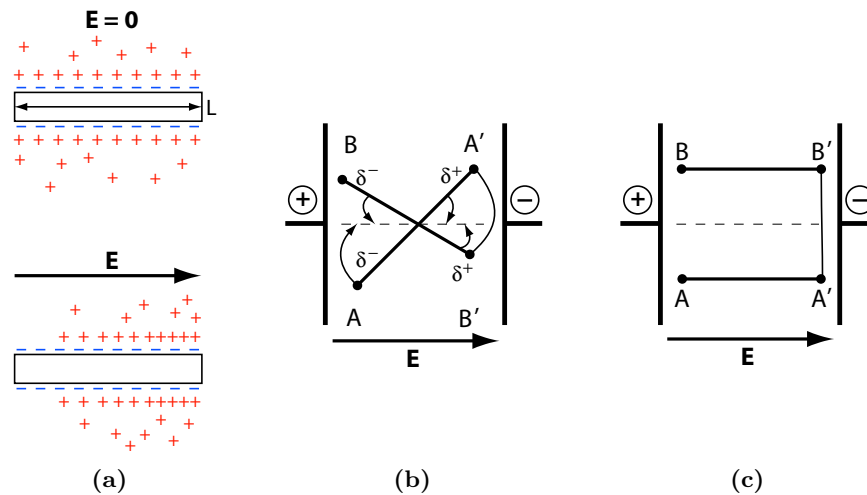


Figure 1.11: Polarization (a) and orientation (b)–(c) of DNA segments in an electric field. (a) Cartoon of the positive counterion cloud surrounding a negatively charged DNA segment of length L and its distortion due to an externally applied electric field. (b) Two randomly oriented DNA segments AA' and BB' are polarized in an electric field of a plate capacitor and (c) align parallel (AA') and antiparallel (BB') with the field.

There are two possible contributions to the polarizability of DNA, induced or permanent dipoles. It is widely assumed that DNA possesses no permanent dipole [58]. Instead, a DNA molecule in solution is polarizable [59] due to the counterion cloud in the surrounding of the polyanionic backbone.⁵ The counterions can be displaced by an electric field inducing a dipole (Figure 1.11a), whose magnitude depends on the frequency of the applied field. The frequency dependence of the polarizability is well documented and covers a wide frequency range from 10^{-1} to 10^7 Hz [61–63]. The ion displacement discussed so far is only possible in the low frequency range below 200 kHz as otherwise the time is too short for the required charge transport. In the higher frequency bands around 2 and 12 MHz, the polarization mechanism is attributed to concentration dependent interactions of DNA molecules and fluctuations in the double layer [58]. The polarization at 12 MHz is also attributed to a so called MAXWELL-WAGNER interface polarization [64]. However, the DEP manipulation of DNA is not possible over the full frequency range. Especially in the low and high frequency range, there are several more effects that contribute and

⁵There have been many publications, both theoretical and experimental, on the interaction between polyelectrolytes like DNA and an external electric field, and on the mechanism of polarization and orientation (see references in [59]). The counter-ion polarization model [60] is one model among others like the proton fluctuation model and the surface conductivity model.

complicate the analysis. There are hydrodynamic effects and electroosmotic motions which will be discussed in detail in the next subsection.

However, due to the fact that the ions are bound radially but are relatively easy to move axially, the polarization of DNA is anisotropic, i.e. it is highly polarizable along its length. Another feature to be noted is, that, because of this anisotropy of DNA, the dominant dipole moment occurs axially, so that also in an oscillating electric field the orientation parallel to the external field is often described (for ease of understanding shown in a stationary electric field in Figure 1.11).

Thus, in an electric field of sufficient strength and frequency a polarized DNA molecule is thought to stretch from a compact coil into an elongated conformation, orient along the electric flux lines and migrate parallel to the electric field gradient. WASHIZU *et al.* [59, 65, 66] for the first time studied effects of DEP on DNA. Their work was already aimed at site-specific integration of DNA bridging over an electrode gap [65]. Trying to realize that task they encountered a flow of the medium associated with heating due to the very high field intensity at the electrode edges preventing the unfixed molecule end to approach to the adjacent electrode. This problem was solved designing floating-potential electrodes (Figure 1.12) where the potential is applied to other electrodes than the ones where the molecules should be stretched, thus keeping thermal flow minimal near the latter. GREEN *et al.* [67, 68] then in detail studied experimentally as well as from a more theoretical point of view forces other than dielectrophoretic affecting the behavior of macromolecules like DNA in microelectrode structures. Their findings will be discussed in detail in the next subsection. For the moment the results of GERMISHUIZEN *et al.* [69–71] will provide the basis for the discussion on the applicability of DEP for DNA stretching and integration into microelectrode structures. Following the conclusions of GREEN, the group of GERMISHUIZEN found that for a number of different frequencies, electric field strengths, DNA lengths and across different electrode gap separations the elongation of the DNA is restricted by the geometry of the stripe electrode arrangement,

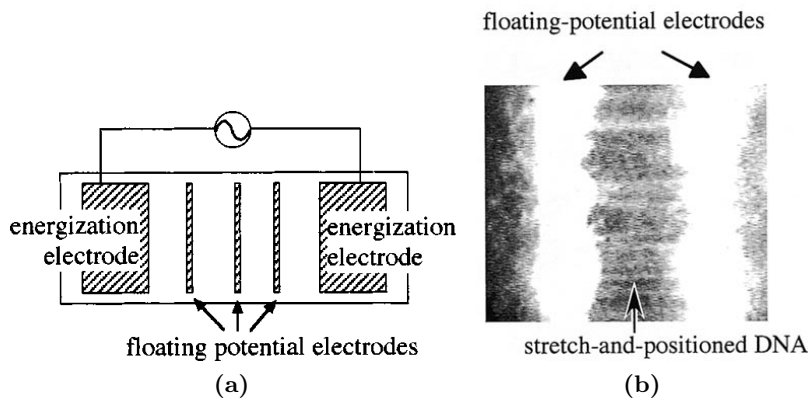


Figure 1.12: Stretching of DNA with floating potential electrodes. (a) Sketch of the electrode design and their potential feed. (b) Fluorescently stained λ -DNA stretched by an electric field of 1 MV/m and 1 MHz and immobilized at aluminium electrodes with a spacing of 15 μm . Both images taken from [66].

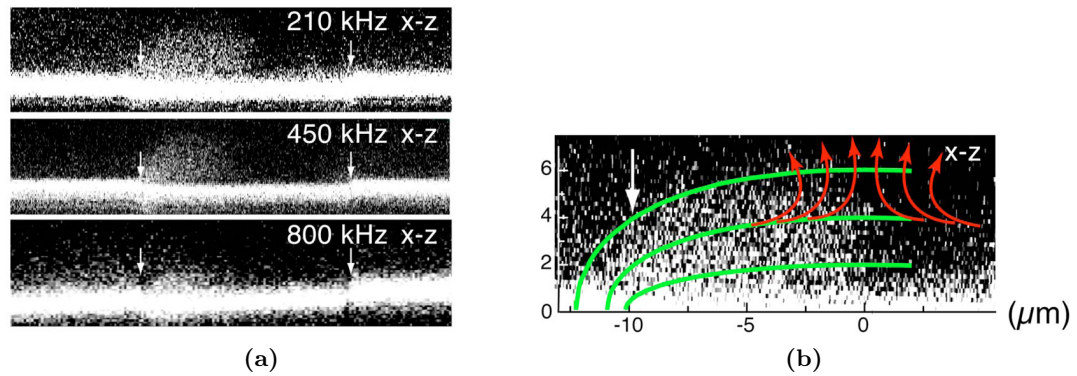


Figure 1.13: Side views of elongated, fluorescently labeled λ -DNA across a 20 μm wide electrode gap. (a) Side views at 210 kHz, 450 kHz and 800 kHz with the edges of the electrodes marked as white arrows; (b) Side view at 210 kHz where superimposed the electric flux lines (green) and the induced fluid flow (red) are shown. Taken from [70].

i.e. elongation is only possible up to the center of the electrode gap. The reason for that is the fluid flow pattern which as mentioned above WASHIZU already came across and which was analytically described by GREEN. As shown in Figure 1.13 the fluid flow only points in a direction suitable to lead to an elongation in the first half of the gap (looking across the gap). In other words, it becomes obvious that the stretching of a DNA molecule across a gap between parallel electrode plates is impossible.

However, the authors point out, that the fluid flow is essential as a bias force to allow for elongation of the DNA molecules at all. Their argumentation is the following: Modeling a DNA double strand as a long string of connected short segments (worm-like chain model [72]) in each of which a dipole is induced due to an external electric field, no elongation is expected as the parallel and antiparallel alignment of the segments with the field are equal probable (Figure 1.11). To make one alignment to be favored over the other, an additional bias force is said to be needed e.g. a point force pulling on the free end of the DNA. This bias force cannot be provided by the electric field itself because a positive dielectrophoretic force would point with the gradient of the electric field towards the ends of the molecules that are tethered to the surface and therefore would not result in elongation.⁶ Alternatively, a fluid flow induced viscous drag force could assume this role—but with the consequence of being not oriented in the favorable direction throughout the full gap length of a symmetric electrode setup.

To overcome the problem of fluid flow in left-right symmetric setups NAMASIVAYAM *et al.* [73] altered the shape of the electrodes from two parallel stripes to a tapered tip pointing towards the edge of a stripe. Using this system, a DNA molecule could be captured at the tapered electrode, immobilized using a thiol linker, and then stretched above its full length to bridge the entire gap. However, as the DNA used was only one-sided thiol-functionalized the stretched DNA recoils back to the pointed electrode after switching off

⁶Concluding, in the following text not the term “dielectrophoretic stretching” will be used, but the stretching mechanism resulting from effects related to an electric field are referred to as “electric field induced stretching”.

the electric field and no permanent connections were established not to mention networks of differently aligned interconnections between a number of electrodes.

Flow Regimes Induced by Oscillating Electric Fields

In this section the movement of liquid and the behavior of polarizable objects like DNA in aqueous solutions subjected to spatially non-uniform, oscillating electric fields will be discussed. The high-strength electric fields used in DEP manipulation systems often give rise to fluid motion, which in turn results in a viscous drag on the object. The results of object motion under the influence of these forces as reported in the literature will be explained.

First, fluid flow in electrolytes above microelectrodes occurs because electrical power is produced in the fluid surrounding the electrodes to a degree proportional to the conductivity of the medium and the field magnitude squared. Since the electric field used here is highly non-uniform, also the power density of this JOULE heating is highly non-uniform and generates temperature gradients in the fluid and therefore gradients in its mass density, permittivity and conductivity. They in turn can give rise to fluid flow in one of two ways: the first mechanism that produces the buoyancy force on the fluid is natural convection, where the denser fluid elements displace less dense. But for all situations involving microelectrode structures the effects of natural convection are negligible compared with those of the subsequent explained electric forces, because buoyancy only dominates at typical system sizes of the order of or greater than 1 mm. The second effect is termed “electrothermal” and therein the electric field interacts with the gradients in conductivity and permittivity induced by the temperature variations to effect electric forces [67]. The conductivity gradient produces free volume charge and the COULOMB force whilst a permittivity gradient produces the dielectric force.⁷ For planar electrodes with a finite gap these forces result in the formation of oppositely rotating eddies above the electrodes (qualitatively shown in Figure 1.14), whose directions depend on the frequency of the applied electric field [67].

In addition, non-uniform, oscillating electric fields produce forces on the charges in the electric double layer which forms in an electrolyte solution on the electrode surface. The normal component of the electric field thereby induces electrode polarization via COULOMB force, so that for low frequencies, the tangential component of the electric field forces the accumulated electric charge to move along the electrodes with the highest coulombic force predicted and observed at the electrode edges [74]. This steady motion of the charges acts through friction with the surrounding liquid to produce a flow referred to as ac electroosmosis because of its similarity to electroosmosis in a dc electric field. In combination, the result is the formation of eddies above the electrodes (Figure 1.14) similar to those expected from electric forces induced by JOULE heating and experimentally proved [75]. Additionally, it has been found, that the direction of fluid pumping is also frequency and amplitude dependent [76, 77], whereas this phenomenon has not been adequately explained yet. Moreover, besides a limited scope of ac electroosmosis relying on the capacitive charging mechanism, that is in the frequency range around 100 kHz

⁷For the theory of electrothermally induced fluid flow the reader is referred to [63, 67, 68].

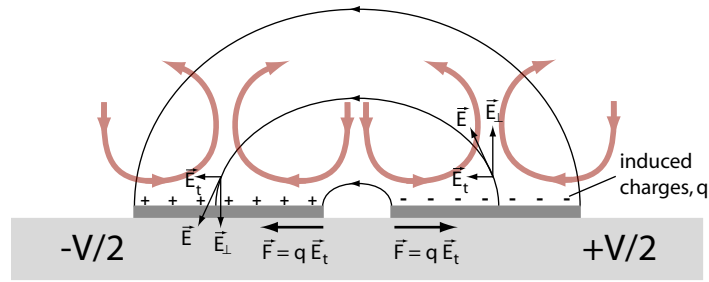


Figure 1.14: A cross-sectional diagram showing the electric field induced motion of fluid for two parallel electrode plates with a very small inter-electrode gap, across which a potential V is applied. The flow pattern shown, applies for electrothermally induced flow as well as ac electroosmosis. Fluid moves down into the inter-electrode gap and out across the electrode or vice versa, depending on the frequency of the electric field. Additionally, the principle of ac electroosmotic flow is explained.

[67], also ac electroosmosis based on the ac faradaic electrode polarization was reported for much higher frequency ranges up to 10 MHz [78]. Herein, if the amplitude of the ac electric field is higher than the electrochemical limit, the electric charge on electrodes is produced via electrochemical reactions instead of the capacitive charging.

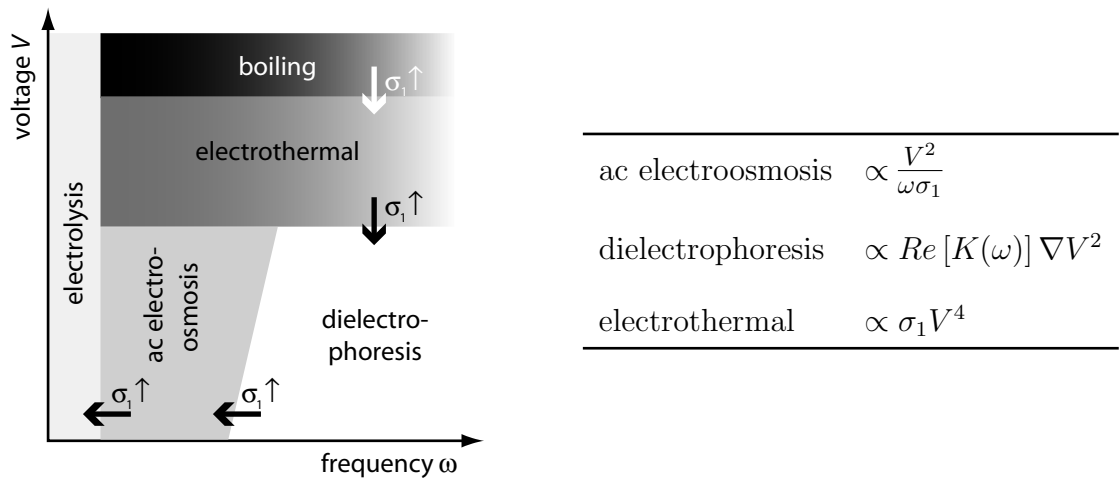


Figure 1.15: A qualitative illustration of fluid flow phenomena including indicators for changes upon increasing fluid conductivity and fluid conductivity dependencies of the displacement of a spherical object in an interdigital electrode array.

However, for the present thesis, mainly the following dependencies are of importance: For ac electroosmosis, the velocity of the flow pattern rises with increasing applied voltage, approximately proportional to V^2 (Figure 1.15). But as the electrolyte conductivity [75, 79] and/or the frequency of the electric field [67] is increased, it disappears and the effect of electrothermal flow becomes more important. The electrothermal fluid velocity increases directly with the medium conductivity, which is a clear indication of JOULE heating, and more important scales with the applied voltage as V^4 . Also, the

1.5 Relevant Tasks for DNA Integration

electrothermal effect is rather independent of the frequency of the electric field, except around a critical frequency, where the inversion of direction occurs, and gets progressively bigger for increasing system size, thought of as the distance to the electrode edge. In contrast, DEP scales with the gradient of the electric field and hence, dominates close to the electrode edges, i.e. for small characteristic lengths. This means objects can be trapped at electrode edges by DEP while they are moved by fluid motion in the bulk.

In a concentrated and simplified form—as illustrated in Figure 1.15—it can be stated that ac electroosmosis dominates fluid motion at low frequencies and small system sizes, electrothermal flow dominates at high voltages and DEP governs the motion of micrometer size objects for small systems and at high frequencies. Additionally, it should be noted that certain regions are inaccessible: electrolysis at the electrode surface occurs at very low frequencies and high voltages, and boiling due to JOULE heating occurs at high voltages and medium conductivities.

1.5 Deriving Relevant Tasks for the Integration of DNA into Microelectrode Structures

Within the scope of this thesis, as a model system DNA molecules shall be stretched between electric contact pads in an addressable manner so that they can not only serve as electric interconnection between the contacts, but also as a guide for the further arrangement of functional objects along them. Besides the transformation of single DNA molecules from a coiled into a wire-like conformation, this task requires specific

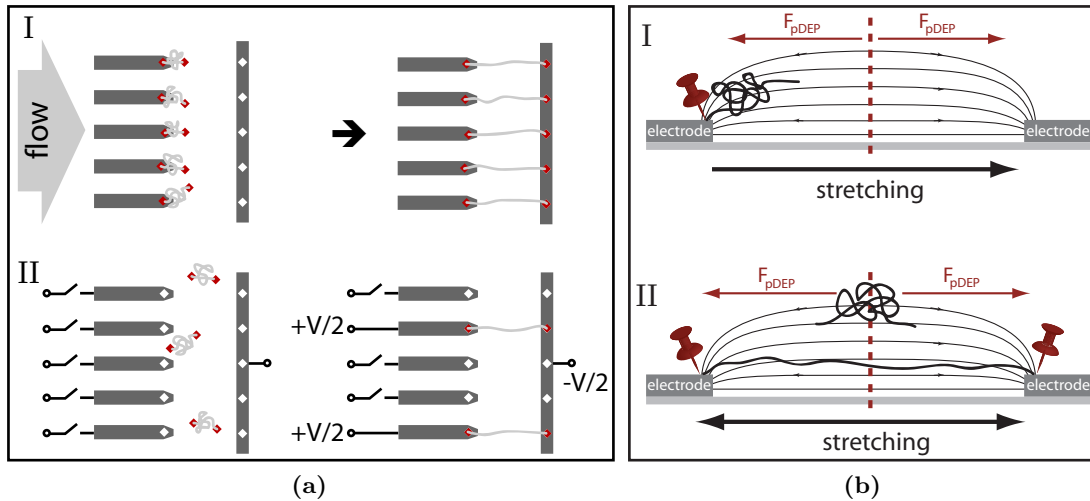


Figure 1.16: Schemes representing tasks to solve. (a) (I) Parallel-fashioned flow induced stretching versus (II) selective switchable electric field induced stretching. (b) (I) How to stretch a single-end tethered DNA molecule over the first half of the electrode gap against the counteracting pDEP? versus (II) Can a DNA molecule situated centric in the electrode gap be stretched simultaneously with either end towards one electrode?

recognition between the DNA and the interface where it is to be positioned to allow for the attachment of both DNA ends to defined contact pads.

In a first approach, hydrodynamic shear flow shall be used to provide the stretching force. Together with an anti-sense functionalization of both ends of the DNA duplexes and of the appropriate metal contacts, this method is preferentially seen as a possibility for the controlled batch-wise assembly of interconnections. Thereby the idea is, that the equality of the type of linkage at all integration sites allows for the “saturation” of all attachment sites with a single-end tethered DNA molecule in a first step, which can then in *one* more step all be stretched and fixed with their second end (Figure 1.16a,I).

In contrast, for the targeted assembly of DNA bridges at certain specific pairs of contact pads one either has to come up with a unique combination of linkers for each integration site to be able to recognize only those positions of purpose with DNA in the first step. Or, there must be a possibility to constrict the application of shear flow to a certain integration site, which is a top-down problem probably limited by the availability and positioning accuracy of such a miniaturized tool. However, for such an application, where single connections need to be assembled according to a “wiring diagram”, a switchable electric field induced stretching is considered favorable, making use of the electric access to the integration site through the prefabricated electrode arrays (Figure 1.16a,II). Thus, the question is: How can a single-end tethered DNA molecule—assumed to experience positive DEP—be stretched across an electrode gap, where in half the interelectrode area the DEP force counteracts stretching (Figure 1.16b,I)? Or is it possible to pull each end of a DNA molecule, which is situated in the center of the electrodes, towards one contact by means of positive DEP (Figure 1.16b,II)? More general, does DEP at all have the ability to stretch DNA or is an electric field induced flow the underlying mechanism? How does then an electrode design have to look like to be suitable for a directed stretching and furthermore, for the construction of networks in terms of a “wiring diagram”?

This goal of (i) batch-wise establishment of interconnects is pursued in Section 2.2 and (ii) the open questions concerning an electric field induced stretching are addressed in Section 2.3.

1.6 Bottom-up Nanofabrication with DNA

The specific base-pairing of nucleic acids cannot only be used to localize DNA molecules to predetermined surface sites but also to direct the assembly of material on the subnanometer to micrometer scale. The highly specific interaction between pre-designed building blocks and biomolecules in general and DNA in particular leads thereto that the components find—“recognize”—each other and spontaneously form the desired, more complex hierarchical structure, without the addition of an external force. Thus, recognition on the molecular level, so called *molecular recognition* and the resulting *self-assembly* drive the bottom-up construction of ensembles with all the information encoded in the components and, choosing the right building blocks, with almost no limitations in geometry and complexity.

1.6 Bottom-up Nanofabrication with DNA

The specific bonding between DNA base pairs has been used in this way to create complex synthetic DNA structures which have experienced substantial success during the past decades benefiting from SEEMAN and his coworkers' pioneering work. They developed the "tile model" which uses multi-arm junction motifs as basic building block (tile). These tiles are designed to include crossover points between DNA strands, so imparting stiffness to the structure, and contain free single-stranded regions extruding

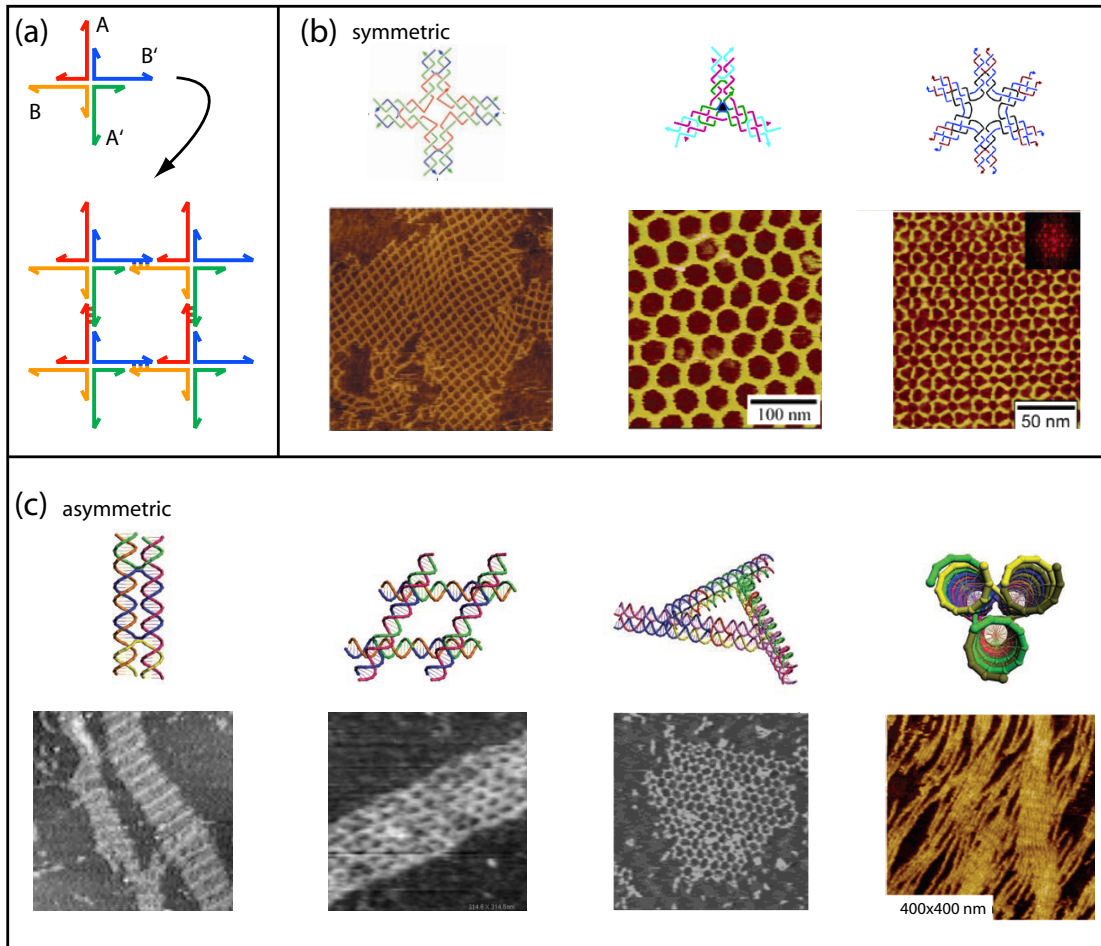


Figure 1.17: 2D DNA structures. Schematic diagrams (top) and atomic force microscopy images (bottom) of commonly used building blocks. (a) Key concept of DNA tile-based self-assembly: combining branched DNA junctions via sticky-end association (A-A',B-B') to self-assemble into 2D periodic lattices. Whereas a general rule of sequence design demands a minimum of sequence symmetry in the branched structure to avoid undesired pairing, the concept of sequence symmetry makes use of it, thus simplifying the design and more importantly allowing arrays to grow to larger size. (b) Apart from the cross-shaped tile [80], symmetric tiles are the three-point- [81] and six-point star [82] tiles, that self-assemble into lattices with square and hexagonal cavities, respectively (from left to right). (c) Examples for asymmetric tiles, given from left to right, are the double-crossover (DX) tile [83], the parallelogram tile composed of 4 four-arm junctions [84], the triangle tile formed from DX DNA molecules [85] and the three-helix bundle tile [86].

1 DNA-Based Nanowire and Network Fabrication

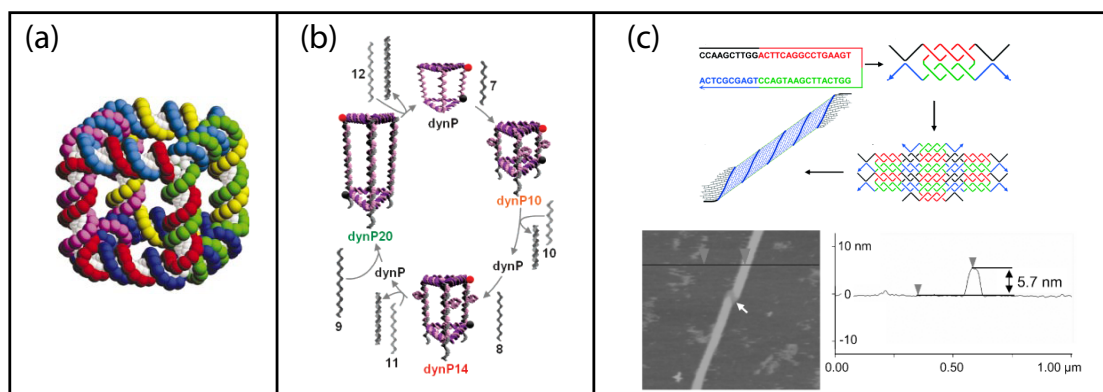


Figure 1.18: 3D DNA structures. Starting from (a) the SEEMAN cube [97] different approaches were used to assemble 3D DNA structures. For instance, (b) a triangular prism was built from a triangular rigid organic molecule and single-stranded DNA and the addressability of this assembly was demonstrated by constructing a dynamic triangular prism capable of structural oscillation between three predefined lengths [96]. (c) In a minimum approach only one DNA single strand is used, whereof two associate to form a DX-like structure, which can further assemble into 2D lattices and fold into tubes (top). In AFM long tubes can be visualized with about 6 nm height and defects here and there where the tubes are not completely closed [90].

from each corner thus, permitting self-assembly into a wide variety of structures by sticky-end cohesion. Depending on the number, orientation, and layout of the crossover pairs structures such as 2D lattices [87], nanoribbons [88] and nanotubes [89, 90] were built (Figure 1.17) and logical computation could be established [91, 92]. The fabrication of 3D objects via this scheme was also investigated (Figure 1.18) and examples include polyhedrons like a cube [93], octahedra [94], buckyballs [95] and dynamic capsules that switch between three different states [96].

A second design theme was introduced by the group of JOYCE [98] and ingeniously generalized by ROTHEMUND [99]. In this “DNA origami” (Figure 1.19) a long continuous single strand of DNA is systematically folded into the desired shape by the addition of a number of short single strands (staples) which are computationally designed to be complementary to selected regions of the initial long strand. The power of this approach lies in its addressability. Because each staple strand has a unique sequence, appendices like e.g. loop structures can be incorporated spatially addressable to “write” a desired bit in the molecular fabric. Although the large number of unique staple strands required for this scaffolding approach increases the expense in experimental development, a huge variety of 2D as well as 3D shapes has been validated experimentally, e.g. ROTHEMUND’s famous smiley face, the world map [99] and a 12-tooth gear [100], to mention some figurative shapes. Recently, also a hollow box was assembled, whose lid can be opened in the presence of externally supplied DNA “keys” [101].

Among a multitude of directions the field of DNA nanotechnology is growing in (see for example [102]) few examples will be mentioned in the following which are thought to be attractive approaches for bottom-up nanofabrication of electronic circuits with DNA.

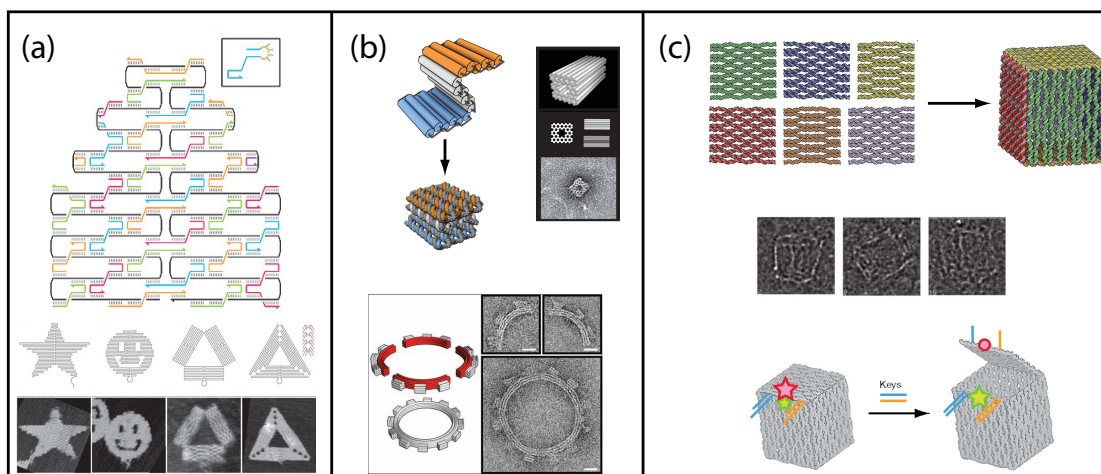


Figure 1.19: 2D and 3D DNA origami. (a) Concept of DNA origami: A single-stranded scaffold strand is folded into the designated shape and joined by a multitude of short staple strands which can also be modified as the 4-T loop shows for instance. In this way different 2D shapes like a star, smiley face and triangles were formed (top row: folding paths; bottom row: AFM images) [99]. (b) Extension of this method to building custom three-dimensional shapes formed as pleated layers of helices constrained to a honeycomb lattice (top left). Assembly was for example demonstrated for a square nut (top right) [104] and a 12-tooth gear (bottom) [100]. (c) DNA origami box [101]. Model of the six DNA sheets in a flat and cubic structure, respectively (top), cryo-electron microscopy images of the assembly (middle) and illustration of the opening of the box lid by the addition of “key” strands and its visualization by fluorophores (bottom).

First, two-dimensional DNA arrays provide the opportunity to template the positioning of materials like nanoparticles and proteins with nanoscale precision. As their collective properties, such as electron transport, optical coupling, and magnetic interactions, depend on their relative arrangement, DNA-mediated control of material organization promises to affect the fields of nanoelectronics (see Section 1.7), nanooptics and sensors, among others. Also, MAO *et al.* [103] employed a 2D DNA array as a reusable “mask” to create gold patterns via vapor deposition into the array’s cavities. By the use of thicker DNA templates high aspect features are conceivable as well as multilayer deposition, all at higher resolution than conventional photolithography.

In a different approach called “supramolecular DNA assembly” intrinsically functional synthetic molecules can bring a number of additional interactions into DNA nanotechnology. For example, SLEIMAN *et al.* reported the synthesis of single-stranded and cyclic DNA structures with rigid organic corners and used them as dynamic scaffolds to organize gold nanoparticles with the ability to write/erase and structurally switch these assemblies upon addition of specific DNA strands [105]. The group further constructed 3D DNA cages capable of switching and changing their size between three predefined states [96]. Besides, there have been many elegant designs for DNA nanomachines that respond to specifically added DNA strands or other molecules [106]. All these examples have led to the development of molecule-responsive DNA materials, i.e. devices that change state in

1 DNA-Based Nanowire and Network Fabrication

response to an external trigger and which might be used for molecular sensing, intelligent drug delivery or programmable chemical synthesis.

Recently, SHARMA *et al.* [107] demonstrated an interesting type of 3D nanoparticle assembly. Starting with DNA nanotubes formed through either self-association of multi-helix DNA bundle structures or closing up of 2D DNA tile lattices, they produced nanoparticle architectures ranging from stacked rings to spirals. Multi-stranded DNA structures like DNA nanotubes or bundles in general provide some advantageous properties for their application in nanoelectronic devices: in comparison to double-stranded DNA their higher stiffness facilitates an oriented integration into electrode arrays. Additionally, the increased number of interwoven strands results in a larger density of metal nucleation sites in a DNA templated metallization process (compare Section 1.7) and thus a more continuous nanowire [108].

The most prominent pioneer of DNA nanotechnology, NADRIAN C. SEEMAN, will have the final say in this little overview: “As with any craft material, the structural applications of DNA are limited only by the imagination” [109].

1.7 DNA Metallization

In the previous sections it was shown, how DNA is currently explored as a new material for functional, molecular nano-architectures. In this context it was illustrated how the polymer DNA can be handled, i.e. integrated and manipulated on surfaces, and how it can self-assemble into complex networks and arbitrary structures. This represents first steps in the bottom-up construction of functional devices. Further beyond that might be electronic circuits in the sense of employing DNA with a diameter of only 2 nm and the large aspect ratio as a ready-to-use wire which connects functional elements in future electronics by self-assembly into electronically active networks. However, it seems unlikely that the intrinsic conductance properties of DNA can be used for nanodevices: taking only in consideration those experiments that have been confirmed using the same experimental conditions and the same type of DNA leads to a rather clear picture: random sequence λ -DNA is insulating on a length scale larger than 100 nm. But as this statement constitutes the justification for half the effort of this thesis, it shall be discussed a bit more in detail before going on.

A Comment on DNA Conductivity

Already soon after WATSON and CRICK discovered the double-helical structure of DNA, this structure was thought to be ideal for electron transfer because some of the electron orbitals (the so-called π -orbitals) belonging to the bases overlap quite well with each other along the axis of the DNA [110]. Extensive experimental and theoretical work over the past 20 years has led to substantial clarification of the relevant charge-transfer mechanisms in DNA. Assuming a donor group at one end of the molecule and an acceptor group at the other, the dominant mechanisms appear to be the following two: the first consists of a coherent electron-tunneling process from donor to acceptor, whose rate decreases exponentially with the distance traveled. The second mechanism—for

long-distance electron transfer—is referred to as thermal hopping. Both charge-tunneling and thermal-hopping mechanisms have been verified in DNA charge-transfer studies [111] and describe the basics, that is, electrons and holes are indeed able to shuttle along a single DNA molecule over a distance of a few nanometers.

However, direct electrical measurements on long DNA molecules by a number of physics groups have yielded conflicting results. With the advent of single molecule measurements and scanning probe techniques, a direct measurement of the resistance of single DNA molecules can be made by hooking the molecule up between two metal electrodes and measuring the electric current running through it. The first direct electrical measurements on small bundles of DNA were made in 1999 by FINK *et al.* [112] leading to the surprising result that DNA bundles almost 1 μm in length appear to behave like an ohmic conductor and not like a semiconductor with a large band gap, as expected in the simplest picture. Resulting from a subsequent series of different experiments, everything from well-insulating behavior to the support of superconducting currents through DNA has been reported. Possible differences could be due to the base sequence or the length of the used DNA, or the properties of the buffer solution in which the DNA is kept. Other factors include the ambient surroundings (whether the experiments are conducted in liquid, air or vacuum), the structural form of the DNA and its organization (whether the bulk material is studied versus bundles or single DNA molecules), and the electrode-molecule interface. However, as stated above, taking only in consideration those experiments that have been confirmed using the same experimental conditions and the same type of DNA leads to the conclusion, that long ($>100\text{ nm}$) DNA molecules are true insulators, as shown most convincingly by STORM *et al.* [113].

In this respect, one major question is how the DNA molecule has to be chemically modified in order to increase the electron transfer efficiency. Fortunately, the multiple functional groups presented by DNA make this molecule reactive toward a variety of other organic and inorganic compounds. Thus, DNA is an ideally suited metallization material because it can either serve as a template or as an assembling agent and both approaches are equally interesting for the build up of metallic nanowires. To do so, three concepts were proven successful (Figure 1.20) which in the following will be explained in more detail.

Concepts for DNA Metallization

In a very interesting first approach, the groups of SHIONOYA [114, 115] and SCHULTZ [116] synthesized novel nucleobases which provide a new double helix containing metal ions stacked on top of each other in its middle (Figure 1.20a). Therein the natural hydrogen bonds are replaced by metal coordination forces. Whereas these complete artificial base pairs might be limited to a very small number in a DNA molecule, AICH *et al.* [117] accomplished the complexation of positively charged metal ions to every base pair. This so called M-DNA is formed in solution upon addition of bivalent metal like Zn^{2+} , Co^{2+} , Ni^{2+} or Hg^{2+} . For Zn^{2+} it was shown that the ion replaces the imino proton of each base, also resulting in a chain of one metal every 3.4 \AA regardless of the DNA sequence and length.

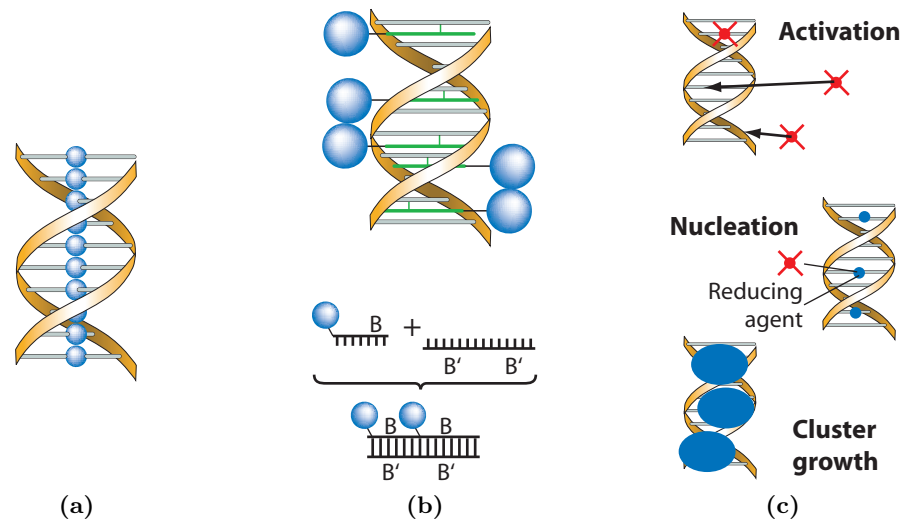


Figure 1.20: Concepts for the creation of metallic nanowires: (a) Metal incorporation in the DNA structure on an atomic level. (b) DNA-directed assembly of prefabricated and labeled metal clusters using intercalation (top) and hybridization of complementary sequences (bottom). (c) DNA-templated growth of metal clusters.

A different approach is the DNA-directed assembly of already prefabricated nanoparticles. To securely attach nanoparticles to DNA, preparations of various surface-functionalized nanoparticles have been reported: PATOLSKY *et al.* [118] have developed a method in which 1.4 nm gold clusters labeled with a small molecule are intercalated into a poly-A and poly-T DNA duplex and the intercalator is bound covalently to the bases of the DNA by a photochemical reaction (Figure 1.20b). Moreover and maybe even more easily, positively charged metal clusters are attracted by the negatively charged DNA backbone, using electrostatic interaction as the driving force. By this technique SASTRY *et al.* [119, 120] added small gold clusters to DNA and thus formed linear superstructures, TORIMOTO *et al.* [121] attached CdS semiconducting clusters and HARNACK *et al.* [122] showed that even negatively charged trisphosphine-capped gold clusters bind densely to DNA. In addition to decorating a DNA double strand with metal particles by specific particle-DNA interactions⁸ interestingly, the principle also works the other way around: single-stranded DNA can be used to modify the surface of metal clusters and thus, endow them with selective recognition and self-assembly capabilities. This allows sequence-specific binding of clusters to other DNA strands and thus, the formation of cluster chains [123] (Figure 1.20b) or networks of clusters with DNA linkers as shown in two landmark papers by MIRKIN *et al.* [3] and ALIVISATOS *et al.* [124] and “perfected” by WINFREE *et al.* [83] who created specific periodic patterns with the size of several μm .

Besides the possibility of DNA-assisted assembly of *ex-situ* prepared metal particles, there is also the way to grow clusters directly—*in-situ*—onto DNA. Thereby, the challenge is to control the nucleation kinetics, because metal clusters naturally nucleate

⁸Basically, all the methods for a surface tethering from Section 1.4 are conceivable.

1.7 DNA Metallization

Table 1.1: Characteristics of DNA-templated nanowires

Material	Thickness [nm]	Length [μm]	Electric behavior	Reference
<i>Semiconducting</i>				
CdS	5	-	-	[125]
CuS	1-10	-	-	[108]
<i>Magnetic</i>				
Co	25	-	-	[127]
Ni	50-70	few	-	[128]
Ni	12-17	-	-	[129]
<i>Metallic</i>				
Ag	100	16	R=7 M Ω	[126]
Ag-Au	-	-	$\rho=1.5 \cdot 10^{-7} \Omega\text{m}$	[130]
Ag	15	7	$\rho \approx 20 \cdot 10^{-6} \Omega\text{m}$	[131]
Ag ⁹	35-40	5	$\rho=[1.4 \dots 3.2] \cdot 10^{-5} \Omega\text{m}$	[89]
Ag ¹⁰	20-50	2	$\rho=[2.25 \dots 2.57] \cdot 10^{-6} \Omega\text{m}$	[86]
Ag ¹¹	43 \pm 2	5	$\rho=2.4 \cdot 10^{-6} \Omega\text{m}$	[80]
Cu	3.1	-	-	[132]
Cu	1.8-3.3	-	-	[133]
Pt	3-5	0.1	-	[134–136]
Pt	1-7	-	-	[52]
Pd	50-100	6	R=[1...3] k Ω	[137]
Pd	50	6.5	$\rho=5 \cdot 10^{-7} \Omega\text{m}$	[138]

homogeneously in the solution as well as heterogeneously at the template. Nonetheless, this template directed growth of a variety of metals on DNA (Table 1.1) has been used successfully for a decade now since the pioneering work of COFFER *et al.* [125] and the well known milestone of BRAUN *et al.* [126] in 1998. COFFER and his coworkers bound Cd²⁺ ions to plasmid DNA and reduced them with H₂S, leading to 5 nm CdS clusters at the circular DNA. BRAUN then adapted this scheme and treated a λ -DNA molecule stretched between electrodes with a silver salt solution to selectively localize silver ions along the DNA through Ag⁺/Na⁺ ion-exchange and to form complexes between the silver and the DNA bases. The silver-laden DNA was reduced by the reducing agent hydroquinone to form small silver aggregates that serve as seeds for further cluster growth in a final “development” step. The resulting granular wire had a width of 100 nm and provided electrical contact between the electrodes.

⁹on DNA tubes

¹⁰on 3-helix DNA bundles

¹¹on 4 \times 4 DNA ribbons

1 DNA-Based Nanowire and Network Fabrication

The basic scheme of electroless DNA metallization already shown in these works as well as in many following ones consists of three steps: (i) First, in the so-called activation step metal ions or complexes from solution bind to DNA. For silver ions [139, 140], platinum and palladium complexes the bases are the preferred binding sites whereas other metal ions like cadmium and copper bind to the backbone (Figure 1.4, page 9). (ii) In the second step, the bound metals are treated with a reducing agent like dimethylamineborane, hydroquinone or sodium borohydride to form initial seeds on the template by heterogeneous nucleation which (iii) in the third step control the growth of clusters selectively on the biomolecule. In the style of the technology widely used in industry to make metallic films, this step is also termed “electroless plating”. By the addition of new metal solution, which might differ from the seeding solution and thus allow for the combination of metals [52, 130], and reducing agent in the third step an autocatalytic process starts wherein metal ions or complexes from solution are preferentially reduced on already reduced metal. Therefore, the initial activation step is crucial in establishing as many seeds as possible onto the DNA molecules to control their growth in the last step and to thus suppress the homogeneous metal cluster growth in solution as much as possible, since it forms metal structures that are not built onto the template. In this context, SEIDEL *et al.* [135, 136] showed experimentally how by variation of the activation time¹² the metallization process can be tuned from non-activated, seedless DNA leading to homogeneous and heterogeneous nucleation to activated DNA with many platinum seeds where clusters are selectively bound to the DNA template and background metallization is completely hindered. Thereby, the key feature of their technique is the long incubation of DNA with the metal salt solution K_2PtCl_4 . As the presence of the thus formed nucleotide ligands both enhances the electronic affinity of the complexes and stabilizes the formation of Pt-Pt bonds during the first reduction stage, upon the addition of the reducing agent the first formed nuclei immediately quickly develop into larger clusters and consume the dissolved platinum complexes. In this way, the above explained steps two and three of the template-controlled growth of metal clusters are merged. Furthermore, first-principle simulations by COLOMBI CIACCHI [134, 141] underline the importance of the activation step, revealing the favored heterogeneous formation of platinum dimers at the DNA bases as a consequence of the strong electron donor character of the nucleotides.

All these methods have their advantages and disadvantages. To evaluate their suitability for the formation of less than 10 nm thin electric conducting nanowires integrated into microelectrode structures—as it is the intention of this work—the selectivity of the metal deposition, the homogeneity of the coverage and the thickness of the wire needed for a reasonable electric conductivity can be appraised.

Whereas the formation of metal containing DNA-inspired double helices up to now is limited to a small number of base pairs that can hold steady in a stack, for M-DNA with zinc a metallic-like behavior with a resistance of about 300 M Ω was measured over a length of 10 μ m [142]. Even though up to now this is the only experimental evidence for an improved electron transfer, M-DNA holds great promise as a new material for the

¹²combined with a careful choice of metal and reducing agent

preparation of self-assembling electronic circuits, because in contrast to growing materials on the exterior of a DNA strand, incorporating metal complexes into DNA can create metallic structures with preserved self-assembly capabilities.

The second method has to deal with the problem of packing defects and nanoparticle size distribution, thus, inhomogeneities in the metal layer. All approaches failed up to now to fabricate almost defect-free 1D arrays large enough for electric measurements due to inherent defects as a result of the coverage with single metal particles, maybe even separated by non-metallized DNA spacers. If one tries to close the gaps in the colloid chains by an additional metal deposition the wire indeed becomes conducting [128], but the wire diameters get quite large in comparison to the size of the particles used for assembly [122].

Hence, nucleation and growth of metal clusters on DNA is the main approach to DNA nanowire fabrication. Therein, the homogeneity of the metal coverage can be controlled to a significant degree by densely packing the DNA molecules with efficient nucleation centers in the activation step. However, the actual metallization and film growth from solution remain stochastic processes and inevitably, metallic ions are reduced in solution and become randomly deposited on the substrate—this is the so-called background metallization or homogeneous nucleation path. Typically, this leads to dendritic-like, irregular branching and necklace structures in the nanowires, despite the favorable growth on the templates by the “DNA-controlled” mechanism. To help overcome this difficulties, further strategies were developed to increase the selectivity of the reduction step. By the addition of aldehyde groups to DNA KEREN *et al.* [143] were able to localize the reducing agent on the DNA template. Gold nanowires with low background were grown by catalysis during a subsequent electroless plating step. In another approach called “ionic-surface masking” BECERILL *et al.* [133] used alkali metal cations to passivate the surface, creating a physical and an electrostatic barrier against nonspecific silver or copper cation adsorption and subsequent metal deposition. A more than 50% decrease in non-specifically deposited nanoparticles was found by this approach. Recently, a completely different approach was followed by BERTI *et al.* [144]. Instead of using a chemical as reducing agent, they reasoned to grow chains of silver nanoparticles through photoreduction of silver-laden DNA. The speculation that DNA itself would act as light harvester and sensitizer, thus triggering the photoreduction of the complexed silver ions, was verified by selective growth of silver particles on DNA upon 254 nm-wavelength UV irradiation.

In order to extend the utility of DNA as a metallization template beyond the formation of plain wires, the idea to use the spatial resolution, i.e. the base sequence, of the DNA for a sequence-dependent metallization, is most challenging. KEREN and coworkers [130] indeed accomplished such a sequence-specific metallization, which can be viewed as lithography on a molecular level. They used a second biomolecule, the *RecA* protein, to cover the backbone of a DNA at a specific sequence. The resist function provided by the *RecA* protein, blocks the access of small molecules and thus, inhibits the formation of silver seeds at the binding region and a gold coating was established on the unprotected regions of the DNA only. Since the position of the different components can be addressed

sequence-specific this allows for a precise manipulation with an accuracy of 3.4 Å, the distance between two base pairs.

The molecular lithography process demonstrated above constitutes an important step toward integrated DNA-templated electronics, broadening the spectrum of constructs which can be designed with the help of the carrier of the genetic code.

1.8 Deriving Relevant Tasks for the Metallization of Integrated DNA

Aiming at the formation of electric conducting nanowires as thin as possible, based on the preceding explanations, it was considered most promising to adopt the fine three-step metallization of DNA in solution from SEIDEL *et al.* [136] to DNA, which was integrated into microelectrode structures before. This aim itself is not new, however, as the work for this thesis started, three problems prevented its realization: (i) The reduction of platinum activated DNA *in solution* by addition of a reducing agent relies on the well-regulated dosage of the reaction components. That is, they have to exist in a certain ratio to assure the full control over the nucleation and growth process and to achieve such a complete dominance of the heterogeneous cluster formation at the DNA template at suppressed homogeneous nucleation in solution. However, it is questionable, if such a well-balanced ratio of reactants can be achieved for a few DNA molecules attached to a surface. (ii) Moreover and more important, first experiments in the group had shown, that the addition of the reducing agent dimethylamineborane to activated DNA, that was fixed in a linear form on a gold surface by thiol-linkers at each of its ends, resulted in the dissolution of the DNA from the surface probably due to a reduction of the gold-sulfur bond going along with the reduction of the metal complexes. Thus, at the end of a metallization step no metalized DNA was present at the surface, where it was positioned before, making a metallization of pre-integrated thiol-functionalized DNA molecules impossible. (iii) Inspired by the work of BERTI *et al.* [144], in a different project in the group, fine platinum clusters were formed on bacterial surface layers by the photoinduced reduction of the salt $\text{Pt}(\text{NO}_3)_2$ [145], resulting in cluster sizes compatible to the ones achieved on DNA templates by the reduction of K_2PtCl_4 with dimethylamineborane.

Given this framework, the questions to be answered in the course of this work are: (i) Is the photoinduced reduction of $\text{Pt}(\text{NO}_3)_2$ applicable to DNA templates and does it result in the controlled formation of fine platinum clusters along the molecules and what are the necessary parameters? (ii) Can the photoinduced reduction of $\text{Pt}(\text{NO}_3)_2$ be adopted to DNA molecules that were integrated into microelectrode structures prior to the metallization to lead to a transformation of the insulating biomolecular connection into a miniaturized electric conducting wire?

2 Integration of DNA into Microelectrode Structures

A decisive step in the construction of future nanoelectronic circuits is the site-specific positioning of devices into larger microelectronic structures which can basically be accomplished by using DNA duplexes to interconnect the functional elements with desired microfabricated contact pads. As a kind of basic model system, in the following the controlled interconnection of metallic contact pads by DNA molecules is demonstrated. On the one hand, first this involves the specific binding of both ends of DNA molecules to different, addressable contacts. For this, a functionalization of the DNA ends and/or the substrate is required, which is specific to the contact structure and excludes unspecific binding of DNA to the surface areas in-between the contacts. On the other hand, since long DNA molecules in solution have the conformation of a random coil, they have to be stretched against the acting entropic forces to pose the shape of a linear wire.

To realize the first point, in the following section it is described how the end-specific binding can be accomplished by a functionalization of the sticky ends of DNA with thiol groups each. The second point will be achieved by stretching of single-end surface-tethered DNA molecules in hydrodynamic flow, demonstrating the suitability for parallel processing within this approach. On the contrary, the addressability of single connections will be investigated by an electric field-based approach.

2.1 Tethering DNA Ends to Electrodes

If one wants to bridge a gap between two electrodes by a DNA molecule, one has to deal with two DNA ends—one end has to bind to the first contact and the other to the second contact. A first approach to this scenario would be to address the single DNA ends differently, i.e. to modify the DNA and the substrate in such a way that one particular end can exclusively bind to one certain electrode. However, this technique requires large effort in the site-specific functionalization of individual electrodes of only micrometer size and distance and this poses an even larger challenge if one wants to bind many molecules in parallel. Nonetheless, as long as the (parallel or antiparallel) orientation of the DNA molecule in the gap is not of importance (as it would be e.g. in the case of sequence-specific subsequent steps), an electrode-specific functionalization is not essential. Instead, it is also possible to use identical binding modes for both surface/DNA-end interfaces and address the two DNA ends successively. That is, a single-end surface-tethered DNA molecule is not only stretched by a force, but at the same time the force also guides the second end away from the first attachment point

2 Integration of DNA into Microelectrode Structures

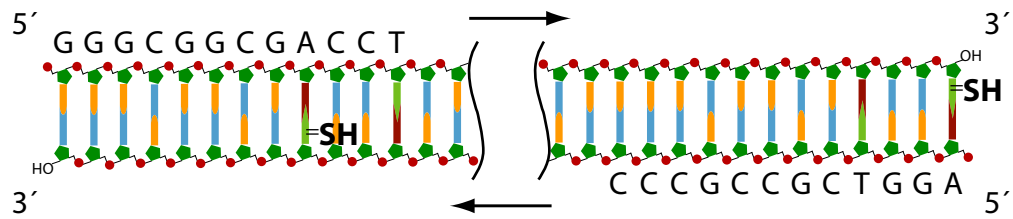


Figure 2.1: Thiol-functionalized ends of the T-DNA-T used in stretching experiments. The sequence of the single-stranded overhangs before filling is given.

toward the second electrode to bind there. As this method is suitable for the stretching mechanisms applied in this work, it is chosen for all the following stretching experiments.

To achieve specific tethering of the two ends of a λ -DNA-molecule to gold electrodes the strong and selective bond of thiol—incorporated at the DNA ends—to gold was selected from the methods introduced in Section 1.4. This approach is also beneficial for the compatibility with microelectronics fabrication as well as for a subsequent metallization step because both binding partners are readily available—the gold contacts as interface to the next higher integration level have to be fabricated anyway and the DNA can be functionalized with a thiol group at each end in a preparative step—and no other components (that might interfere with the metallization step) for an additional functionalization or blocking of selected surface areas are necessary.

To this end, the functionalization was carried out as described in Section 1.3 by filling the 12-bases long sticky ends on *both* sides of the λ -DNA with complementary nucleotides in a Klenow polymerization reaction using dATP, dCTP, dGTP, the altered S⁴TTP, modified to include the desired thiol group, and the Klenow fragment of DNA polymerase. Then, the DNA thiolated at both ends (T-DNA-T, Figure 2.1) was purified (compare Appendix A.1.1).

The efficiency of functionalization of the DNA ends was evaluated by using a simple surface assay allowing direct observation of the number of binding events by fluorescence microscopy. To this aim, T-DNA-T was incubated for 30 min in a thin-slit perfusion chamber, where the upper sealing plate of the chamber consists of a glass cover slip with a patterned gold surface of quadratic pads of $50 \times 50 \mu\text{m}^2$. The glass cover slip was mounted with the gold pads upside down to allow the observation of molecules attached to the pads in the inverted optical microscope used. After the incubation, unbound DNA was removed by flashing the perfusion chamber several times with buffer. The remaining tethered molecules were stained with a 1.6 nM YOYO-1 solution.

Fluorescence imaging revealed that individual T-DNA-T molecules were specifically attached to the gold pads, where the number of molecules bound per $50 \times 50 \mu\text{m}^2$ area averages to 35. The molecules appear as “dotlike” structures undergoing spatial fluctuations due to Brownian motion of the single tethered duplexes in the form of random coils (Figure 2.2a). Nearly no molecules bound non-specifically to the glass surface in-between the gold pads which appears darker in Figure 2.2. To prove whether the T-DNA-T molecules are indeed tethered with one end to the gold film only, hydrodynamic

2.2 Stretching DNA by Hydrodynamic Flow

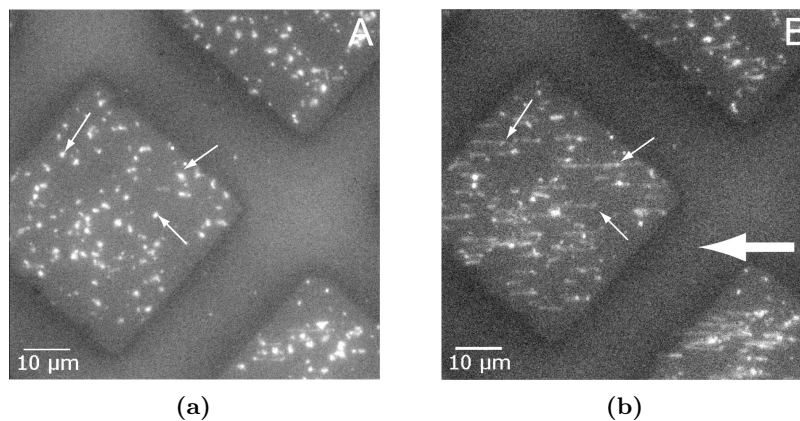


Figure 2.2: Fluorescence micrographs showing (a) specific binding of one end of YOYO-1-labeled T-DNA-T to a patterned gold surface. (b) Under the application of flow in the direction indicated by the thick arrow, single tethered molecules are stretched. For easier comparison same molecules are marked by thin arrows in (a) and (b).

flow was applied to the perfusion chamber for a short time by sucking buffer through the channel with filter paper (Figure 2.2b). As the result, for about 80% of the total number of molecules bound a transition of the molecule conformation from coiled to stretched was effected. Molecules tethered with both ends to the surface and thus stretching in a U-shape under the application of flow are hardly seen. This is supposed to result from the mean-squared distance of $1.3\ \mu\text{m}$ between two DNA ends under no external force, meaning that the probability for the free end to approach the surface is low, once one end is anchored at the surface.

2.2 Stretching DNA by Hydrodynamic Flow

2.2.1 Experimental Setup

The incorporation of T-DNA-T, i.e. the specific binding to and the stretching between photolithographically patterned interdigital electrodes was accomplished in an open flow cell, schematically shown in Figure 2.3. To this aim, the glass slide carrying the electrode structures was assembled into a homemade open flow cell and covered with $200\ \mu\text{l}$ of $100\ \text{mM}$ phosphate buffer, pH 7.5 (PB100). The flow cell is mounted into an inverted optical microscope allowing inspection of the sample from below. In addition, two microcapillaries with an inner diameter of $580\ \mu\text{m}$ are mounted from above to accomplish fluid flow over the sample surface by means of a peristaltic pump which is connected to the microcapillaries by polymer tubes. The main advantage of this experimental setup is the possibility of flexible and accurate positioning of the two microcapillaries inside the fluid cell at variable lateral position and height by means of a micromanipulation system enabling an easy control of the direction of flow relative to the mounted electrode structure. Additionally due to the inclined position of the microcapillaries the flow can be

2 Integration of DNA into Microelectrode Structures

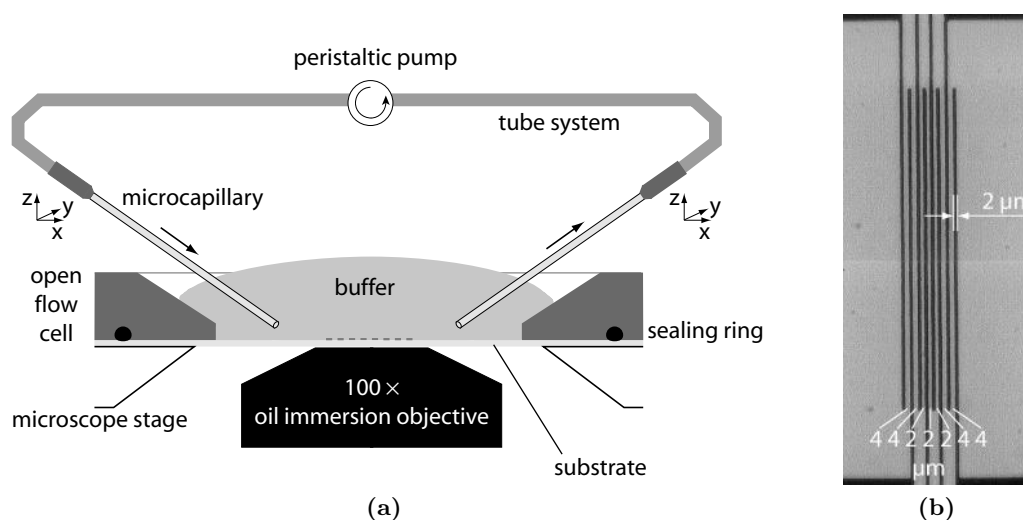


Figure 2.3: Schematic representation of the experimental setup. (a) An open flow cell is mounted on the inverted fluorescent microscope. Microcapillaries can be variably positioned above the substrate with the interdigital electrode array, shown in (b), by means of a micromanipulation system.

directed onto the surface, which assures higher flow velocities at the surface in comparison to a parabolic HAGEN-POISEUILLE velocity profile, with zero velocity at the surface.

As a result of a stretching experiment DNA molecules were observed by fluorescence microscopy. For this, images were acquired with 300 ms exposure time using a cooled, 16-bit frame-transfer CCD camera Cascade 512B and a Zeiss α -Planfluar 100 \times oil immersion objective with a numerical aperture of 1.45, which combines high resolution as well as high light yield. The DNA was fluorescence labeled with YOYO-1 dye, which is excited with blue light at 490 nm and has an emission maximum in the green at 509 nm. This dye is virtually nonfluorescent when free in solution but strongly fluorescent when bound to DNA [146]. Coupled with the very high binding constants, this results in a >1000-fold fluorescence quantum yield difference between the stained DNA molecules and the background, which provides high sensitivity when imaging DNA. Previous studies have shown that YOYO-1 binds to DNA in two modes [147]: (i) The preferred mode is bisintercalation, and the immobilization of the YOYO-1 dye between the base pairs results in strong fluorescence. (ii) A second mode that gives a weaker fluorescence is external binding which appears at mixing ratios where, if the dye is assumed to follow the nearest neighbor exclusion principle, all intercalation sites are filled up, i.e. at a base pair to dye ratio of 4:1.

From that, serious side effects can arise that need to be considered in a stretching experiment as well as for a subsequent metallization of the stretched molecules. (i) One drawback is that dimeric nucleic acid stains like YOYO-1 have been found to increase the contour length of a labeled DNA molecule [45] as a result of their intercalative binding. Thus, an initially 16.2 μm long λ -DNA molecule exhibits a contour length of 21.8 μm under a staining-ratio of 0.72 base pairs per dye [148]. (ii) Additionally, an intercalated

2.2 Stretching DNA by Hydrodynamic Flow

chromophore might interfere with a metal binding mechanism during the activation step of the metallization and thus, needs to be removed before it, e.g. by washing with a destain solution containing cations [149]. Besides the effort for this step, the mechanical stressing of the molecule has to be considered: in a molecule, which was (“over-”)stretched to a certain length in the presence of the intercalating dye and fixed in this conformation, the decrease in base pair-distance due to the removal of the chromophores leads to a tensile stressing of the molecule anchored at its end. If the worst comes to the worst the DNA bridge even breaks. (iii) Another disadvantage of YOYO-1 is its tendency to photocleave the probed DNA [150]¹, especially under the intense illumination that is used for imaging of individual molecules. Without any precautions, YOYO-1 stained DNA will fragment in 1–3 seconds exposure. In microscopy work, cleavage is typically suppressed by removal of oxygen through enzymes that scavenge the oxygen from solution and addition of β -mercaptoethanol, a reducing agent that directly attacks oxygen radicals. At the same time the fluorescence of the stained molecules is commonly observed to bleach less during prolonged illumination [151].

To minimize the problems arising from fluorescence staining, in the following experiments making use of hydrodynamic flow the DNA is only stained after the stretching was completed. In this way, the stretching procedure was performed “blindly”, so to speak, as it was not the intention of this work to study the behavior of DNA in a flow but to build up stable DNA bridges between metallic contacts. Only to keep record of the result (Section 2.2.2) or for analytical reasons as described in Section 2.2.3 a 15 μl droplet of 400 nM aqueous YOYO-1-solution with 20% (v/v) β -mercaptoethanol was added to the buffer volume covering the electrode structure in the open flow cell.

2.2.2 Stretching DNA Between Interdigital Electrodes

Site-specific incorporation of DNA duplexes into an interdigital electrode array was accomplished in the open flow cell by positioning the microcapillaries 100 μm above the structure surface using the motorized focus control of the microscope. First 2 μl of T-DNA-T (0.25 $\mu\text{g}/\mu\text{l}$) diluted in 50 μl PB 100 were flushed in with a flow rate of $\approx 2.5 \mu\text{l}/\text{s}$. The flow direction was chosen to be perpendicular to the long contact fingers of the interdigital electrodes. To enhance the amount of DNA coils binding with one of their thiol-functionalized ends to a gold contact, the DNA solution was pumped for 2 min back and forth over the contact array at minimum flow rate. After some of the T-DNA-T molecules were bound specifically to the gold contacts, PB 100 buffer solution was pumped over the surface with a 5-fold increased flow rate of 12.5 $\mu\text{l}/\text{s}$, resulting in an uncoiling, and thus, stretching of the molecules in the direction of flow. As soon as the free end of a stretched molecule reaches the adjacent gold contact, it can bind via the thiol group there. When the flow is released, the molecule tethered with both ends to contacts forms a permanent linear DNA interconnect.

¹Both YO and YOYO cause single-strand breaks and when two YO chromophores are forced into proximity in YOYO, there is an enhancement of double-strand break cleavage rate because of the nonrandom distribution of single-strand breaks from the dimer.

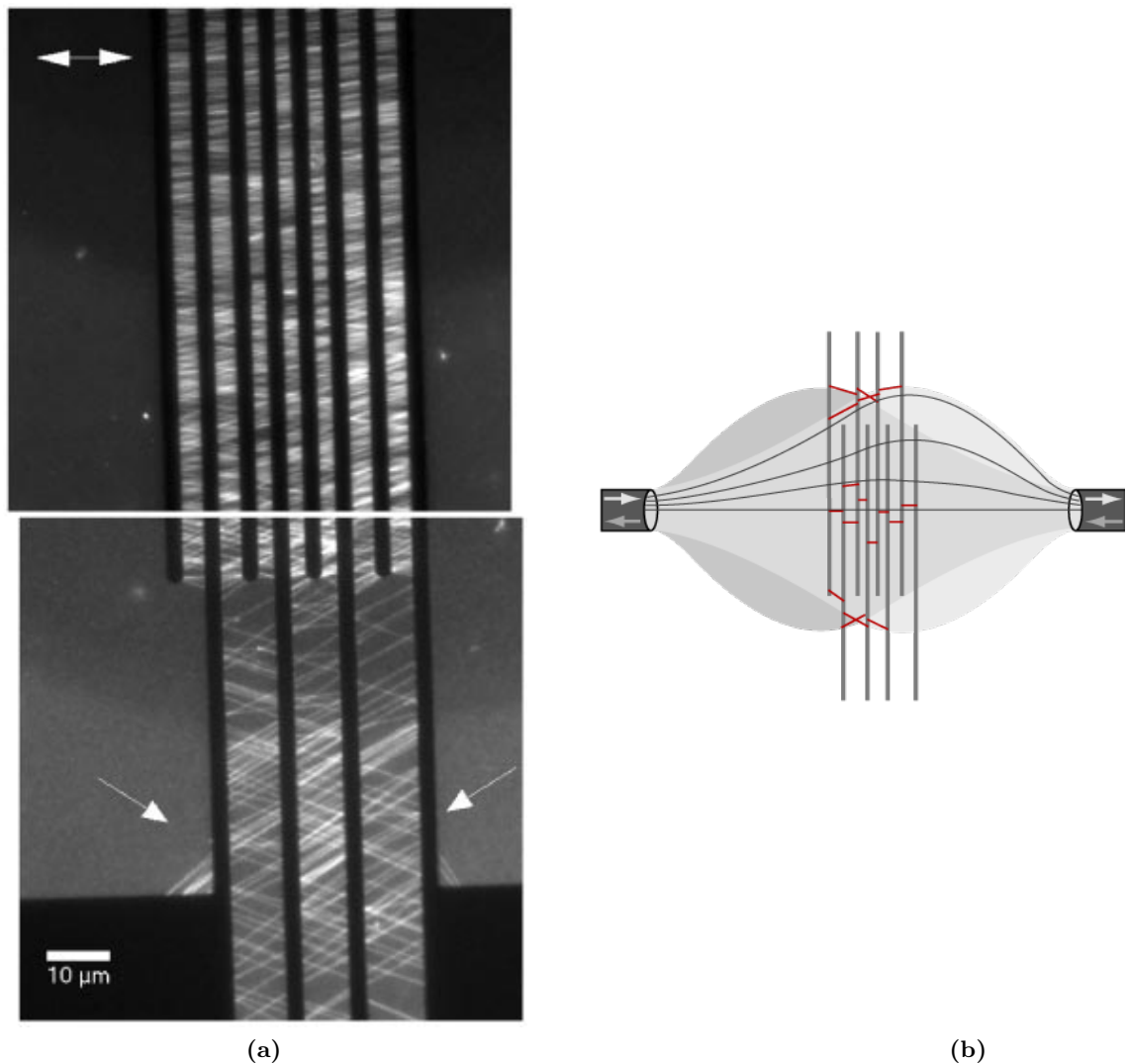


Figure 2.4: T-DNA-T molecules after stretching by alternating hydrodynamic flow. (a) After fluorescence staining, the formation of permanent, linear DNA interconnects in the direction of flow (white arrows) is shown. (b) Illustration of flow regime and alternation of flow direction between the microcapillaries in the open flow cell.

Figure 2.4a shows the result after staining the assembled DNA interconnects with YOYO-1. A massive incorporation of DNA molecules is observed [152]. They are mainly oriented perpendicular to the electrode fingers which is in general agreement with the applied flow direction. However, the orientation of the DNA molecules to each other is not perfectly parallel, which can be attributed to (i) the appearance of short-range thermal fluctuations of the molecules' free ends during the stretching procedure, which can cause that the position of the second attachment point statistically deviates from that attachment point which would be expected from a non-fluctuating molecule, i.e.

2.2 Stretching DNA by Hydrodynamic Flow

a simple linear extrapolation of the site where the molecule was first tethered in the direction of flow. (ii) The flow direction in the open flow cell is not parallel to the centerline of the two capillaries all over the structure and moreover, not symmetric upon inversion of the flow direction. As depicted in Figure 2.4b, the flow profile produced by the micro-capillaries inside the buffer volume of the open flow cell is “fanlike” shaped as it is not confined by channel walls. Only the streamlines close to the notional line connecting the centers of the capillary openings are parallel to that line. With increasing distance from the centerline the curvature of the streamlines increases corresponding to a position-dependent inclination of the flow direction, and thus, of the orientation of the doubly-tethered molecules. As this effect is not symmetric upon inversion of the flow direction, the inclination angles of the molecules are positive as well as negative [153]. In the experiment shown in Figure 2.4a alternating flow has been applied during the assembly of the network, with the centerline position close to the upper edge of the image. In the “outer parts” of the electrode structure in the bottom part of the image the effect becomes most pronounced showing angles of inclination of $(28.3 \pm 8.6)^\circ$ and $(-20.1 \pm 3.6)^\circ$, respectively in comparison to $\pm(9.5 \pm 6.4)^\circ$ for molecules near the centerline.

Besides the parallel processing of hundreds of DNA molecules as shown in Figure 2.5c, by careful adjustment of parameters like the T-DNA-T concentration that is flushed into the open flow cell, the stretching of DNA by hydrodynamic flow can also be tuned towards a single-molecule manipulation technique (Figure 2.5a). But then in the case of the interdigital electrode array, although the anchoring points of the single DNA molecule are confined specifically to two gold fingers, it has to be admitted, that it can not be determined in advance which two fingers will be connected exactly.

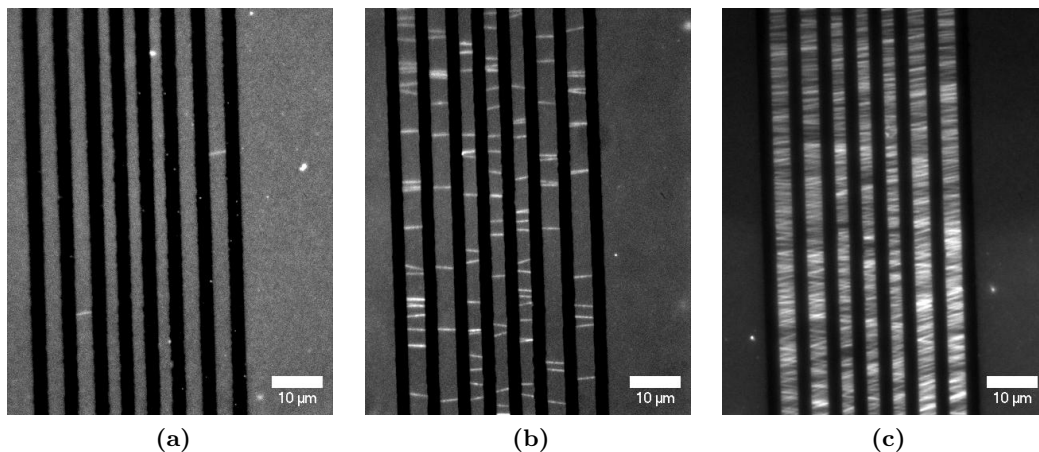


Figure 2.5: Changing the T-DNA-T concentration flushed in, the number of integrated molecules can be adjusted from (a) single molecules at $0.5 \text{ ng}/\mu\text{l}$ via (b) a few tens at $4 \text{ ng}/\mu\text{l}$ to (c) hundreds of molecules processed in parallel at $10 \text{ ng}/\mu\text{l}$.

2 Integration of DNA into Microelectrode Structures

2.2.3 Determination of Anchoring Sites

Resulting from the utilization of a flow of $12.5 \mu\text{l/s}$, in the bottom part of Figure 2.4a the DNA interconnects span gap distances between the input leads of the electrode fingers of up to $10 \mu\text{m}$, whereas the DNA bridges between the electrode fingers themselves are only $2 \mu\text{m}$ and $4 \mu\text{m}$ long, respectively. Under these circumstances the question arises whether the DNA molecules attached in the region where the distances between the electrode fingers is smaller are tethered to adjacent contacts or simultaneously span two gaps, a distance the flow is obviously high enough to stretch out the DNA.

A disadvantage of the used inverted microscopy setup is that, as the DNA can not directly be observed on the opaque gold electrodes, the anchoring points of a molecule can not be seen. Therefore, the above issue was addressed in a statistical evaluation and an additional experiment. For the purpose of the former, fluorescence micrographs from stretching experiments with medium T-DNA-T concentration (like in Figure 2.5b), where single molecules are well separated from each other, were analyzed according to the maximum conceivable elongations of individual molecules. Thereby, as shown in Figure 2.6,I, two cases have to be distinguished: if the notional extension of a fluorescent line in one electrode gap coincides with the one in the neighboring gap (Figure 2.6,I right),

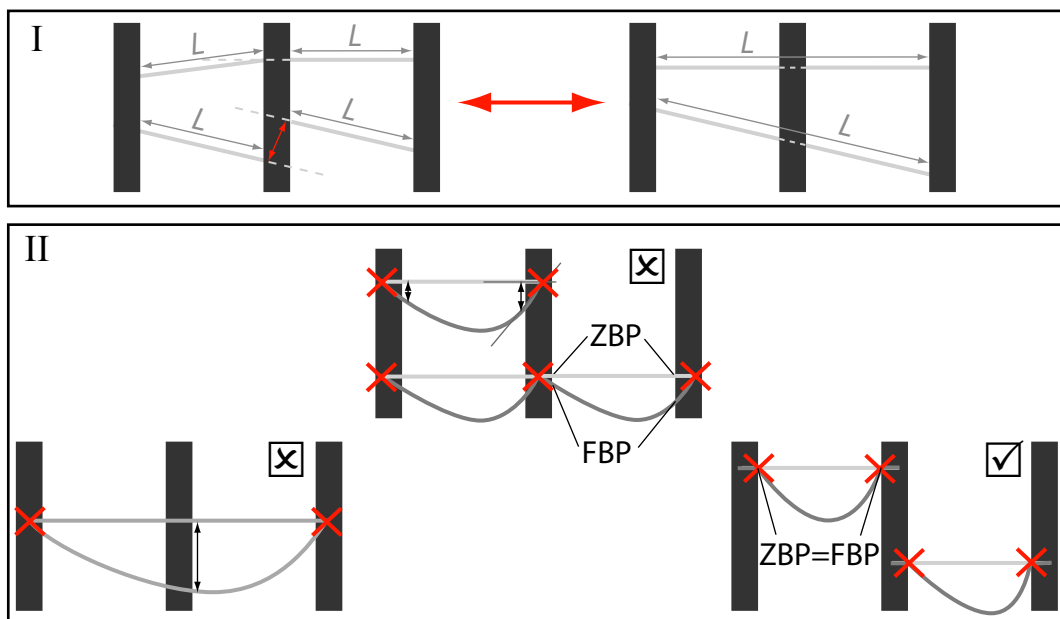


Figure 2.6: (I) Differentiation of DNA molecules bridging one or most likely two gaps by means of an offset between the points where the molecules become invisible at the electrode edges. (II) Conceivable attachment modes of a DNA molecule at the interdigital electrode array and their different behavior under the influence of inclined flow. Left: A solely end-specific tethered molecule sags over its whole length. Middle: In contrast, a molecule spanning one gap only or a molecule, that spans two gaps but is unspecifically fixed at the electrode it bridges, will show reduced bending resulting in a measurable offset between ZBP and FBP. Right: For molecules (additionally) fixed at the electrode edge, ZBP and FBP coincide. Experimentally ruled out versions are marked false by \times .

2.2 Stretching DNA by Hydrodynamic Flow

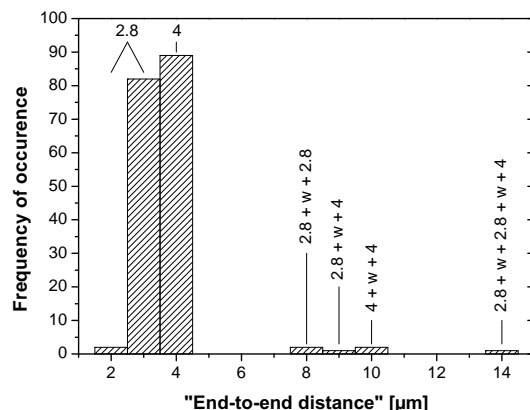


Figure 2.7: Frequency distribution of “end-to-end distances” of T-DNA-T molecules integrated into an interdigital electrode array by hydrodynamic flow. The width of the electrode fingers is $w = 2.36 \mu\text{m}$ and the electrode gaps measure $2.8 \mu\text{m}$ and $4 \mu\text{m}$, respectively.

the two lines are assigned to belong to the same DNA molecule, whose length is measured as the distance between the outermost visible points. On the other hand (Figure 2.6,I left), if an offset exists between the positions of the notional extensions of two neighboring fluorescent lines, they are considered to be different DNA molecules. The same applies for neighboring fluorescent lines without offset, but whose directions are not consistent. Following these aspects, the visible endpoints of 179 DNA molecules were located and their “end-to-end distances” measured. The resulting frequency distribution is shown in Figure 2.7. Therein, it becomes clear, that nearly all determined lengths fall within the two electrode gap widths of $2.8 \mu\text{m}$ and $4 \mu\text{m}$, respectively, with slight variations from these two values due to the inclination of the molecules as described above. For only 6 molecules, that is $\approx 1/30$ of the total number, a length spanning more than one gap is conceivable. Thereof, only one molecule with a (minimum) length of $14.3 \mu\text{m}$ bridges three gaps. All the measured lengths can clearly be classified according to the two gap distances and the electrode width or a combination thereof in Figure 2.7. This gives a first hint to the binding specificity of the thiolated DNA ends to the gold surfaces only, because in case of unspecific binding at the glass surface any other lengths except the restricted ones are possible in equal measure.

Additionally, an experiment was performed, where the positions of the micro-capillaries were symmetrically changed so that the orientation of their centerline was rotated clockwise by 45° . In this way, an oblique-oriented flow can be applied to the DNA interconnects [153]. As a result, the molecules should bend like “sagging ropes” clamped only at their ends somewhere on the opaque electrodes (Figure 2.6,II). The anchoring point can then be determined by analyzing the displacement between the observable “endpoint” of a molecule at the electrode edge in case of zero bending (zero-bending endpoint, ZBP) and finite bending (finite-bending endpoint, FBP) together with the tangent through that point (Figure 2.6,II).

The Figures 2.8 and 2.9 show the result of such an experiment. The molecules which were stretched by a horizontally aligned flow and which appear straightened in the relaxed

2 Integration of DNA into Microelectrode Structures

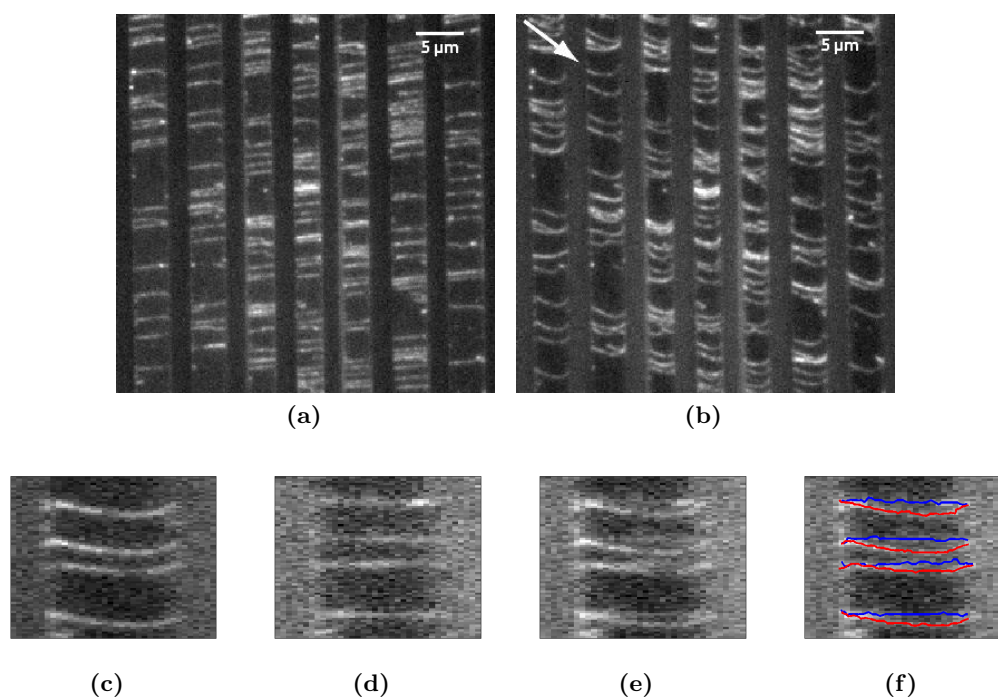


Figure 2.8: Fluorescent micrographs demonstrating the specificity of T-DNA-T attachment to gold and used for the determination of the anchoring site: (a) When the flow is switched off, the molecules exhibit a linear conformation. (b) Applying an oblique-inclined flow in the direction indicated by the white arrow, results in a change in the conformation of the doubly tethered DNA molecules from linear to crescentlike. (c), (d) Details showing 4 DNA molecules from the lower left part of (a) and (b), respectively. (e) Superposition of (c) and (d). (f) corresponds to (e) but includes the tracked lines of highest brightness along the molecules. Blue lines show relaxed molecules and red lines bent molecules under the influence of shear flow, respectively. The visible endpoints ZBP and FBP come to lie on top of one another.

state under no flow (Figures 2.8a and 2.9a), bow during the application of an oblique-inclined flow of $210 \mu\text{l/s}$ (Figures 2.8b and 2.9b). These images give clear evidence (i) that the molecules are specifically attached with both ends at electrodes only and (ii) that the molecules are solely tethered to adjacent electrodes, because no molecules with a lower bending radius spanning more than one gap are observed (compare Figure 2.6,II left). Both observations are in agreement with the above statistical evaluation. A consolidated view of all these facts indicates that, although the flow velocity is high enough to stretch DNA molecules to at least $14 \mu\text{m}$, there must be another efficient mechanism which causes a preferred binding to the adjacent contact finger which is located at a distance smaller than $14 \mu\text{m}$. I suggest the following explanation: When the flow is switched on, and the flow velocity rises within the first seconds to its stationary value, the DNA molecule is extended in the force direction and intermediately adopts—following the stem-and-flower model [48, 49]—a trumpet shape due to the increasing tension along its backbone. In this state, the high affinity of the thiol-functionalized free end of the DNA molecule to

2.2 Stretching DNA by Hydrodynamic Flow

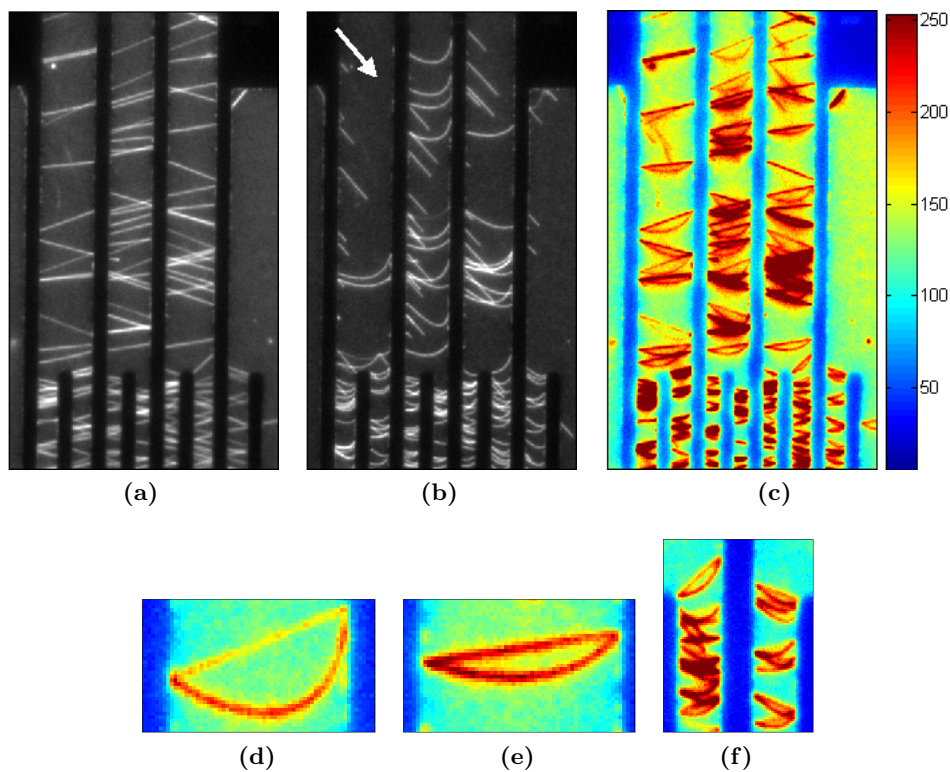


Figure 2.9: Determination of the anchoring sites in the “outer” area of the electrode array: (a) No flow. (b) Application of a oblique-inclined flow in the direction of the white arrow. (c) Superposition of (a) and (b), shown in color for better visibility. (d)-(f) Detailed views onto selected areas in (c).

gold surfaces can result in prompt binding to the electrode closest to the first anchoring point in the direction of flow. The high surface roughness of the electrodes, especially their high-pitched edges (due to the lift-off manufacturing procedure, compare AFM images in Section 4), may then result in a fixation of the “trumpet” onto the electrode area. This suggestion is strengthened by the observation of no horizontally oriented DNA U-loops which would be the case for highly extended molecules tethered with both ends to proximate electrodes. Further and more evidentiary, in Figure 2.8c–f as well as Figure 2.9d–f no shift between the ZBP and FBP can be determined, demonstrating an attachment of the molecule directly at the electrode edge.

The most important reason for the observed behavior probably originates from the open flow cell setup used. Therein, the microcapillaries are oriented under an angle of $\approx 45^\circ$ compared to the substrate surface (Figure 2.3a). Thus, the inflow carrying the T-DNA-T possesses not only a force component parallel to the surface, but also one pointing towards the surface. Therefore, it is assumed, that also the free end of a single-tethered T-DNA-T molecule, which stretches out under the influence of flow, will experience a force component downwards to the surface driving it into close proximity to

2 Integration of DNA into Microelectrode Structures

the gold electrodes and also enforcing the binding to the electrode closest to the first anchoring point.

Summing up, the formation of T-DNA-T bridges by hydrodynamic flow can be described as well controlled in respect of both the formation and specificity of these DNA interconnects. By the application of a diagonal flow it was shown that most of the molecules form “crescent-shaped” structures, which only span one gap, clearly demonstrating that the DNA is specifically attached with both of its ends at contact fingers and solely anchored to adjacent contacts even in the region where the distances between contacts is small compared to the contour length of the λ -DNA used. Only an insignificant fraction of the DNA molecules form “double crescentlike” structures like in the upper right part of Figure 2.8b, which is a sign for the occurrence of a third unspecific adsorption side at the glass surface between two electrode fingers. After switching off the hydrodynamic flow, in the central region of the electrode array (Figure 2.8) the original linear form of the DNA bridges is recovered and no molecules are detached. Moreover, the flow rate applied in Figure 2.8b was $210 \mu\text{l/s}$ which is about a factor of 20 larger than the flow rate applied for the integration of the DNA into the electrode array, thus manifesting the large stability of DNA tethering via thiol groups. However, the direct comparison between Figures 2.9a and 2.9b shows, that in the outermost regions of the electrode array, where molecules span distances of 6 to $10 \mu\text{m}$, a few molecular bridges break upon the application of the strong inclined flow. The result are shortened DNA strands attached to an electrode with one end only and stretched in the direction of flow (upper part of Figure 2.9b). This effect is attributed to photoinduced cleavage of the stretched DNA molecules. Because, if it was a result of the increased bending of the molecules bridging larger gaps, the highest torque would not act on the center of the molecules but on its attachment points and disruption should appear there. This is obviously not the case and points again to the strength of the anchoring.

2.3 Stretching DNA by Electric Field Induced Flow

This section describes how the bridging of an interelectrode gap by a DNA molecule can be achieved by the application of an electric field at the electrodes constituting the integration sites. As described in Section 1.4.2, besides dielectrophoresis several effects can be induced by an oscillating electric field in microelectrodes. Thus, an investigation concerning the occurrence and dependencies of these effects is put in front of the actual purpose to construct interconnect patterns in a switchable manner. That is, according to the derived tasks in Section 1.5, first the questions are answered concerning the mechanism that underlies the potential electric field induced stretching of DNA and the parameters or electrode designs that are needed for its successful application. Then, in Section 2.3.2 this gained experience is put into practice by the attempt to interconnect the four tips in a cross electrode structure in a variable manner to form different interconnection patterns.

2.3 Stretching DNA by Electric Field Induced Flow

2.3.1 Stretching DNA in Heterogeneous Electric Fields

To investigate the influence of dielectrophoresis and other electric field induced effects of fluid motion impacting on the DNA, an altered electrode layout was chosen. An array of tapered electrode tips pointing perpendicularly towards a stripe electrode (Figure 2.10) provides the foundation for the following experiments. In contrast to a design where two electrode tips or stripes face each other and a migration of DNA based on pDEP is equally probable to either of the two electrodes, this layout offers the advantage that it is not symmetric and the direction of the electric field gradient is unambiguously defined, namely pointing towards the tip electrode. Thus, at least the direction of a dielectrophoretic motion—following the gradient of the electric field—is well determined.

With such an electrode array photolithographically fabricated on a glass substrate fluorescence microscopy is used to investigate the motion and/or stretching of fluorescently labeled (thiol-functionalized) DNA molecules (Figure 2.11). By the addition of 20% (v/v) β -mercaptoethanol to the buffer solution it becomes possible to continuously watch the processes running upon application of an oscillating electric field of certain strength and frequency without photocleavage or bleaching of the molecules of interest. Thus, uninterrupted time series of 500 images were recorded with 35 ms exposure time per frame of 512×512 pixels size. For this maximum image size needed to survey processes also outside the interelectrode space, this period of time constitutes an acceptable compromise between captured intensity and time resolution. Especially the latter is important to resolve the conformational changes and the “cruising speed” of single DNA molecules. The electric potentials $V_{pp} \cdot \sin(2\pi ft)$ with the peak-to-peak amplitude V_{pp} and frequency f and ground are applied to the two contact pads of interest via tungsten needles positioned by the micromanipulator system already used above (see Appendix A.1.1 for details). Thereby, to avoid electrolysis at the needles the contact points are located outside the liquid volume which is confined by a sealing ring to a region of 2 mm diameter around the center of the electrode array. For ease of comparing experiments with different distances d between the tip and the plate electrode, in the following the maximum

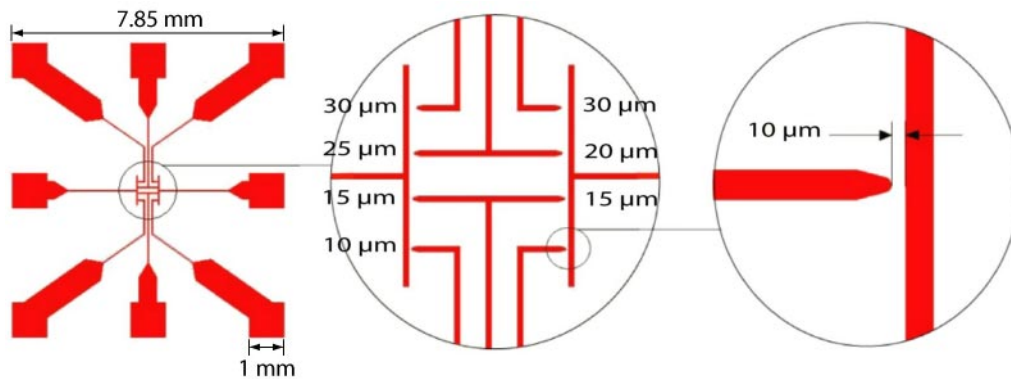


Figure 2.10: Layout of the photolithographically produced tip-plate electrode array with gap sizes of 10 to 30 μm . The tip electrode width is 5 μm to reduce electrolytic bubbling sharp tips are prone to.

2 Integration of DNA into Microelectrode Structures

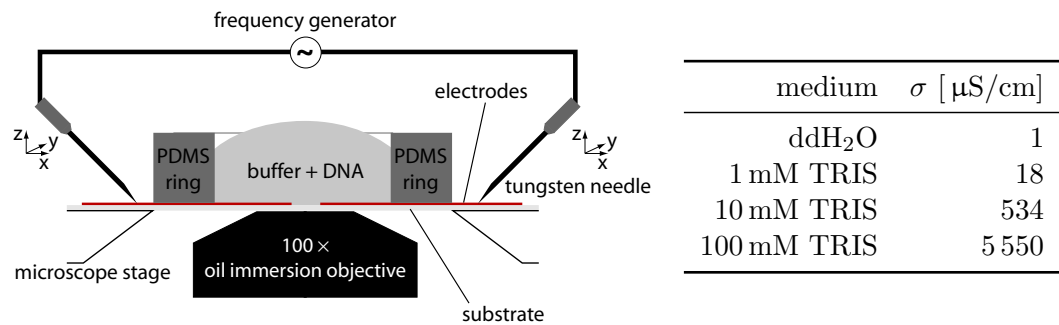


Figure 2.11: Schematic representation of the experimental setup for the electric field induced stretching of DNA and measured electric conductivities σ of different media (all TRIS buffers have pH 8.0).

strength of the electric field calculated as V_{pp}/d and its frequency are referred. Besides dependencies on these two parameters, also the influence of the electric conductivity of the used buffer was investigated. For this purpose, DNA was diluted in TRIS buffers of different concentrations (1, 10, 100 mM) and thus electric conductivities² (Figure 2.11). Concentrations smaller than 1 mM as well as higher than 100 mM were not considered because unspecific DNA adsorption to the glass substrate prevented from their use in the first case and enhanced electrolysis of the electrodes in the latter case. Thus, the solution typically used consists of 76.5 μl TRIS buffer (1, 10 or 100 mM), 20 μl 14.2 M β -mercaptoethanol, 2.5 μl DNA (0.01 $\mu\text{g}/\mu\text{l}$) and 0.1 μl 40 μM YOYO-1.

In the following the experimental observations will be described and discussed. First, a characterization of the detected flow patterns caused by the impact of dielectrophoresis and electrothermal flow is carried out. Subsequently, the domains' dependencies on the parameters electric field strength and frequency and buffer conductivity are compiled. Then, those parameter regions can be deduced, where electric field induced stretching of DNA molecules is possible.

Dielectrophoresis

For low-strength electric fields ($E \approx 1 \cdot 10^5$ V/m) dielectrophoretic trapping of λ -DNA molecules was observed throughout the whole frequency range (50 kHz...16 MHz). As the sequence of images in Figure 2.12 illustrates, in such cases DNA molecules migrate towards the pointed electrode with a mean velocity of 20 $\mu\text{m}/\text{s}$. Independent of the frequency applied, the movement of the molecules is directed into regions of highest field strength, that is positive dielectrophoresis is observed. During the migration the coiled DNA molecules become more or less disentangled (compare conformations at $t=197$ ms and $t=328$ ms in Figure 2.12), but never really stretched. That is, even with T-DNA-T single-tethered at the electrodes no single molecule was observed to stretch from the stripe electrode into the regions of highest field strength at the pointed electrode, thus

²Electric conductivity measurements were performed on a WTW Conductivity measuring apparatus inoLab Cond 720 at Fraunhofer IKTS, Dresden with the help of Dr. Thomas Rabbow.

2.3 Stretching DNA by Electric Field Induced Flow

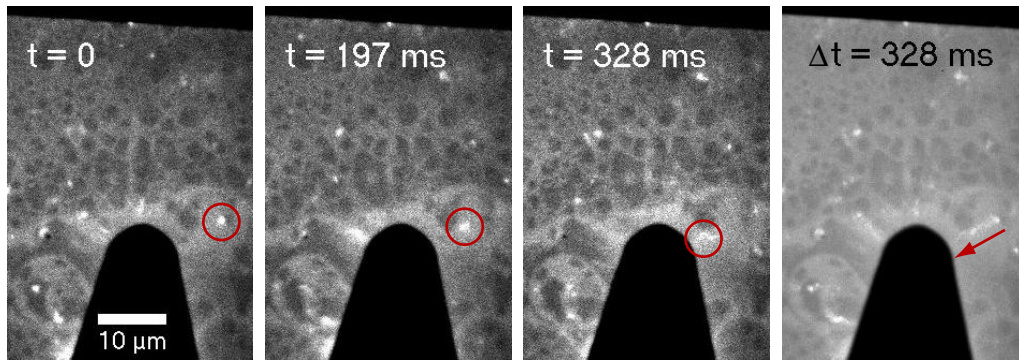


Figure 2.12: Time series of a λ -DNA molecule (encircled in red) under dielectrophoretically induced movement in 10 mM TRIS buffer under an electric field of $E=1.5 \cdot 10^5$ V/m and $f=250$ kHz. For the total covered distance—as shown in the maximum intensity projection of the whole period of time (right)—a mean velocity of 20 $\mu\text{m/s}$ was determined.

spanning the gap between them. Instead, the view onto the electrode gap region and its adjacencies reveals a different picture (Figure 2.13). In the maximum intensity projection of 100 consecutive frames the trajectories of the DNA molecules moving by pDEP become apparent (Figure 2.13a): like a “corona” the trajectories enclose the pointed electrode tip, thereby following the shape of the electric field lines (Figure 2.13b). From a distance of about 7 μm on the pDEP force is strong enough to attract molecules towards the pointed electrode. Furthermore, in Figure 2.13a also short trajectories emerge that strike the stripe electrode perpendicular on either side. DNA molecules are attracted also by the edges of the only 30 nm thick electrodes where in the 3-dimensional space also a gradient of the electric field exists (Figure 2.13c,III). However, the attractive force at the electrode

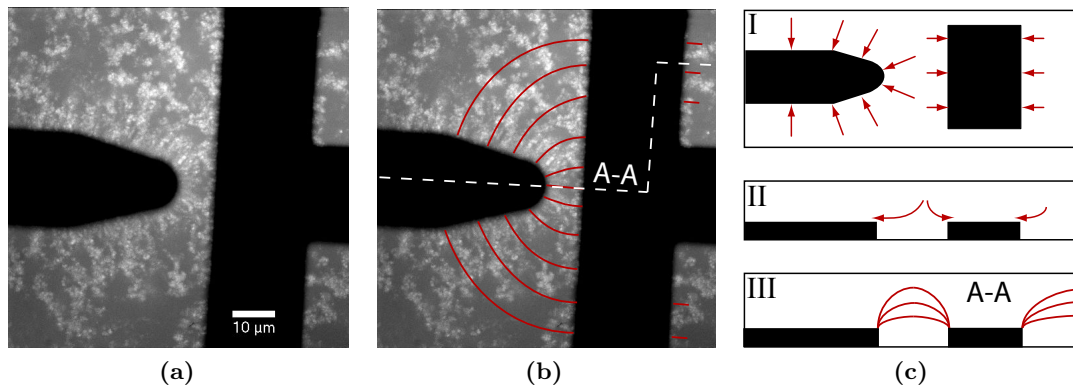


Figure 2.13: Dielectrophoretic movement of λ -DNA in 10 mM TRIS buffer under an electric field of $E=1.5 \cdot 10^5$ V/m and $f=100$ kHz. (a) Maximum intensity projection. (b) Electric field lines (red) superimposed with the maximum intensity projection in (a). (c) Schematic representation of the direction of dielectrophoretic movement (I) viewed from above and (II) in side view and (III) electric field lines in sectional view along A-A as depicted in (b).

2 Integration of DNA into Microelectrode Structures

edges suffices only for the trapping of molecules from the immediate vicinity. Thus, the increased electric field gradient at the pointed electrode induces the preferential migration of DNA molecules to that electrode (different length of arrows in Figure 2.13c,I and II). Outside the attracting range the DNA molecules undergo Brownian motion resulting in “cloudy” trajectories.

Small-Scale Electrothermal Flow

In contrast to a dielectrophoretically induced motion towards the regions of highest electric field strength at the electrodes, for higher frequencies and slightly stronger electric fields the DNA molecules move away from the electrodes into the interelectrode space (Figure 2.14). There, an upwards motion is detected consistent with observations in other experiments [70]. The determined speed of the molecules is with $15.1 \mu\text{m/s}$ similar to the case of pDEP. The reason for this movement is attributed to an electrothermally induced flow.

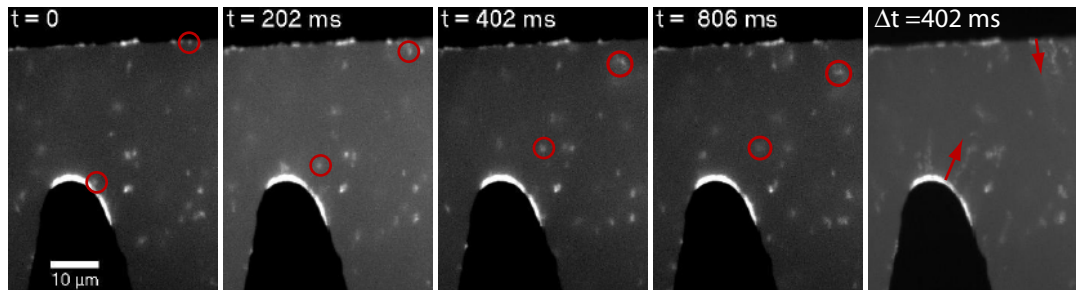


Figure 2.14: Time series of λ -DNA molecules (encircled in red) under electrothermally induced movement in 10 mM TRIS buffer under an electric field of $E=7.1 \cdot 10^5 \text{ V/m}$ and $f=10 \text{ MHz}$. Note the blurring of the molecules at $t=806 \text{ ms}$ due to their upwards movement. For the covered distances—as shown in the maximum intensity projection of the first 402 ms (right)—a mean velocity of $15.1 \mu\text{m/s}$ was determined.

In the overview in Figure 2.15a the narrowness of the electrothermal flow becomes apparent. Only directly in the gap region upwards directed eddies (Figure 2.15b,II) were detected. More outside, the molecules are mainly pushed away from the electrodes and the upwards motion diminishes. That’s why this flow pattern, watched at electric field strength below $1 \cdot 10^6 \text{ V/m}$ and low to intermediate medium conductivities, is termed small-scale to distinguish it from the following observation.

2.3 Stretching DNA by Electric Field Induced Flow

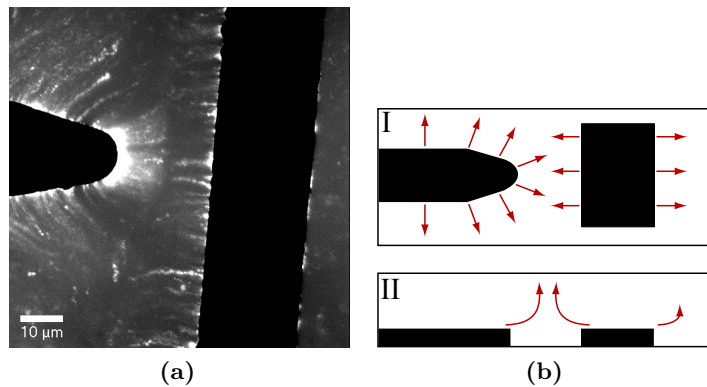


Figure 2.15: Movement of λ -DNA under the effect of a small-scale electrothermal flow. (a) Maximum intensity projection of λ -DNA in 1 mM TRIS buffer under an electric field of $E=8 \cdot 10^5$ V/m and $f=1$ MHz. (b) Schematic representation of the direction of movement (I) viewed from above and (II) side wise.

Large-Scale Electrothermal Flow

At electric field strengths of $E \geq 1 \cdot 10^6$ V/m and high buffer conductivities (100 mM TRIS with 5.5 mS/cm) the small-scale electrothermal flow pattern with eddies out of the substrate plane merges into a pattern with extensive in-plane vortices on either side of the pointed electrode (Figure 2.16). They rotate in opposite directions, thus producing in their center a straight fluid stream directing molecules from the pointed electrode tip to the stripe electrode and beyond (Figure 2.16c,I). According to an electrothermal origin, the detected velocity of the DNA molecules increases to 32.5 $\mu\text{m/s}$ due to the higher electric potential applied (Figure 2.17). This value is rather an estimation of the lower velocity range as the molecular positions start to smear over during 35 ms of exposure.

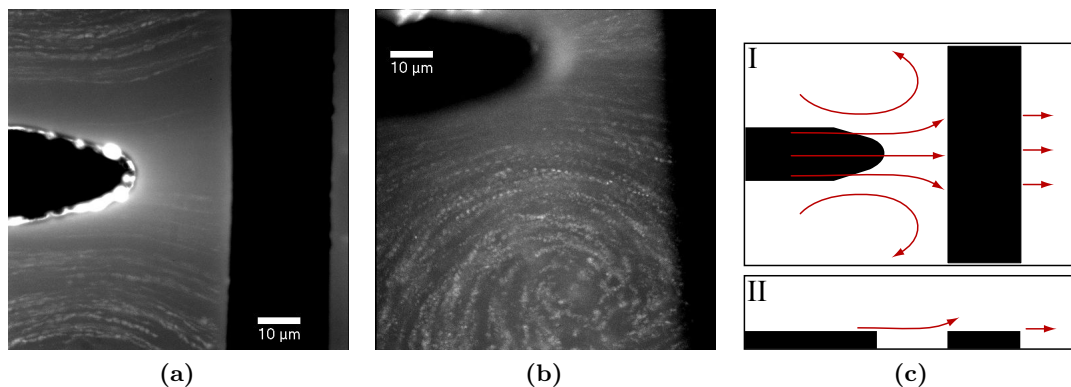


Figure 2.16: Movement of λ -DNA in a large-scale electrothermal flow. (a) and (b) Maximum intensity projection of λ -DNA in 100 mM TRIS buffer under an electric field of $E=2 \cdot 10^6$ V/m and $f=10$ MHz. (c) Schematic representation of the direction of movement in (I) top and (II) side view.

2 Integration of DNA into Microelectrode Structures

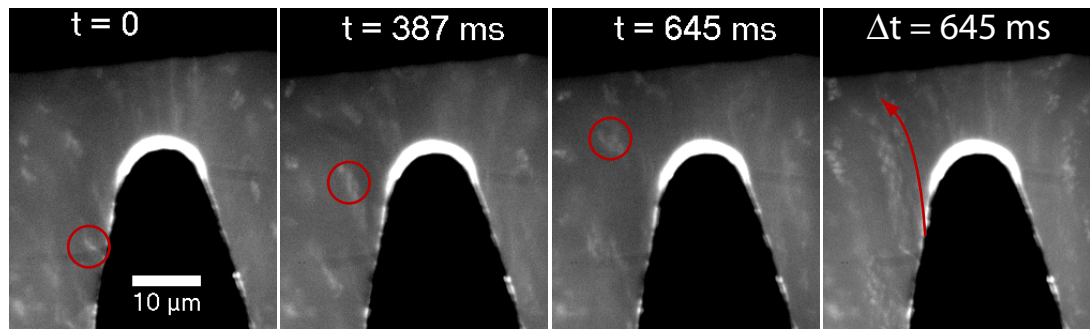


Figure 2.17: Sequence of images illustrating DNA movement in an extensive electrothermal flow in 100 mM TRIS buffer under an electric field of $E=1.3 \cdot 10^6$ V/m and $f=5$ MHz. For the covered distance—as shown in the maximum intensity projection (right)—a mean velocity of $32.5 \mu\text{m/s}$ was determined.

However, the fact that the fluid velocity increases with medium conductivity and the applied potential is a clear indication of JOULE heating. Furthermore, the direction of the vortices is constant independent which electrode is set to ground and which the oscillating potential is applied to.

Parameter Domains of the Flow Effects

In the style of the abovementioned experiments qualitative examinations were performed changing the parameters electric field strength, frequency and buffer conductivity and analyzing the resultant flow patterns. To illustrate the domains of influence of the different forces (pDEP, small-scale and large-scale electrothermal flow and combinations thereof) Figure 2.18 shows symbolic maps where the observed effects are plotted against the

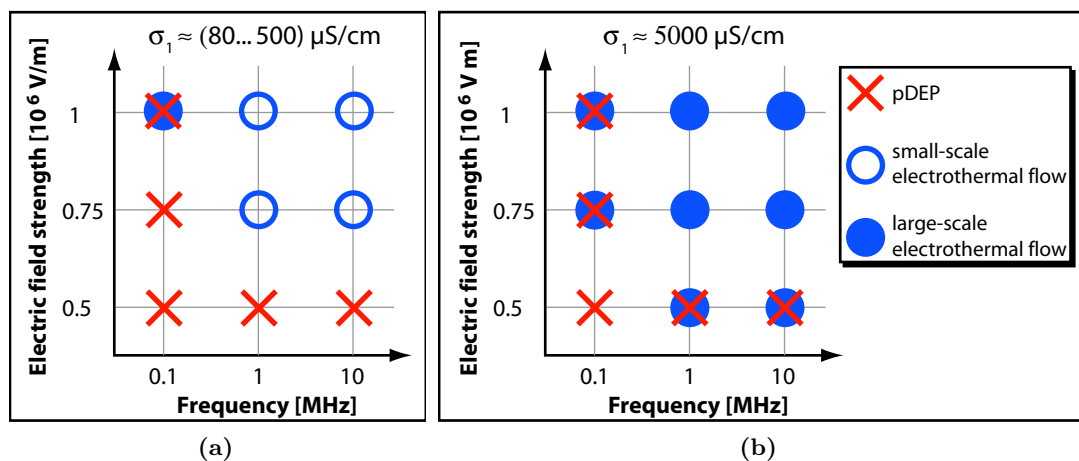


Figure 2.18: Domains of influence of the different effects pDEP, small-scale and large-scale electrothermal flow at (a) low to intermediate buffer conductivity and (b) high buffer conductivity.

2.3 Stretching DNA by Electric Field Induced Flow

applied electric field strength and frequency. For low to intermediate buffer conductivities (Figure 2.18a) pDEP is the dominant effect at low electric field strengths throughout the entire investigated frequency range. For increasing electric field strengths, pDEP only dominates at low frequencies. Otherwise the voltage and thus the JOULE heating is high enough to produce small-scale electrothermal flows.

For a high buffer conductivity it is evident from Figure 2.18b that pDEP is overridden by large-scale electrothermal flows. For high frequencies and electric field strengths, solely the large-scale electrothermal flow is dominant, whereas for the cases where one of these two parameters is low and the other one high the superposition of pDEP with a

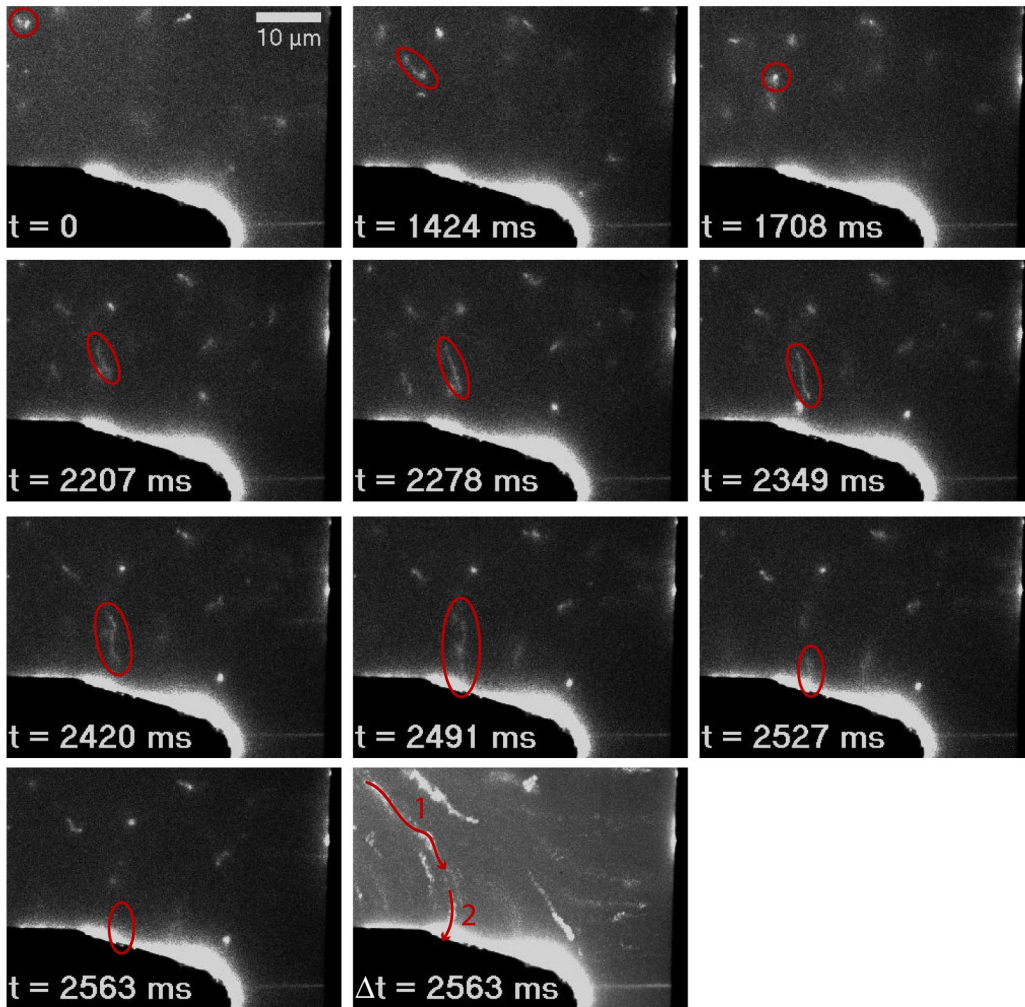


Figure 2.19: Time series illustrating the movement of T-DNA-T under the influence of pDEP superposed with an electrothermal flow at $E=1.3 \cdot 10^6$ V/m, $f=100$ kHz in 10 mM TRIS buffer. Note the slow motion at $7.4 \mu\text{m/s}$ and partial disentanglement as the molecule is attracted from the bulk (path 1) and the 10 times faster attraction ($78.5 \mu\text{m/s}$) under a considerable disentanglement by pDEP trapping close to the electrode edge (path 2).

2 Integration of DNA into Microelectrode Structures

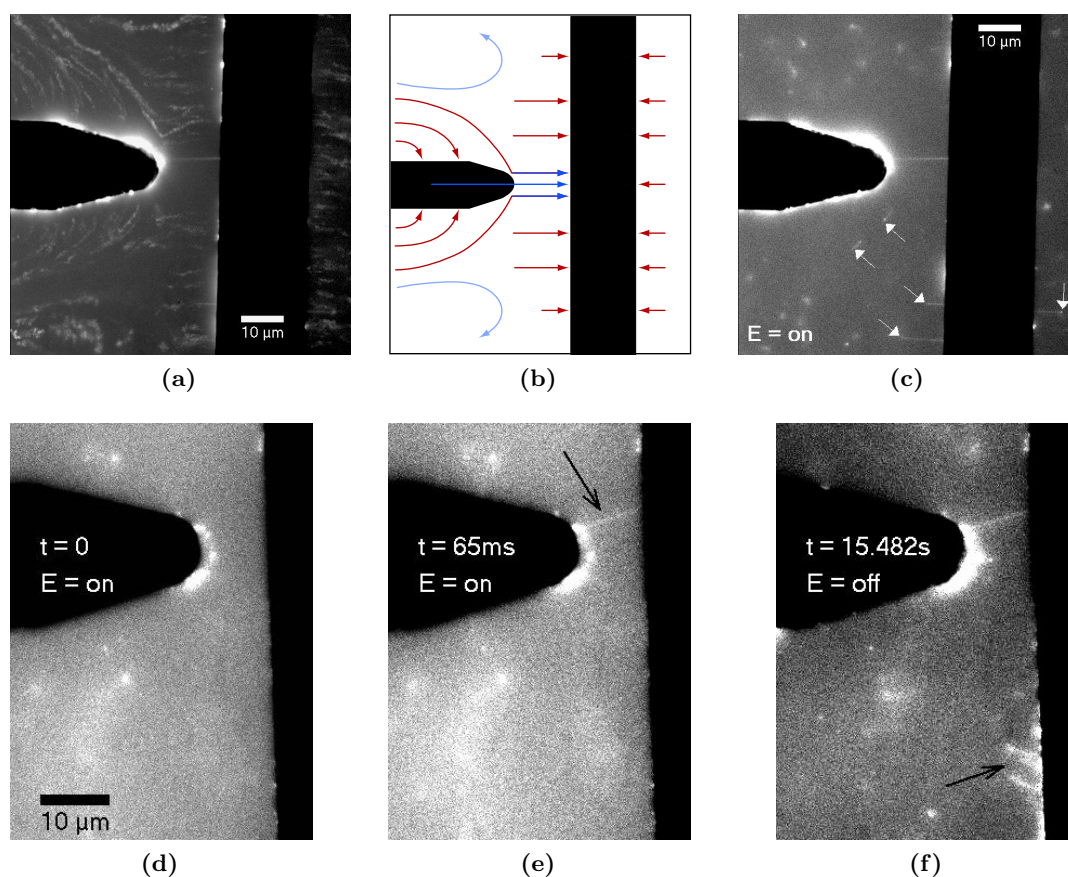


Figure 2.20: A sequence of images showing the trapping, immobilization and stretching of T-DNA-T under the influence of pDEP superposed with an electrothermal flow at $E=1.3 \cdot 10^6$ V/m, $f=100$ kHz in 10 mM TRIS buffer. (a) Maximum intensity projection. (b) Schematic representation of the movement: molecules between the electrode gap move linearly with the electrothermal flow (dark blue) and are stretched, molecules are attracted (red) to regions of highest electric field strength at the electrodes and molecules outside of the gap region have the motion of cofield rotation (light blue). (c) T-DNA-T molecules unspecifically attached to the glass surface (white arrows) are stretched in the flow and by pDEP towards the electrodes, respectively, thus illustrating the direction of the acting force. (d),(e) When the electric field is switched on, within one frame of 35 ms exposure time a T-DNA-T molecule (black arrow) is stretched from the pointed electrode above the 15 μm gap to the stripe electrode. (f) Long after the electric field was switched off, the DNA bridge remains established while other molecules move away from the electrodes under Brownian motion (black arrow).

large-scale electrothermal flow is observed (Figure 2.19). The same result is found for a moderate buffer conductivity where at low frequencies the electric field strength is high enough to induce the electrothermal flow pattern. The combination of the two effects is characterized by pDEP trapping of DNA molecules at electrode edges while they are moved by a large-scale electrothermal flow directly in the electrode gap region and in the bulk (Figures 2.20a and 2.20b). In consequence of the strong forces particularly at high

2.3 Stretching DNA by Electric Field Induced Flow

electric field strengths, the DNA molecules are considerably disentangled already at a pDEP governed motion (Figure 2.19).

Furthermore, if T-DNA-T is used instead of λ -DNA, the single-end tethered molecules are stretched from the tip of the pointed gold electrode in the direction of electrothermal flow over to the stripe electrode (Figures 2.20d and 2.20e). In other words, the directed electrothermal flow appearing under these conditions in the gap between a pointed and a stripe electrode is capable for the construction of DNA bridges. In this process, the preferred direction of the flow is attributed to the non-symmetric electrode geometry. Therein, electrothermal pumping, with the temperature gradients arising from JOULE heating ($\sigma_1 E^2$), is also non-symmetric, i.e. major heating at the pointed electrode leads to a flow preferentially emanating from there. Beyond that, the combined occurrence of pDEP and the electrothermal flow in the described manner allows for the systematic capture of DNA molecules at the tapered electrode from the bulk solution by pDEP, the immobilization of the trapped functionalized molecules using the thiol-linkage to the gold electrode surface and then the directed stretching in the electrothermal flow. Finally, after the binding of the second DNA end to the stripe electrode, the DNA bridge is stable and both DNA ends remain bound even after the electric field is switched off (Figure 2.20f).

In conclusion, the results indicate that pDEP dominates the molecule motion at low electric field strength or low frequency ranges. The dielectrophoretically induced motion is clearly dominant at small scales, i.e. pDEP can trap DNA molecules at electrode edges. For high electric field strengths and high frequencies, electrothermally induced flow is the dominant effect. The domain of its influence increases with medium conductivity, thus leading to a superposition with pDEP in its former dominant area of application. Only the flow pattern resulting from this combination allows for the stretching of single-end tethered DNA molecules which in addition takes place in a directed manner between a tapered and a stripe electrode. In contrast, in the cases of separated occurrence of pDEP and electrothermal flow DNA molecules are only moved in their coiled formation and no relevant stretching appeared. Care should be taken to avoid boiling at very high electric field strengths ($\geq 5 \cdot 10^7$ V/m) and electrolysis at frequencies below 10 kHz.

2.3.2 Construction of Interconnect Patterns

In the above section the behavior of DNA molecules subjected to electric field induced phenomena under variation of the parameters electric field strength, frequency and buffer conductivity were described. It became apparent that a localized stretching of single-end tethered DNA molecules is only achievable using the non-symmetric, directed electrothermal flow in the gap between a tapered and stripe electrode. However, application oriented contact electrode structures rather consist of opposing contact pads of more or less tapered shape. Thus, such electrode structure are in the spotlight of this section aiming at the construction of more complex, “interwoven” patterns than a single interconnection of two electrodes. First, a symmetric geometry of opposing tip electrodes is used to verify the establishment of a localized continuous flow in-between them. Then, the geometry is expanded to four electrodes opposing each other in a cross-like configuration.

Opposing Tip Electrodes

Also contradictory to earlier experiments [70] where a limited stretching of DNA molecules was observed as result of oppositely rotating eddies above the symmetric electrode tips, in fact here it was possible to achieve a continuous flow in the $10\ \mu\text{m}$ wide gap between two opposing tip electrodes (Figure 2.21). At an electric field strength of $1\cdot 10^7\ \text{V/m}$, which is twice as high as in the experiment of WÄLTI *et al.* [70], and a comparatively two orders of magnitude higher frequency of 10 MHz a continuous electrothermally induced flow was established (Figures 2.21b and 2.21c) leading to a directed stretching of single-end tethered T-DNA-T molecules (Figure 2.21b) and finally the formation of a single interconnection after the electric field was switched off (Figure 2.21a). The reason for the one-way directed flow in the itself symmetric electrode layout is attributed to inhomogeneities in the electrodes such as random protrusions as a result of the lift-off manufacturing inducing slightly higher electric field strengths there and thus leading to non-symmetries, i.e. the activation of one electrode as “source” of the flow.

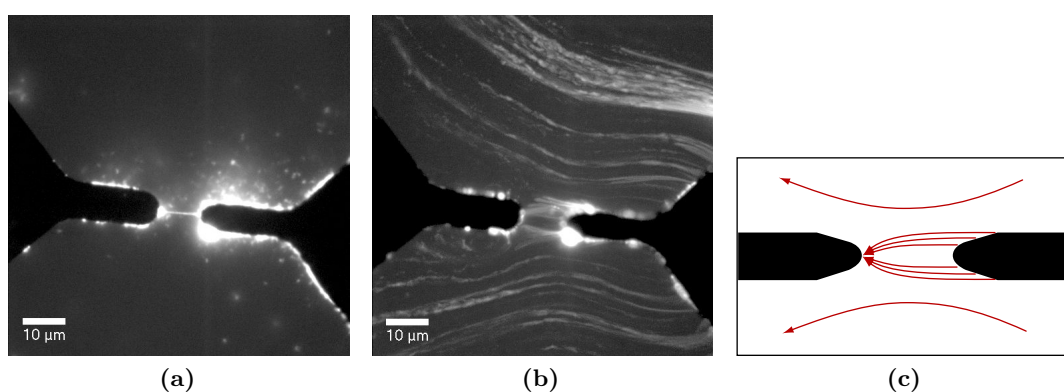


Figure 2.21: Continuous electrothermally induced flow between opposing tip electrodes at $E=1\cdot 10^7\ \text{V/m}$, $f=10\ \text{MHz}$ in 10 mM TRIS buffer. (a) A single T-DNA-T bridge was established and is held up even after the electric field is switched off. (b) Maximum intensity projection showing the stretching of several T-DNA-T molecules from the right to the left tip electrode. (c) Schematic representation of the induced flow.

Cross Electrode Structure

The cross electrode structure was used to test the assembly of complex interconnect patterns thought to be achievable by the selective, consecutive switching of the electric field between certain electrodes. But, since in the cross electrode structure the applied electric field between the selected electrodes is affected by the presence of the metallic areas of the other electrodes, electric field gradients also arise elsewhere than between the contacted electrodes. In consequence, they disturb the directed fluid flow between the selected electrodes and thus hinder the systematic immobilization of the second end of a single-end tethered T-DNA-T molecule. Nevertheless, the interconnection of electrodes in the cross structure was successful. As shown in Figure 2.22 during the application of

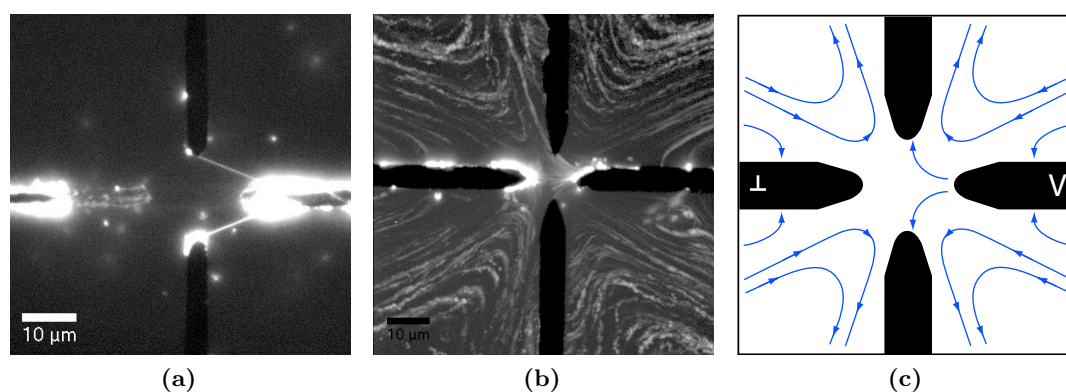


Figure 2.22: Electrothermally induced flow in the cross electrode structure at $E=2 \cdot 10^6$ V/m, $f=10$ MHz in 10 mM TRIS buffer using T-DNA-T. (a) Two T-DNA-T bridges were established between the connected left and right electrode and are held up even after the electric field is switched off. Note the stressing of the contacted electrodes and the halo around them resulting from trapped molecules diffusing away after the electric field is switched off. (b) Maximum intensity projection showing the stretching of several T-DNA-T molecules from the right to the left tip electrode. (c) Schematic representation of the induced flow and the applied electric potentials.

an electric field between opposing electrodes the arising electrothermal fluid flow in the vicinity of the tips is directed in such a way that T-DNA-T molecules could be stretched to both neighboring electrode tips. However, the fluid motions are so strong and distorted that already formed DNA bridges do not withstand the inclined fluid flows generated by contacting a different electrode pair in a subsequent step. Thus making it impossible to organize the assembly of DNA interconnects in a switchable manner.

2.4 Conclusion

The aim of this chapter was the stretching of DNA molecules from a coiled conformation into a linear, wire-like form and the positioning of these wires between defined contact pads. To this end, the end-specific functionalization of λ -DNA molecules with one thiol-group at each end was used to allow for the attachment of both DNA ends to lithographically patterned gold electrodes. The stretching of such single-end surface-tethered DNA molecules by hydrodynamic flow in an open flow cell resulted in the directed formation of T-DNA-T bridges spanning single gaps in an interdigital electrode array. This assembly is not only well controlled in respect to the specificity and stability of the DNA interconnects but also the number of integrated DNA molecules can be adjusted from single molecules to the batch-wise assembly of hundreds of interconnects.

In a second approach the realization of single connections in an addressable and switchable electric field based stretching method was investigated. It became clear, that the electric field induced effect DEP does not have the ability to considerably stretch DNA molecules as it leads to the trapping of a DNA coil as a whole to regions of highest electric field strength. Instead, an electric field induced, electrothermal fluid flow is the

2 Integration of DNA into Microelectrode Structures

mechanism that leads to a directed stretching of single-end electrode-tethered T-DNA-T molecules. In an altered electrode layout consisting of a tapered tip opposed by a stripe electrode with a straight edge the electric field strength is increased at the tip, thus inducing the preferential JOULE heating of that electrode and a fluid flow emanating from there. However, the construction of complex networks in terms of a “wiring diagram” could not be achieved based on this approach as a highly controlled deposition (meaning that the location of each end of the DNA molecule is predefined) is not realizable in an array of electrode tips. The applied electric field between the “turned on” electrodes is affected by the presence of the metallic areas of the other electrodes, so that electric field gradients and fluid flows also arise elsewhere than between the contacted electrodes.

3 Photoinduced Platinum Deposition on DNA Templates

The challenge in the application of a metallization procedure to DNA templates is to establish a method where continuous nanowires with a diameter as thin as possible, favorably below 10 nm, can be fabricated *in place*, i.e. *after* the integration into the circuitry. First, the demand on such a DNA metallization is, that it is highly specific, i.e. metal deposition should take place selectively on the DNA, but not at the surrounding areas. However, under wet-chemical conditions in the experiment one always deals with both processes—the biomolecule-templated heterogeneous reaction as well as the homogeneous reaction, which leads to unwanted background metallization. These two metallization routes are competing. Therefore, in order to avoid the background process, methods have to be developed, where the heterogeneous reaction channel at the biotemplate is strongly favored compared to the homogeneous reaction channel.

Second, the DNA molecules preliminary integrated into the e.g. electronic structure of the higher hierarchy level (towards the exterior of the device) with the help of their molecular recognition and self-assembly properties, have to withstand the metallization procedure. That is, once assembled connections or networks are not allowed to get lost or loose, respectively during the metallization.

Third, the metallization procedure must be applicable to single, immobilized DNA molecules. In other words, no “ensemble methods” come into consideration as they rely on the control of reaction kinetics by fine adjustment of the ratios between reactants. That this is feasible in solution was conclusively demonstrated by SEIDEL *et al.* [136]. However, this approach is not thought to be suitable for the metallization of single molecules which do not constitute an ensemble and for a subsequent positioning of metalized DNA molecules their molecular recognition capability is no longer available, as it is lost during the metallization.

A potential approach for all three issues is the use of DNA itself as a reducing agent [144] induced by short-wavelength UV light. The idea is that DNA acts as photosensitizer, i.e. at 254 nm wavelength—the absorbance maximum of double-stranded DNA—only DNA bases are photooxidized leading to a reduction of the bound metal complex ions. As thus the reduction energy is only available at the DNA molecule, simultaneously the background metallization is suppressed. However, the investigations on silver-laden DNA shown by BERTI *et al.* [144] result in coarse metallization.

In order to improve the method towards the formation of thin and continuous structures, platinum is a promising candidate. In comparison to silver its lower surface energy leads to smaller clusters. Furthermore, platinum complexes are known to strongly bind to DNA [154] and the cluster growth from initially formed nuclei upon further reduction

3 Photoinduced Platinum Deposition on DNA Templates

proceeds via an autocatalytic mechanism [155]. It is speculated, that these advantages of platinum resulting from the reduction with a chemical reducing agent, also appear upon the photoinduced reduction as could recently be shown on bacterial surface layers using $\text{Pt}(\text{NO}_3)_2$ as platinum source [145].

Therefore, in the following the DNA metallization using aqueous $\text{Pt}(\text{NO}_3)_2$ solutions is studied. In the preliminary investigations of this chapter, double-stranded λ -DNA absorbed onto mica is the starting point to investigate the parameters that control the heterogeneous cluster formation on surface-immobilized DNA. Straightforward atomic force microscopy (AFM) is used to identify the influence of metal salt concentration in Section 3.1.1 and other control parameters like UV irradiation time in Section 3.1.2. For reasons that will be presented in the course of the discussion, the investigation of the binding of $\text{Pt}(\text{NO}_3)_2$ to DNA is complicated, whose examination is therefore put last in Section 3.1.4, although it is the initial step in the procedure. In Section 3.2 the continuity of the synthesized cluster chains is studied by transmission electron microscopy (TEM), also in correlation with atomic force microscopy. Furthermore, in Section 3.4 the photoinduced platinum deposition is applied to the metallization of tubular DNA templates.

3.1 Formation of Platinum Cluster Chains on Double-Stranded DNA

The formation of platinum clusters on DNA comprises the loading of the template with the metal species as a first step, termed *activation*. As shown in previous investigations with the platinum complexes of the salt K_2PtCl_4 in our group [136], this important step guarantees a dense coverage of the template with initial nucleation centers and therefore leads to a favored reduction and growth of clusters there. As the binding of the tetrachloro platinate to DNA is rather slow, activation times of up to 24 hours were used in these works for a subsequent reduction with a chemical reducing agent. However, for a photoinduced reduction the use of $\text{Pt}(\text{NO}_3)_2$ revealed better results in preliminary experiments [145]. Nevertheless, at this point it has to be stated, that until now the result of the dissociation of $\text{Pt}(\text{NO}_3)_2$ salt in water is not known. That means, that at the beginning of this work it could not be determined whether a potential Pt^{2+} -ion electrostatically interacts with the negatively charged phosphate groups in the DNA backbone or a $\text{Pt}(\text{II})$ -complex binds covalently to the bases, e.g. the N7 or N3 sites and what reaction kinetics are underlying. Further experiments for the clarification of this dilemma were performed and will be discussed in Section 3.1.4. The results therein can be read as hints for an electrostatic interaction behavior between the products in the $\text{Pt}(\text{NO}_3)_2$ aqueous solution and the λ -DNA. Anticipating this outcome, on the one hand the term “platinum ion” will be used consistently throughout the text to refer to the metal species that binds to DNA. On the other hand, activation times of 5 hours are initially used as a compromise to ensure saturation of all binding sites on the DNA.

3.1 Platinum Cluster Chain Formation on DNA

3.1.1 Metal Salt Concentration Dependence During Activation/Reduction

Before the metallization of λ -DNA, that is the heterogeneous formation of platinum clusters on the DNA template, is investigated, several control or rather reference experiments are carried out. These include (i) experiments about the photoinduced cluster formation without DNA. From the comparison with the subsequent studies performed in the presence of DNA one can determine the influence and the role of the DNA during the cluster formation process. Similarly, a comparison between (ii) DNA, which was only activated, but not reduced, and (iii) DNA, which was activated and reduced, demonstrates the photo-reducing capability of DNA and reveals the autocatalytic growth process.

To guarantee comparability, for these reference experiments the same protocol was applied like in the following proper preparations. In short, the sample preparation followed throughout this chapter comprises the following steps (for details refer to Appendix A.1.2). Muscovite mica pieces of standardized size of $5 \times 5 \text{ mm}^2$ serve as substrate. Its atomically flat surface dedicates mica for AFM studies. Clean surfaces were prepared by cleavage immediately before exposure to solutions. That surface is hydrophilic and carries a negative surface charge. However, ion exchange with divalent cations like Mg^{2+} in the buffer will produce a positive surface charge which allows for the electrostatic binding of λ -DNA via its negatively charged phosphate backbone. Consequently, λ -DNA is adsorbed from a $10 \text{ }\mu\text{l}$ droplet of buffer solution (40 mM HEPES, 5 mM MgCl_2 , pH 7.6), containing 1 ng/ml λ -DNA, left to sit on the mica piece for 5 min. After rinsing with water, $15 \text{ }\mu\text{l}$ of the activation solution are placed on the surface and stay there in a humid and dark environment for the activation time t_A , which is 5 hours in the experiments in this section. Then, either this droplet covers the surface during UV-light exposure or it is replaced with $15 \text{ }\mu\text{l}$ of a different solution after an intermediate washing step in water. After the reduction, i.e. the UV-light irradiation, the preparation is completed with a final washing step in water and the sample is blown dry with nitrogen.

Cluster Formation in the Absence of DNA

Figure 3.1 shows the result of such an experiment where no λ -DNA was adsorbed but 1 mM, 10 mM and 100 mM aged $\text{Pt}(\text{NO}_3)_2$ solution, respectively, was added directly to the freshly cleaved mica surface. The term “aged” thereby means, that the metal salt solutions are at least 24 hours old to ensure an equilibrated state after potential hydrolysis, which is known to have an influence over the result [136]. After 5 min of UV exposure the samples only contain particles of up to 30 nm size in case of the 1 mM $\text{Pt}(\text{NO}_3)_2$ solution (Figure 3.1a). For increasing $\text{Pt}(\text{NO}_3)_2$ concentration larger agglomerates (Figure 3.1b) or even a nearly complete deposit (Figure 3.1c) can be seen. Two conclusions can be drawn from these results. First, the energy impact during 5 min UV exposure with 10 mJ/cm^2 —which are the same characteristics as used in the subsequent experiments with DNA—is enough to lead to spontaneous cluster formation via homogeneous nucleation and growth in the droplet of $\text{Pt}(\text{NO}_3)_2$ solution. Second, in the absence of an organic catalyst

3 Photoinduced Platinum Deposition on DNA Templates

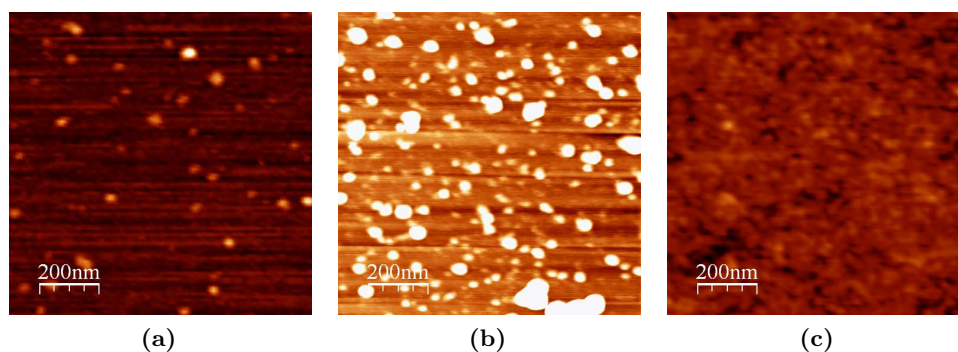


Figure 3.1: Photoinduced particle formation in the absence of DNA. AFM images of Pt particles from $\text{Pt}(\text{NO}_3)_2$ solutions of (a) 1 mM, (b) 10 mM and (c) 100 mM concentration. z-scale 0–3 nm.

like DNA only random aggregates are formed, no regular structures with a chain-like morphology are present.

Appearance of Activated, Non-Reduced DNA

As stated at the beginning, the experiments without DNA only serve as a reference. The intention of this work is to suppress the homogeneous nucleation path in solution and instead, to catalyze the photoreduction process by the use of the photosensitive template DNA to directly synthesize particles there. So the aim of the following experiments is to initiate heterogeneous cluster growth at the DNA and densely, i.e. preferably continuously electric conducting, cover the DNA. To do so, λ -DNA was first immobilized at the mica surface as described above and then *activated*, that is loaded with metal ions so that all

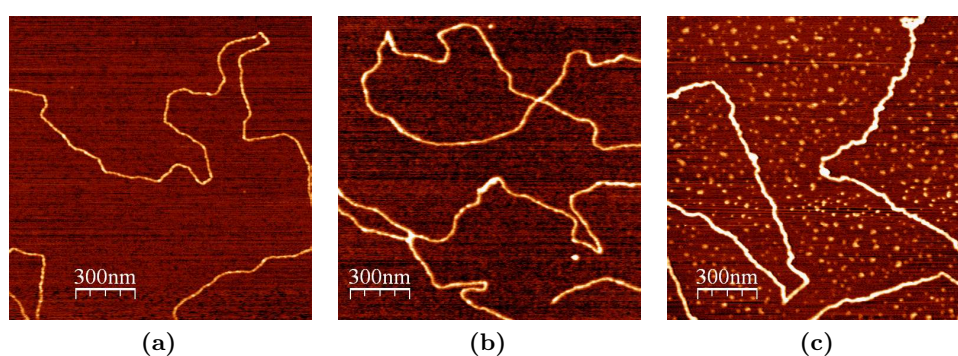


Figure 3.2: AFM images of λ -DNA, which was only activated in (a) 1 mM, (b) 10 mM and (c) 100 mM $\text{Pt}(\text{NO}_3)_2$, respectively, but not reduced. z-scale: 0–2 nm

3.1 Platinum Cluster Chain Formation on DNA

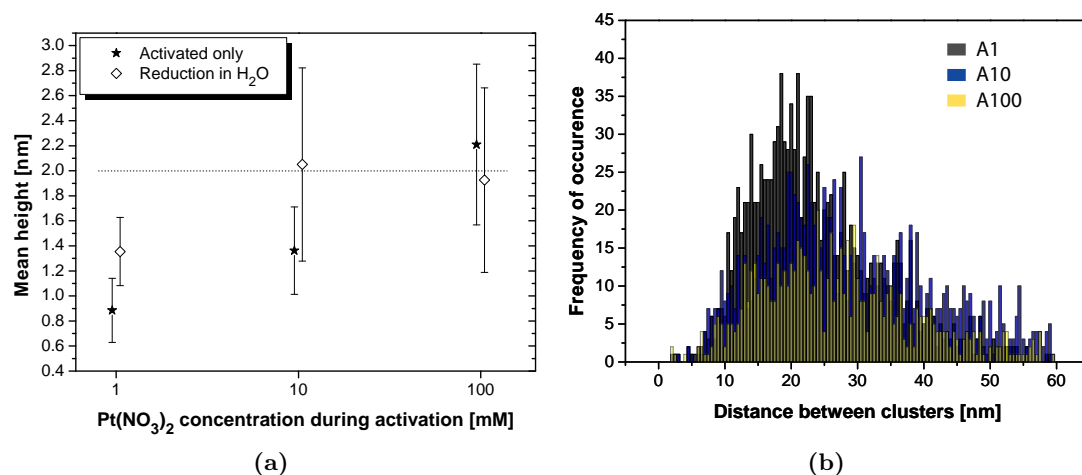


Figure 3.3: Analysis of AFM data for λ -DNA activated for 5 h in 1, 10 and 100 mM $\text{Pt}(\text{NO}_3)_2$, respectively. (a) Mean height of the cluster chain. For comparison the results for λ -DNA that was reduced in a water droplet are included (identical data points as in Figure 3.5a). (b) Overlay of the cluster distance distributions upon increasing $\text{Pt}(\text{NO}_3)_2$ concentration during activation.

possible DNA binding sites are saturated.¹ This primary bound metal ions shall serve in the subsequent reduction step as nucleation centers.

Again as a reference, the surface-immobilized λ -DNA was first activated only to quantify the DNA height increase upon metal binding. The result is shown in Figure 3.2 where λ -DNA adsorbed to mica was activated in 1, 10 and 100 mM $\text{Pt}(\text{NO}_3)_2$ for 5 h. In comparison to native λ -DNA, whose height on mica averages to (0.5 ± 0.1) nm after activation in pure water under identical conditions, the height of the platinum activated DNA is increased to (0.89 ± 0.26) nm for 1 mM $\text{Pt}(\text{NO}_3)_2$ and (1.36 ± 0.35) nm for 10 mM $\text{Pt}(\text{NO}_3)_2$. As beyond 100 mM $\text{Pt}(\text{NO}_3)_2$ the enhancement is not continued ((2.20 ± 0.64) nm), apparently all binding sites are saturated and the DNA can not be loaded further with platinum as shown in Figure 3.3a. Therein, for comparison the results from the following paragraph are included showing the mean height of the DNA after the reduction of the initially bound amount of platinum in a water cover, that is where only the initially bound platinum can be reduced because no further material is available. For this case it seems reasonable to assume, that clusters of 2 nm diameter (dotted line in Figure 3.3a) form on DNA with saturated binding sites. Supposing further, that then one Pt atom is situated at each phosphate group in the 48 502 base pairs of λ -DNA, one can estimate, that the Pt atoms throughout a length of about 20 nm have to coalesce to form a sphere of 2 nm size. As can be seen in Figure 3.3b, cluster distances in that range are indeed measured.

¹Assuming the adsorption of one λ -DNA molecule out of hundred to the sample surface from a 10 μl droplet containing 1 ng/ml λ -DNA, the ratio of platinum ions per adsorbed base pair is already $3 \cdot 10^4:1$ in 15 μl of 1 mM $\text{Pt}(\text{NO}_3)_2$.

3 Photoinduced Platinum Deposition on DNA Templates

Concluding, with this series of experiments the base amount of bound platinum ions was determined which can then be exposed to UV light to initiate the cluster formation at the DNA template.

Cluster Chain Formation at Activated DNA upon Reduction

Cluster formation in the presence of activated λ -DNA is achieved by exposing the DNA-Pt compound to 254 nm UV light through a film of aqueous solution. This can either be the activating droplet itself or it is exchanged for a droplet of solution of different $\text{Pt}(\text{NO}_3)_2$ concentration. The combination of constant substrate size and droplet volume thereby guarantees a constant film thickness of about 1 mm the UV light has to radiate through. The result is shown in Figure 3.4 wherein the outcome of a series of different combinations of solutions in the activation and reduction step is compiled. Each of the images is a representative one out of about 30 $1 \times 1 \mu\text{m}^2$ detail sections, that were recorded on each sample. They provide the basis for an image processing routine (for details of the code refer to A.2). Therein, every image is on the one hand analyzed regarding the mean height of a cluster chain. This is the averaged height of the tracked ridge of the chain, corrected for the substrate mean height. Additionally, the height profile along the chain's ridge allows for the calculation of certain lengths, e.g. the distance between local maxima. On the other hand, also the fraction of the background area is determined, which is covered by non-chain-like particles. The results of these calculations for the set of investigated samples from Figure 3.4 are shown in Figure 3.5. The two figures will in the following be discussed together. For ease of communication labels analogous the type “*a1r10*” will be used, which means that this sample was *activated* with a 1 mM $\text{Pt}(\text{NO}_3)_2$ solution and photoinduced *reduced* in a film of 10 mM $\text{Pt}(\text{NO}_3)_2$.

Let us first concentrate on the bottom line of Figure 3.4 where λ -DNA was activated with 1 mM, 10 mM and 100 mM $\text{Pt}(\text{NO}_3)_2$, respectively and reduced in water, i.e. 0 mM $\text{Pt}(\text{NO}_3)_2$. The AFM images in the lowest part of Figure 3.4 show dense chains of particles, where one particle sits so close by the other that no gaps can be visualized with the tip of the AFM. Though this disallows the detection of the underlying DNA, it is assumed that the cluster chains indeed follow the trace of the biomolecules as their contour (curve radius) is identical. For an increasing $\text{Pt}(\text{NO}_3)_2$ concentration from 1 to 10 mM, the increase in height (brighter color) is accompanied by a coarser appearance of the particle chain, i.e. a variance of cluster size along the chain. No significant changes are observed for a further concentration increase to 100 mM. These two observations are verified by the measurements in Figure 3.5a (open diamonds): For a concentration increase from 1 to 10 to 100 mM $\text{Pt}(\text{NO}_3)_2$ the mean height of the cluster chain rises from (1.35 ± 0.27) nm to (2.05 ± 0.77) nm and saturates at (1.93 ± 0.74) nm. Thereby, the increasing deviations from the mean value reflect the increased variations in measured heights along the cluster chain ridge, which is a consequence of the enlargement of particle size: the larger the height of single particles in a row, the larger the detected height difference between the top of a particle and the valley formed by the attachment point of two neighboring particles. Furthermore, only very few aggregates or particles in the background are obtained, i.e. independent of the $\text{Pt}(\text{NO}_3)_2$ concentration during activation only about 2% of the

3.1 Platinum Cluster Chain Formation on DNA

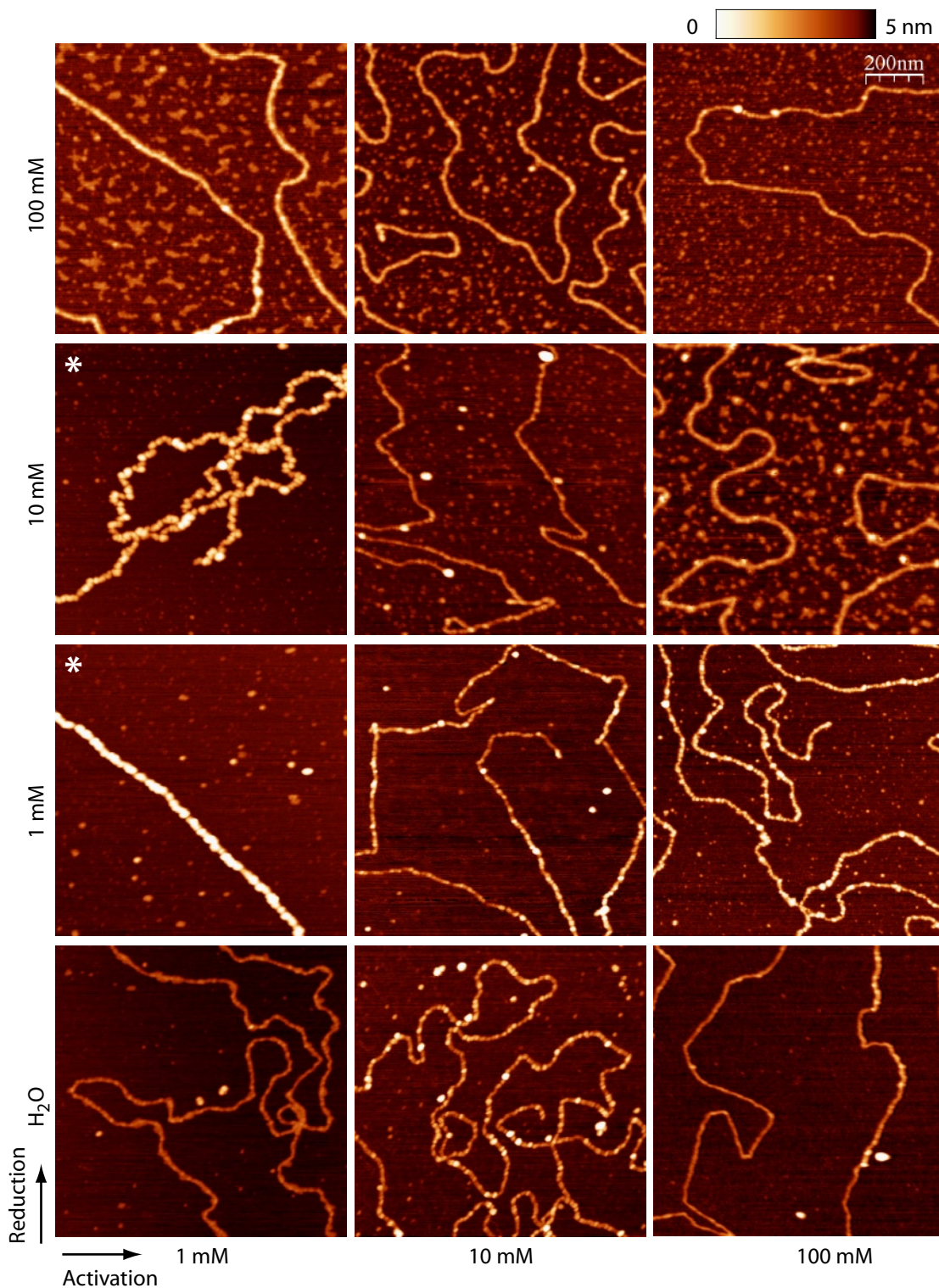


Figure 3.4: Representative AFM images of metalized λ -DNA on mica under different combinations of $\text{Pt}(\text{NO}_3)_2$ concentrations during activation and reduction. Concentrations increase from left to right during activation and from bottom to top for the reduction step. For better visualization the two starred images are scaled between 0 nm and 9 nm, whereas all the other images are scaled between 0 nm and 5 nm as shown in the z-scale colorbar. The scale-bar applies to all images.

3 Photoinduced Platinum Deposition on DNA Templates

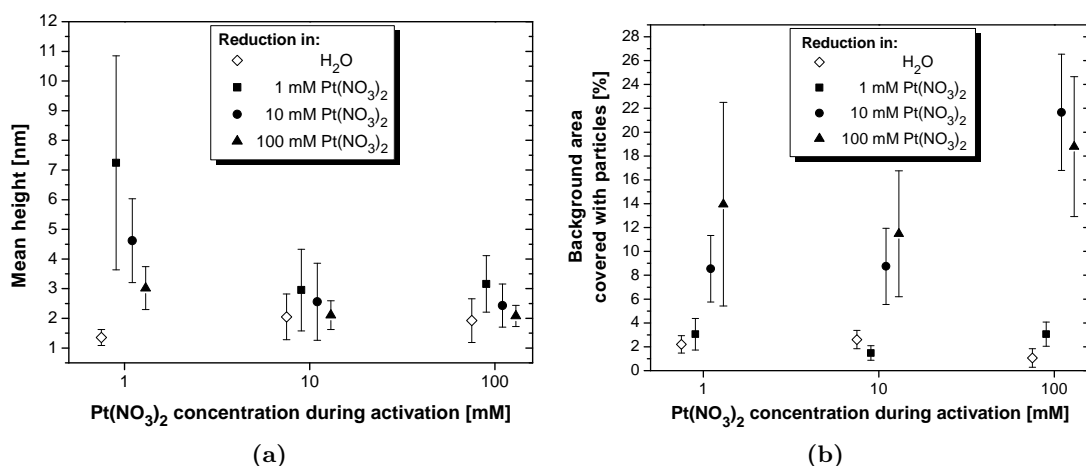


Figure 3.5: Analysis of AFM data for λ -DNA on mica under different combinations of $\text{Pt}(\text{NO}_3)_2$ -concentrations during activation and reduction. (a) Mean height of the cluster chain and (b) percentage of background area covered with particles as a function of the $\text{Pt}(\text{NO}_3)_2$ concentration during UV-reduction for three different $\text{Pt}(\text{NO}_3)_2$ concentrations during the activation step. Each data point is the averaged result of the Matlab-based image processing of about 30 $1\ \mu\text{m} \times 1\ \mu\text{m}$ AFM images on a sample of the particular set of reaction conditions. For all samples activation time was 5 h and reduction took place during 5 min of UV exposure at $10\ \text{mJ}/\text{cm}^2$.

background area are covered. This row of experiments thus represents kind of another reference, because in water only that amount of Pt-ions can be reduced that was bound to the DNA during activation time as there is no further platinum for an autocatalytic growth available during reduction in pure water. The determined mean heights mark a minimum height for the particular activating $\text{Pt}(\text{NO}_3)_2$ concentration which is reached without autocatalytic growth of the initially formed clusters by additional material available in solution. Provided a constant irradiated reduction energy and a further reducing potential of the DNA, i.e. DNA oxidation beyond the already reached level, then even larger clusters should be grown upon autocatalytic growth under $\text{Pt}(\text{NO}_3)_2$ concentration larger than zero.

As we now do not look line by line, but column by column at Figure 3.4 this assumption is not confirmed. In each column the $\text{Pt}(\text{NO}_3)_2$ concentration during activation is constant, and the one during the reduction step increases from 1 mM at the second row to 100 mM $\text{Pt}(\text{NO}_3)_2$ at the top row. A view on one column, e.g. the first one with 1 mM $\text{Pt}(\text{NO}_3)_2$ activation concentration where differences become particularly apparent, reveals the following features: from an enormous high strand of densely packed clusters at a1r1 and an equivalently compact particle chain even though of less height at a1r10 the appearance changes to a blurred particle chain surrounded by diverse other structures in the background at a1r100. Accordingly, a drop in the mean height of the cluster chain is determined at increasing $\text{Pt}(\text{NO}_3)_2$ concentrations in the film during UV irradiation, i.e. whereas the mean height at a1r1 averages to (7.2 ± 3.6) nm it is only measured to be (3.0 ± 0.7) nm at a1r100 (Figure 3.5a). At the same time the background area covered with particles is augmented from $(3.0 \pm 1.3)\%$ to $(14.0 \pm 8.5)\%$. These trends are the same

3.1 Platinum Cluster Chain Formation on DNA

for the other two rows of a10r1–100 and a100r1–100 and can possibly be explained by an increased uptake of light energy by the layer of higher concentrated $\text{Pt}(\text{NO}_3)_2$ solution that covers the surface-immobilized DNA (Figure 3.6b). In such a case less energy reaches the surface to excite the DNA there, whereas at the same time the high energy amount available in solution leads to an increased number of homogeneously nucleated particles that appear in the background. This supposition is in agreement with the results from cluster formation in the absence of DNA (Figure 3.1) and is endorsed by the observation, that an augmentation of $\text{Pt}(\text{NO}_3)_2$ concentration in aqueous solution highly intensifies the yellow tinge of the solution as a result of an increased absorbance in the visible blue wavelength range (Figure 3.6a). This absorbance is far above the upper detection limit of the UV/VIS spectrometer also at 254 nm wave length. In other words, a film of 10 mm thickness—the length of the light path in the used cuvette—is not transparent for light of 254 nm wavelength.

Another characteristic of the metallization process can be found by contrasting the lines of different reduction solutions in Figure 3.4 and drawing comparison between the sets of full symbols in Figure 3.5, respectively. It can be seen that for each concentration of the reduction solution the analyzed mean height as well as the measured height variations around that value decrease for increasing $\text{Pt}(\text{NO}_3)_2$ -concentrations in the activation step. This effect can be attributed to the increment of nucleation centers after the activation in a higher concentrated solution. That constant amount of platinum that

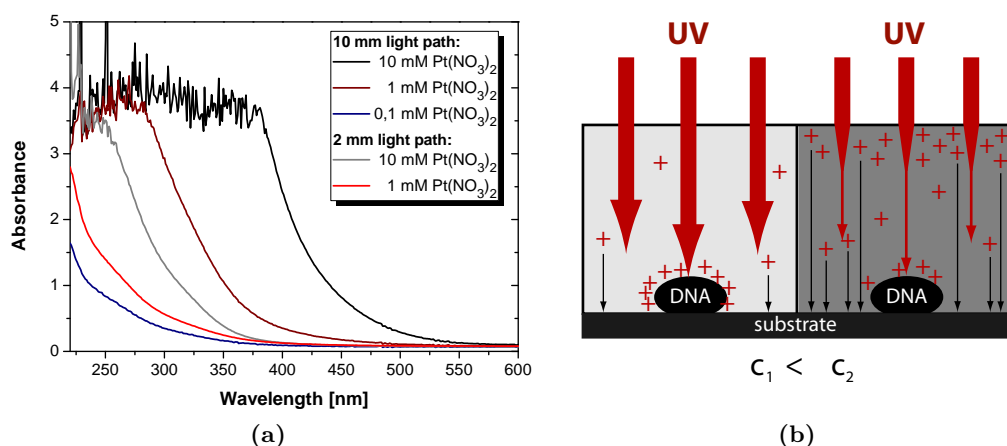


Figure 3.6: Absorbance of aqueous $\text{Pt}(\text{NO}_3)_2$ of different concentrations. (a) Absorbance spectra of $\text{Pt}(\text{NO}_3)_2$ solutions of different concentrations and for light path lengths of 2 and 10 mm, respectively. Absorbances higher than 2 are not reliable. (b) Scheme illustrating the effect of a lowly (left) and highly (right) concentrated $\text{Pt}(\text{NO}_3)_2$ solution sitting on the substrate during reduction. In comparison to the lowly concentrated $\text{Pt}(\text{NO}_3)_2$ for the highly concentrated solution a significant amount of the UV light is unspecifically absorbed in the top film layer resulting in intensified homogeneous nucleation in the solution followed by sedimentation to the surface and reduced UV exposure of the DNA at the substrate.

3 Photoinduced Platinum Deposition on DNA Templates

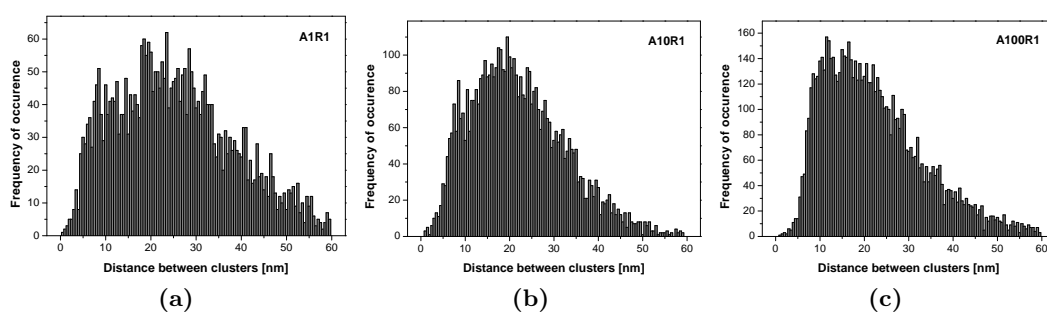


Figure 3.7: Histograms of measured metal cluster distances for reduction in 1 mM $\text{Pt}(\text{NO}_3)_2$ and activation in (a) 1 mM $\text{Pt}(\text{NO}_3)_2$, (b) 10 mM $\text{Pt}(\text{NO}_3)_2$ and (c) 100 mM $\text{Pt}(\text{NO}_3)_2$, respectively.

is grown autocatalytically from the solution under a particular irradiation intensity² is then evenly distributed to the number of nucleation centers, leading to overall lower, but smoother cluster chains at higher activation concentrations, e.g. (4.62 ± 1.41) nm at a1r10 and (2.43 ± 0.73) nm at a100r10. Also, the cluster distance distributions reflect this interpretation. Figure 3.7 shows three distributions of the distances between local maxima—particle summits—in the height profile along the cluster chain ridge. In the figure from left to right the $\text{Pt}(\text{NO}_3)_2$ concentration during the activation step, i.e. the number of nucleation sites, increases whereas all the samples were reduced in 1 mM $\text{Pt}(\text{NO}_3)_2$. The cluster distance distribution of a1r1 (Figure 3.7a) appears full of fissures, humps can roughly be seen at multiples of approximately 10 to 11 nm, which is the measured particle height (upper end of error bar in Figure 3.5a). For a10r1 and a100r1 these humps level out leading to smoother distributions with maxima at progressively smaller values. However, caution has to be exercised looking at the absolute height values for a10 and a100: although their maximum values obtained upon reduction (upper end of error bars in Figure 3.5a) are higher, the range of their mean values is only slightly higher than it is the case for DNA which was activated only. Besides the interpretation heading for an increased number of nucleation sites, this might also be another hint for a reduction of UV light energy getting through to the DNA. That is, not only a high concentration of $\text{Pt}(\text{NO}_3)_2$ in the reduction step hinders transmission, but also the saturation of DNA with platinum seeds might already block the UV irradiation of the biotemplate. Transmission electron microscopic investigations in Section 3.2 will throw light onto this problem.

One last, but perspicuous notice can be made: The amount of background nucleation (Figure 3.5b) is similar for each series of samples r0 to r100 (except for the outlier a100r10). However, this is necessarily the case, as the amount of dissolved platinum, which is available for homogeneous nucleation under constant energy input in the reduction solution, is constant throughout each series. Furthermore, the amount of background nucleation enlarges with increasing $\text{Pt}(\text{NO}_3)_2$ concentration in the reduction step, as

²Both, $\text{Pt}(\text{NO}_3)_2$ concentration during reduction and irradiation energy, are constant throughout each series of measurements.

3.1 Platinum Cluster Chain Formation on DNA

the amount of unspecific homogeneous nucleation in solution scales with its $\text{Pt}(\text{NO}_3)_2$ concentration (compare Figure 3.6b and Figure 3.1).

3.1.2 Influence of Other Control Parameters

Besides the platinum concentration in the activation and reduction process step two more parameters are variable and need to be optimized. This is first the activation time, necessary to densely load the DNA with potential initial nucleation sites, and second the UV exposure time and intensity, controlling the available amount of reduction energy.

In a first survey, the activation time t_A , which the droplet of 1 mM $\text{Pt}(\text{NO}_3)_2$ is allowed to sit on the surface with DNA before UV exposure, was varied between 1 min and 24 h. Subsequently, the different samples were irradiated for 5 min with UV light ($10 \text{ mJ}/\text{cm}^2$), analyzed by AFM and their mean DNA height and background area covered with particles measured. The outcome, displayed in Figure 3.8, is a set of virtually constant values, i.e. the mean height of the DNA molecules as well as the amount of homogeneously nucleated particles do not change with activation time. Thus, in the time range of one minute all possible binding sites are already saturated, that is activation is completed. Otherwise, if the binding kinetic was slower, with higher activation time an increase in height would be expected. Additionally, in consequence of this instantaneous binding one arrives at the conclusion, that for $\text{Pt}(\text{NO}_3)_2$ the activation time does not control the balance between homogeneous nucleation in solution and heterogeneous nucleation at the template, as the also for short activation time constantly low background metallization demonstrates.

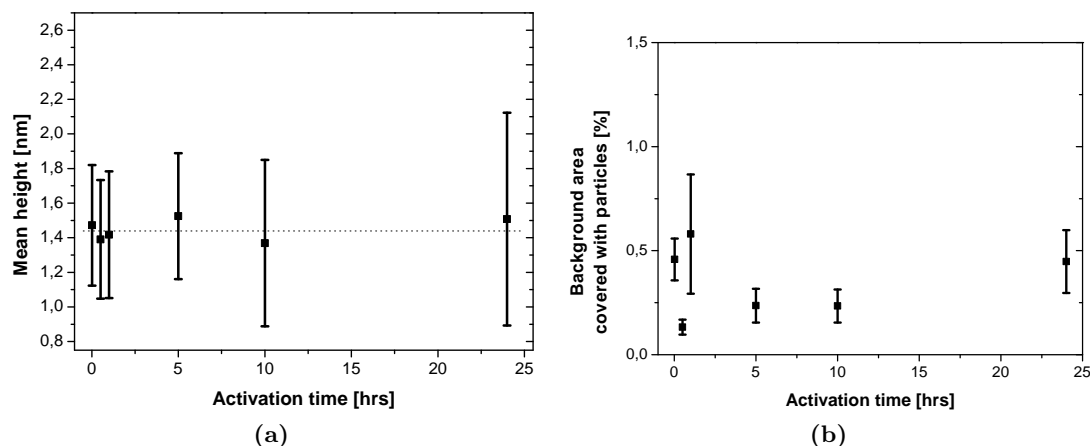


Figure 3.8: Characteristics of platinum cluster formation (a) on DNA and (b) in the background after different activation times. 1 mM $\text{Pt}(\text{NO}_3)_2$ was used for activation as well as reduction and the UV exposure parameters were 5 min and $10 \text{ mJ}/\text{cm}^2$.

In another series of experiments, the UV light exposure time and intensity were varied. In Figure 3.9 the resulting changes in the mean height of the DNA and the amount of background metallization are shown. The basis of this data is again a series of samples imaged by AFM and analyzed. The data illustrates, that the UV light intensity plays a less important role, as changes therein are neither reflected in the mean height of

3 Photoinduced Platinum Deposition on DNA Templates

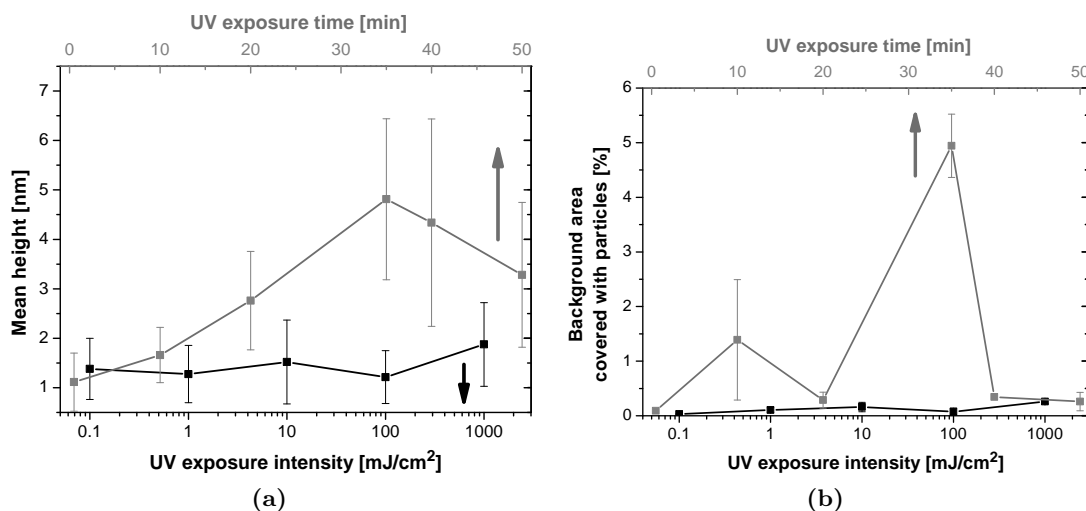


Figure 3.9: Effects of changes in the reduction parameters UV exposure time (gray symbols and lines) and intensity (black symbols and lines). For both series of samples activation time in 1 mM $\text{Pt}(\text{NO}_3)_2$ was 5 h, in case of changing the UV intensity the exposure time was set to 5 min, and for altering the UV exposure time the intensity was kept constant at 10 mJ/cm².

the DNA molecules (black symbols in Figure 3.9a) nor in the amount of background metallization (black symbols in Figure 3.9b). In other words, an enhanced irradiation intensity does not lead to an increased metallization of the template and at the same time also no augmentation of the homogeneous nucleation in solution can be detected (at least no increased number of clusters sediment on the sample surface).

In contrast, an extension of the UV exposure time from 30 s to 35 min results in a continuous heightening of the DNA (gray symbols in Figure 3.9a). For a further prolongation of the exposure the growth process seems self-limiting as no further increase in height is detected, but even a small decrease. Two reasons are thought to account for that: First, the DNA template has a stabilizing effect preventing the platinum clusters to grow beyond a certain size through aggregation with other clusters, which was shown for chemical reduction of K_2PtCl_4 in the presence of DNA [136]. Second, once the clusters have reached a critical size, they might stop UV light from reaching and photooxidizing the DNA, or platinum reduction might stop as soon as the DNA becomes completely photooxidized. Then as the result of a equilibrium reaction, some smaller clusters might dissolve from the DNA back into the solution leading to a decreased mean height for very long UV exposure. Furthermore, even if the reducing behavior of DNA diminishes for long UV exposure, no dominance of the homogeneous nucleation process is observed for that time domain, because again no augmented amount of background metallization was found (gray symbols in Figure 3.9b, the value at 35 min UV exposure time is considered as outlier).

3.1 Platinum Cluster Chain Formation on DNA

3.1.3 UV/VIS Spectroscopy

Ultraviolet/Visible (UV/VIS) spectroscopy is not only useful for determining DNA concentrations, but also for assessing DNA helix structure transitions e.g. due to melting, hybridization or association of metal ions/complexes with the bases, because this spectroscopic technique is sensitive to the arrangement of the bases. The underlying effect is called hypochromism and describes the decrease in absorption intensity of the closely packed bases in the ordered helix structure in comparison to single-stranded DNA, where base stacking is completely lacking. Thus, UV/VIS spectroscopy studies can demonstrate the formation of DNA-metal complexes associated with perturbations of the base stacking and witnessed from an increase in the UV absorbance intensity at 260 nm wavelength (A_{260}), where DNA shows an absorption maximum. In this way, BERTI *et al.* used the response of the 260 nm peak to notice the instantaneous formation of a DNA- Ag^+ complex upon mixing λ -DNA with AgNO_3 [144]. They observed an increase in the 260 nm absorbance maximum of about 0.08 (corresponding to 30% increase of the initial value). In similar studies with K_2PtCl_4 SEIDEL *et al.* also obtained an A_{260} increase of 0.06 (= 50%) as a result of PtCl_4^{2-} binding associated with distortions of the base stacking caused by tilted base planes [136]. Additionally, in both studies the absorbance increase comes along with a slight red shift of the DNA absorbance maximum.

To gain more insight into the interaction of $\text{Pt}(\text{NO}_3)_2$ with λ -DNA and to learn about the nature of the platinum species in solution UV/VIS absorbance studies were performed. For this, the DNA was incubated with 1 mM $\text{Pt}(\text{NO}_3)_2$ and complete absorbance spectra between 220 nm and 1000 nm were recorded over the incubation time to provide not only information about potential distortions in the base stacking upon binding of platinum

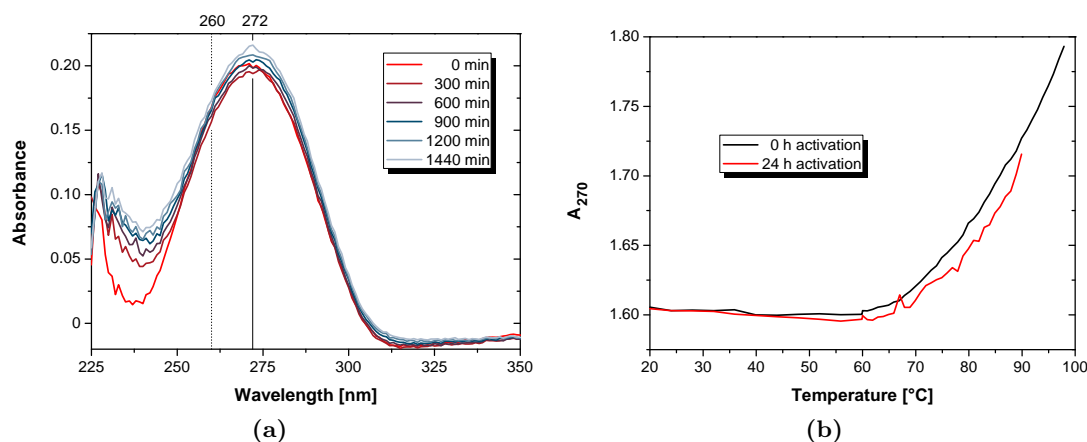


Figure 3.10: Response of the UV/VIS absorbance to association of λ -DNA with Pt^{2+} . (a) Time course of DNA incubation with 1 mM $\text{Pt}(\text{NO}_3)_2$. The spectrum of the pure 1 mM $\text{Pt}(\text{NO}_3)_2$ solution is subtracted from the spectra of the 1 mM $\text{Pt}(\text{NO}_3)_2$ solution containing 50 ng/ml λ -DNA obtained at different times after mixing. Note the red shift of the absorbance maximum to 272 nm due to the acidic character (pH 3.0) of the solution. (b) Melting curves of activated and non-activated λ -DNA. A 1 mM $\text{Pt}(\text{NO}_3)_2$ solution containing 38.5 ng/ μl λ -DNA was measured directly after mixing and 24 h after mixing, respectively.

3 Photoinduced Platinum Deposition on DNA Templates

ions but also about the time scale in which this takes place. Figure 3.10a shows the time evolution of the DNA spectrum, obtained as the difference between a series of spectra of a 1 mM $\text{Pt}(\text{NO}_3)_2$ solution containing 50 ng/ml λ -DNA and a reference spectrum of a 1 mM $\text{Pt}(\text{NO}_3)_2$ solution. (In a comparable time series it was ensured that the absorbance of a $\text{Pt}(\text{NO}_3)_2$ solution does not alter due to hydrolysis after the addition of an equivalent amount of buffer instead of λ -DNA.) First, it has to be noted in Figure 3.10a that there is a shift of the absorbance maximum from the expected 260 nm to 270 nm for $t_A=0$ min and further to 272 nm for $t_A=24$ h and accordingly of the minimum from 230 nm to 237 nm ($t_A=0$ min) and 240 nm ($t_A=24$ h). This is in agreement with the shift of both the maximum and the minimum to higher wavelengths measured by ZIMMER *et al.* for the pH of a DNA solution decreasing from 6.9 to 2.8 [156]. And in fact, a 1 mM $\text{Pt}(\text{NO}_3)_2$ solution has a pH of 3.0.

Furthermore, during the first 600 min of activation basically no changes in A_{270} occur, whereas for incubation times beyond that a slight increase is determined, e.g. the maximum absorbance rose by 0.014, that is 7%, in comparison to its initial value at 0 min. This is a considerably smaller increase than determined for Ag^+ and PtCl_4^{2-} complexation with DNA that induced altered orientations of the bases relative to the helix axis (*vide supra*). However, the question arises, whether the $\text{Pt}(\text{NO}_3)_2$ indeed interacts with the DNA bases and thus the detected absorbance increase is a sign of resulting base distortions or an electrostatic interaction of platinum ions with the DNA backbone can cause the conformational rigidity of the helix to ease and unwind the two strands as described for cationically surface modified Au nanoparticles of mass ratios greater than DNA:nanoparticle=1:5 [157]. Additionally, it has to be kept in mind, that the absorbance change around 270 nm may only indicate a conformational change from the DNA double helix structure to the disordered random coil in consequence of the low pH of 3.0 alone [156].

To answer the question and to conclude about the origin of the absorbance increase, melting transitions of a freshly prepared and a 24 h aged λ -DNA- $\text{Pt}(\text{NO}_3)_2$ solution were obtained by monitoring the UV light absorption at 270 nm wavelength, while the temperature of the solution was gradually increased. The resulting A_{270} -temperature sequence, typically called melting curve, gives the temperature required for the separation of two DNA strands as the midpoint of the transition (Figure 3.10b). If the interaction of $\text{Pt}(\text{NO}_3)_2$ with λ -DNA induces denaturation of the double strand, λ -DNA activated for 24 h in $\text{Pt}(\text{NO}_3)_2$ should exhibit a smoother melting curve with a lower melting temperature in comparison to λ -DNA which was just mixed with $\text{Pt}(\text{NO}_3)_2$ and for which no instantaneous A_{270} increase is observed (Figure 3.10a). Instead, Figure 3.10b reveals a rise in A_{270} at higher temperatures for the 24 h activated DNA. Although the experimental setup precluded the achievement of a plateau phase after melting and thus the determination of the exact melting temperature, the shift in the melting behavior to higher temperatures for activated DNA is distinct. Thus, due to the loading of λ -DNA with Pt-ions no denaturation occurs, but a strengthening of the double-strand as a result of the neutralization of the anionic DNA phosphate backbone by cationic Pt-ions. These findings harmonize with investigations of BLAGOI *et al.* [158] showing an increase in the

3.1 Platinum Cluster Chain Formation on DNA

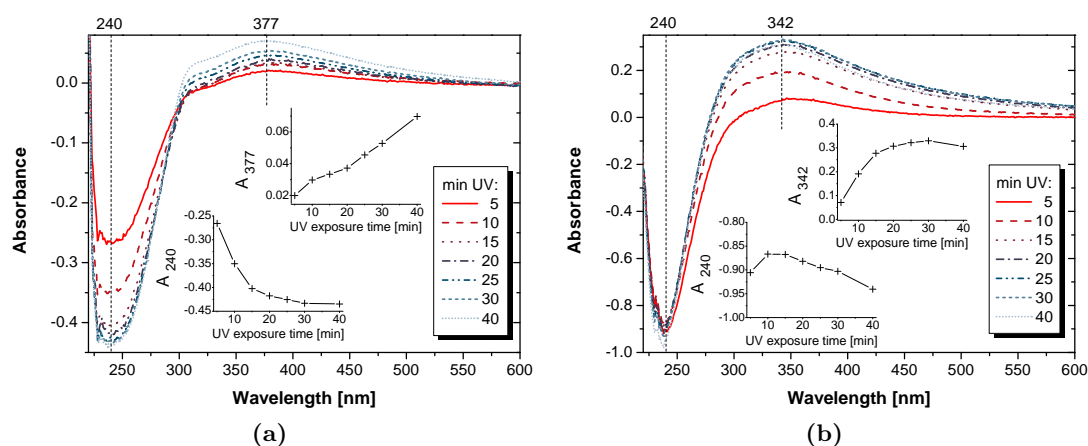


Figure 3.11: Effect of UV light exposure in the presence and absence of DNA. (a) Absorbance spectra of a 1 mM Pt(NO₃)₂ solution containing 50 ng/ml 24 h activated DNA upon UV light exposure. The insets show the time evolution of the absorbance at 240 nm and 377 nm. (b) Spectra of a 1 mM Pt(NO₃)₂ solution without DNA upon UV light exposure for comparison. The insets show the time evolution of the absorbance at 240 nm and 342 nm.

DNA melting temperature at elevated magnesium concentrations in the buffer with a maximum at 1 to 10 mM Mg²⁺.

Analogous to the evolution of the absorption spectra during activation the spectral changes upon UV-induced reduction were investigated. For this purpose, a glass cuvette transmissible down to wavelengths of 220 nm was filled with the solution of interest, so that for reduction the cuvette could be placed underneath the UV light source for a certain time and then the spectrum was measurable. These two steps were repeated. In Figure 3.11 the effects of UV light exposure on a 1 mM Pt(NO₃)₂ solution containing DNA (Figure 3.11a) and the same solution not comprising any DNA, but simply buffer instead (Figure 3.11b), are opposed. The general trends are similar in both curves with two transitions being noticeable. Distinct minima occur upon irradiation at wavelengths around 240 nm. Since for both series the initial spectra before UV exposure are subtracted, these regions of negative absorbance are a consequence of a diminishing absorbance in this range indicating the consumption of dissolved Pt(NO₃)₂ salt. At the same time a rather broad absorption band emerges between 300 nm and 450 nm. According to previous reports [159, 160], this absorption band is related to the surface plasmon resonance of platinum nanoparticles.

While the two sets of spectra are comparable with respect to the overall absorbances and the wavelengths of the transitions, essential differences were observed in the time evolutions of the transitions. They are extracted in the insets of Figure 3.11 for the minima and maxima positions. In the presence of activated DNA in solution the absorption intensity around 240 nm dramatically drops further after each of the first three exposure cycles and levels out for the subsequent 25 min of irradiation. Concomitantly, at 377 nm wavelength the spectral component from particle scattering increases only slowly in

3 Photoinduced Platinum Deposition on DNA Templates

that first time range and steepens thereafter, indicating an increase in the number of the nanoparticles in the solution [52]. In contrast, in the absence of any DNA the absorption intensity at 240 nm only slightly decreases with cumulative exposure duration. Furthermore, in the absence of DNA the 300–400 nm band shows converse behavior in comparison to the solution containing DNA, i.e. the peak increases drastically (and broadens slightly) in the initial 20 min of exposure but stays constant thereafter. Taking the above shown AFM investigations into consideration, which revealed particle formation along the surface-immobilized DNA template, the differences in the time evolution of the spectral features can be attributed to the heterogeneous nucleation at the biotemplate. Thus, in the range of 240 nm the absorbance does not only drop due to decreased unspecific absorption as a result of reducing platinum ions to metallic platinum. But in the solution containing DNA this effect overlaps with a decrease in intensity of the DNA absorption peak and only this leads to the dramatic fall in absorption, which is not present in the absence of DNA. As already observed for DNA templated formation of silver clusters [144, 161], the dipole coupling between the excited electronic states of the bases is altered by structural changes induced upon cluster formation and, as the nanoparticles grow, the absorptivity decreases. Not until this effect reaches completion, i.e. the valley at 240 nm as well as the DNA peak do not deepen significantly further after 15–20 min of UV irradiation, the homogeneous nucleation in solution dominates as indicated by the increase and broadening of the 380 nm band. In contrast, when there is no DNA at all in solution, the latter effect is the determining one from the very first UV exposure step on.

3.1.4 Discussion of the Cluster Formation and Growth Mechanism

In the preceding sections the formation of platinum cluster chains on immobilized double-stranded λ -DNA was studied in the dependence on the $\text{Pt}(\text{NO}_3)_2$ concentration of the solution applied in the activation and reduction step, the activation time and reduction energy and time. Investigations were carried out by AFM and UV/VIS spectroscopy. The results up to here can be summarized as follows:

1. Stable cluster chains with typically 2–4 nm—maximal 11 nm—high clusters are formed on immobilized λ -DNA molecules. The cluster chains can only be synthesized in the presence of DNA, proving that cluster nucleation takes place heterogeneously at the template that provides the reduction energy upon UV irradiation.
2. The height of the cluster chain is determined by two parameters: First, the amount of UV light penetrating the $\text{Pt}(\text{NO}_3)_2$ solution during reduction controls the growth of the platinum seeds. That is, the higher the $\text{Pt}(\text{NO}_3)_2$ concentration the more opaque the solution is, thus absorbing more UV light and reducing the amount available at the DNA on the surface. Second, the $\text{Pt}(\text{NO}_3)_2$ concentration applied during the activation step plays a role. Increasing the platinum load by allocating higher $\text{Pt}(\text{NO}_3)_2$ concentrations during activation resulted in a more homogeneous cluster coverage, rather than in the enlargement of individual clusters.

3.1 Platinum Cluster Chain Formation on DNA

3. Already in the time range of one minute DNA molecules are saturated with platinum ions which were present in large excess (estimated, on a $5 \times 5 \text{ mm}^2$ area with $3 \cdot 10^6$ adsorbed DNA molecules, covered by $15 \mu\text{l}$ of $1 \text{ mM Pt}(\text{NO}_3)_2$ there are $3 \cdot 10^4$ platinum ions per base). In consequence, that short activation durations are enough to result in preferential heterogeneous nucleation at the biotemplate, whereas no appreciable background metal deposition could be detected.
4. The slight distortion of the DNA structure upon activation in $\text{Pt}(\text{NO}_3)_2$ solution does not cause denaturation of the double-strand.
5. The $\text{Pt}(\text{NO}_3)_2$ concentration present in solution during UV irradiation determines the amount of homogeneous nucleation since 100 mM and higher concentrated $\text{Pt}(\text{NO}_3)_2$ solutions are virtually not transparent for UV light any longer thus inhibiting photooxidation of DNA and leading to precipitates from solution.
6. Consistent with the catalytic effect of the DNA template, the UV-induced reduction of platinum and the growth of platinum clusters is a self-limiting process. That is, DNA can only act as photooxidizer as long as the clusters themselves do not hinder the UV light in reaching the template. It should be borne in mind that a platinum nanoparticle of a certain size will reduce the incident flux of photons with enough energy to zero, i.e. the nanoparticle will act as a shield and block incident photons.
7. Reduction energies of 0.1 mJ/cm^2 are enough to initiate the photooxidation of DNA and reduction of bound platinum. Intensified UV irradiation neither leads to a dominance of homogeneous nucleation in solution nor accelerates the reduction process.

Although the formulation of a detailed mechanism on the molecular level for $\text{Pt}(\text{NO}_3)_2$ interaction with DNA as well as for the reduction process is not possible at this stage, it seems reasonable to assume that DNA bases act as photosensitizers due to their strong absorption in the range of 260 nm wavelength.

Concerning the binding of $\text{Pt}(\text{NO}_3)_2$ to DNA, from the above findings—mainly the constancy of the cluster height irrespective of short- or long-term activation—it is believed, that no complexation with or covalent binding to DNA bases is underlying, but an electrostatic interaction with the DNA backbone is present. That is, that the magnesium cations from the buffer—condensed by the phosphate groups in the DNA molecules until charge neutrality is achieved—are exchanged for platinum cations which are present in large excess during activation. To confirm the active role of the phosphate groups in the DNA, the sensitivity of the $\text{Pt}(\text{NO}_3)_2$ affinity to competing phosphate ions in solution was investigated. For this purpose, the activating $\text{Pt}(\text{NO}_3)_2$ solution was laced with a certain amount of phosphoric acid, thus introducing potential electrostatic interaction possibilities other than the phosphate groups in the DNA backbone for the platinum ions. In Figure 3.12 the results of such an experiment are displayed where the $10 \text{ mM Pt}(\text{NO}_3)_2$ solution during activation contained 0.07 mM to 7 mM phosphoric acid and the reduction took place in pure $10 \text{ mM Pt}(\text{NO}_3)_2$. With increasing H_3PO_4 concentration the AFM images reveal an accumulation of enlarging particles sitting on

3 Photoinduced Platinum Deposition on DNA Templates

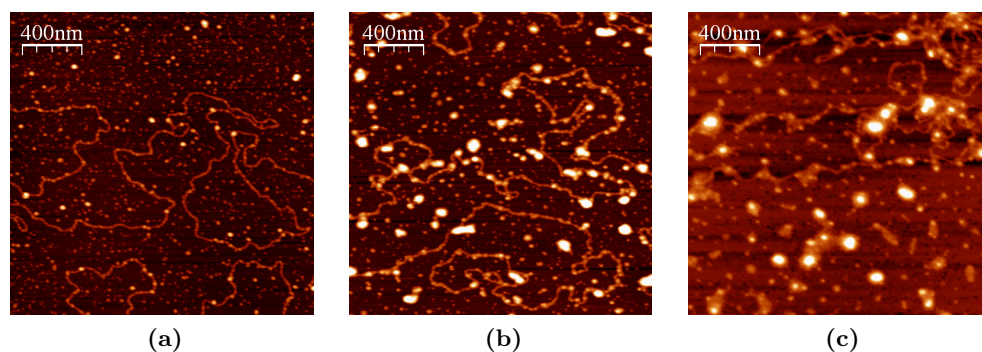


Figure 3.12: AFM height images showing the sensitivity of $\text{Pt}(\text{NO}_3)_2$ affinity to DNA under the influence of competing phosphate ions from H_3PO_4 . From left to right the concentration of H_3PO_4 in the activating 10 mM $\text{Pt}(\text{NO}_3)_2$ solution increases from 0.07 mM to 0.7 mM to 7 mM. Assuming $3 \cdot 10^6$ DNA molecules adsorbed to the substrate surface, that is a ratio of different deprotonated species of H_3PO_4 to PO_4^{2-} groups from immobilized DNA strands of about (a) $2 \cdot 10^3:1$, (b) $2 \cdot 10^4:1$, (c) $2 \cdot 10^5:1$. The z-scale is 0–10 nm for all images.

the DNA molecules or scattered on the substrate. This means that the PO_4^{2-} -derivatives from H_3PO_4 competing with the DNA result in an increased amount of homogeneous nucleation because at constant $\text{Pt}(\text{NO}_3)_2$ concentration comparatively less platinum ions are available at the DNA for a preferential heterogeneous nucleation and autocatalytic growth there. This in turn implies that the PO_4^{2-} groups in fact play an active role in the binding behavior of $\text{Pt}(\text{NO}_3)_2$ to DNA.

3.2 Investigation of Continuity of Cluster Chains

The morphological changes from an extended thread outlined smoothly on the surface to a chain of particles, which DNA undergoes upon its metallization could be nicely visualized and analyzed by means of AFM. However, the method is not sufficient to fully characterize the metallization result as on the one hand it does not allow for a determination of the material of the particles and their crystallinity. On the other hand and more crucial, as the radius of curvature of the AFM tip is comparable to the size of the metal particles to be imaged, tip broadening arises which prevents reproduction of gaps between the particles of about 5 nm or less. But the identification of potential gaps, i.e. discontinuities, in the cluster chain is of great importance for an application of the chain as a continuous electric conductor. Hence, TEM is here applied in order to visualize the metal clusters and potentially their lattice fringes as well as to investigate the continuity of the cluster chains, i.e. answer the question if the single clusters are in contact or appear separated. The drawback is the transparency of native DNA itself, formed of light organic molecules making it invisible in TEM.

3.2 Investigation of Continuity of Cluster Chains

3.2.1 Analysis by Transmission Electron Microscopy

To answer the question concerning the chain continuity left open from the AFM studies the sample preparation protocol has to be adapted in such a way, that it is applicable for TEM but maintains those conditions that came out on top in the AFM survey. At the best, that culminates in correlative studies, where samples of identical metallization procedure can be investigated “one-to-one” by AFM as well as by TEM.

The essence of such a method is to treat a supporting surface—in TEM commonly a thin carbon coated polymer film—such that it will adsorb and disentangle λ -DNA from solution but not interfere with the metallization thereof. Commonly applied spreading methods involve a carrier protein like cytochrome c which wraps around the DNA. As a result, individual DNA molecules are embedded and spread out in a monolayer of denatured protein [162]. This is an undesirable initial state for a subsequent metallization. Thus, staying with low-background and stable carbon supported polymer films at the beginning, it was tried to render the surface of carbon supported polymer films suitable for direct adsorption of λ -DNA by exposing the carbon coated grids to a nitrogen (or “air”) plasma in a SPI Plasma Prep II Plasma Etcher for 20 s [163]. It is thought to generate charges on the surface of the carbon film, at least the wettability is improved to a great extent. In this way, samples are prepared by placing a small droplet of DNA solution containing 10 ng/ml λ -DNA onto the plasma treated grids. After 5 min adsorption, the grids are washed on distilled water and a droplet of $\text{Pt}(\text{NO}_3)_2$ solution is deposited for activation and UV light-induced reduction like on mica.

However, the adsorption efficiency under these conditions is very low and a reasonable number of molecules was very rarely observed. Even harsher methods like plasma treatment of the grids in an oxygenated atmosphere, higher initial DNA concentrations and longer resting times for adsorption to the grid, respectively did not help and screenings with different metallization parameters were impossible being in need of a certain number of molecules for statistics. Anyhow, some successful examples are shown in Figure 3.13. Micrometer long dark threads contrast with the granular background (Figure 3.13a), which a view on a smaller scale (Figure 3.13b) reveals as densely packed bands of metal clusters with diameters of 3 to 5 nm. Along the band the clusters are compactly adjoined on widths of 5 to 12 nm whereas elsewhere on the grid particles are randomly arranged and lie widespread. High resolution transmission electron microscopy (HRTEM), which is able to resolve the lattice planes of the formed clusters (Figure 3.13c) confirms the monocrystalline character of the clusters. In agreement with the unit cell parameter of bulk platinum of 3.92 Å the distance between two adjacent lattice planes in the inset of Figure 3.13c is 4.0 Å. In Figures 3.13c and 3.13d one can furthermore see, that the clusters are partly grown together, connected via grain boundaries, thus resulting in shapes of the clusters not inevitably spherical, but also oval or kidney-shaped. However, no long-range coalescence is observed. Instead, the main part of the clusters in the chain are separated from their neighbors by gaps of about 1 to 2 nm size. Thus, no continuous wires are formed. Interesting is also the defined edge of the cluster band, indicating that the growth proceeds along the DNA.

3 Photoinduced Platinum Deposition on DNA Templates

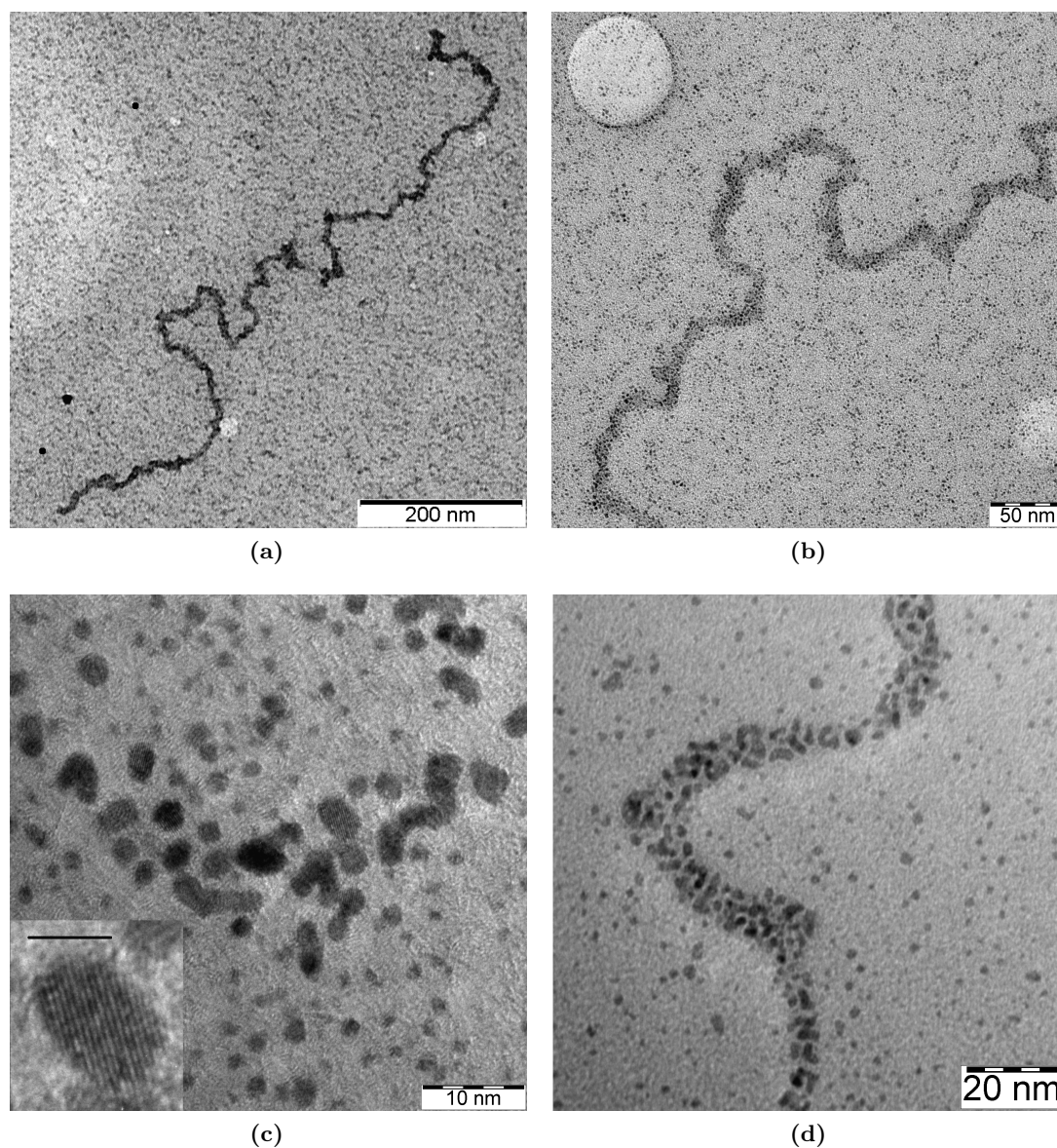


Figure 3.13: Pt cluster formation on λ -DNA adsorbed to plasma treated grids. (a) Large-scale TEM micrograph on a cluster chain formed on a carbon film by 5 h activation with 10 mM $\text{Pt}(\text{NO}_3)_2$ and subsequent exposure to UV light for 5 min at $10 \text{ mJ}/\text{cm}^2$ with 1 mM $\text{Pt}(\text{NO}_3)_2$ present. (b) Small-scale view on the same grid. (c) HRTEM image of the cluster chain. The scale bar in the inset is 2 nm. (d) TEM micrograph of a similar experiment (A1R1) performed on a silicon oxide film.

Another promising method for DNA adsorption to TEM grids involves positively charging the support films by submitting them to glow discharge in an ammonia gas flow [164], thus generating a surface functionalized with NH_2 -groups. On formvar[®]

3.2 Investigation of Continuity of Cluster Chains

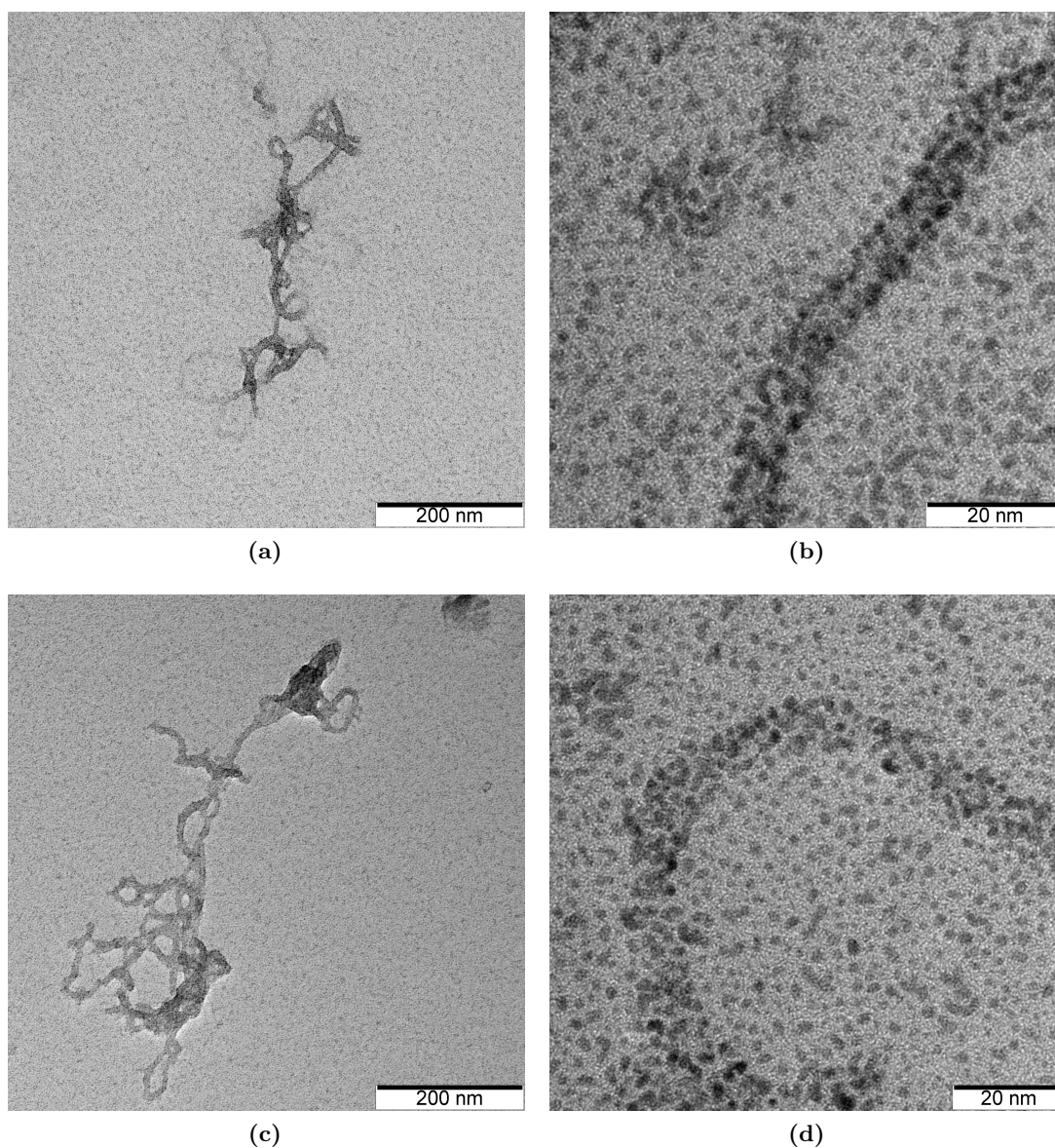


Figure 3.14: Pt cluster formation on amino-functionalized formvar grids. (a) Large-scale and (b) detailed TEM micrograph of a λ -DNA molecule metalized under A1R1. (c) and (d) show corresponding results for A100R1.

(polyvinyl formal) and pioloform[®] (polyvinyl butyral) grids treated that way³ samples were prepared essentially in the same way as described for the carbon grids. This time a reasonable distribution of molecules is observed in TEM, allowing for the correlation of different metallization conditions in analogy to the AFM investigations above. This was

³Obtained from Mirko Nitschke, IPF Dresden.

3 Photoinduced Platinum Deposition on DNA Templates

done in Figure 3.14, where the results on formvar following activation in 1 and 100 mM $\text{Pt}(\text{NO}_3)_2$ and subsequent reduction in 1 mM $\text{Pt}(\text{NO}_3)_2$ are compared⁴. Large-scale views (Figures 3.14a and 3.14c) reveal, that the again densely packed cluster bands are not well extended and appear tangled. This is the result of the strong interaction between the negatively charged DNA backbone and the positively charged grid surface, which leads—despite reducing the adsorption resting time to 5 s only (in comparison to 5 min on carbon)—to a direct attachment of the still partly coiled molecules from solution and less disentanglement. But it also nicely proves the templating effect of the DNA as the cluster band follows the twisting of the DNA strands. A closer look (Figures 3.14b and 3.14d) unveils cluster bands of equal widths, namely 15 nm, and particles of about 5 nm in diameter, the same size as on carbon supports.

In summary it has to be stated that the TEM investigations up to this point do not reveal an essential difference in metal cluster size between low or high $\text{Pt}(\text{NO}_3)_2$ concentrations during activation which would be in correspondence to the large difference in heights measured by AFM. Nonetheless, the observation of a defined band of small clusters supports the concept of a large number of nucleation sites along the DNA for high $\text{Pt}(\text{NO}_3)_2$ concentrations where reduction simultaneously takes place. However, for low $\text{Pt}(\text{NO}_3)_2$ concentrations no reduced number of larger clusters was found in agreement to a height increase in AFM and a decreased number of nucleation sites where cluster growth concentrates to. Additionally, the surface, where the DNA is attached to prior to metallization, seems to play a decisive role, especially in regard to the amount of background metallization.

3.2.2 Correlated AFM/TEM Study

A final investigation by AFM—capable to image DNA and metal clusters simultaneously, but tip convoluted—and TEM—revealing the actual morphology of the cluster chain—under identical preparation conditions, eliminating all unfavorable influences thereof, can only be done by so-called *correlated* microscopy. That is, to image identical samples with both techniques. In consequence, this means to image the result of DNA metallization on a mica support by TEM, as a mica surface features the best compromise between strong physisorption of DNA molecules with sufficient disentanglement and additional the lowest amount of background metallization. Moreover, it was considered possible to cleave mica by a repeated peeling-off process into a film comprising only a few single layers, possessing a thickness of 10 Å each [165], which can then be transferred to the TEM on a grid support and which is transparent therein. However, despite of the recent effort in exfoliating graphite into monolayers of graphene and other materials like boron nitride and dichalogenides into atomic layers [166], the application of this cleavage technique to mica did not result in layers the electron beam in the TEM could sufficiently shine through.

Thus, the direct visualization of metalized DNA on mica by means of TEM was not possible and a method had to be found to replicate the result in such a manner that it

⁴The same results were obtained on amino-functionalized pioloform grids.

3.2 Investigation of Continuity of Cluster Chains

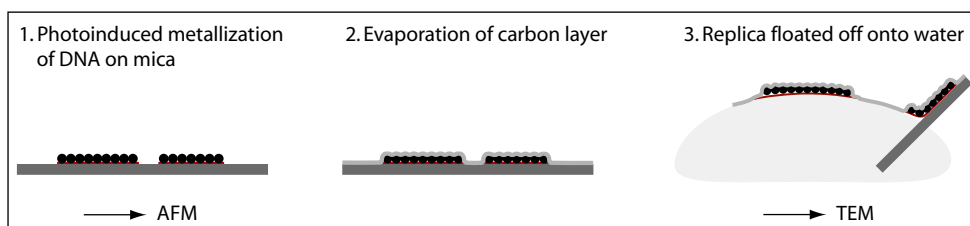


Figure 3.15: Illustration of carbon replica technique.

can be investigated in the TEM. For exactly this purpose the “carbon replica” technique was developed already in the 1980s. There, after adsorption to mica the native DNA is replicated by shadowing with a heavy metal and a carbon layer is evaporated in order to float the replica off the mica onto the surface of a distilled water droplet from where it can be picked up on a grid [167]. For a DNA template already decorated with platinum clusters upon metallization the carbon replica technique reduces to a relocation process making use of the floatable carbon layer that directly “peels” the cluster chain off the mica and allows for a one-to-one image instead of a replica (Figure 3.15). Hence, it should be possible to image the cluster chains visualized by AFM in Figure 3.4 (page 67) by TEM and settle the question of their cluster morphology and the continuity of the chain.

Figure 3.16a contains as an intermediate result an AFM micrograph of the mica surface upon carbon evaporation but before floating. The carbon layer is disrupted at this position so that the unwrapped metallized DNA molecules on the surface (left) as well as the covered metallized DNA molecules can be seen. The height profile perpendicular to the carbon layer edge (inset in Figure 3.16a) reveals a step of about 8 nm height which represents a carbon layer thickness comparable to commercially available films. Additionally, after floating-off and deposition on grids the self-made films exhibit a low contrast, i.e. the details of the specimen dominate the image, and high mechanical stability under the electron beam in the TEM. This allows the visualization of DNA molecules activated and reduced under different conditions on mica and transferred to the carbon film. Native λ -DNA is in principle invisible, only insufficiently washed samples with accumulations of buffer salt ions along the molecules give very low contrast. This is the same for DNA molecules where platinum ions were bound to in the activation step, but which were not reduced to metal clusters. Figure 3.16b shows such a TEM micrograph, revealing the DNA molecules as dark threads on which darker spots of maximal 1 nm diameter are sporadically situated (marked with arrows in Figure 3.16b). The spots are assumed to be first metal clusters—in accordance to the isolated brighter regions on the DNA in the AFM images of Figure 3.2 (page 64)—although it is impossible to resolve lattice planes of such small crystals of only about 10 atoms. Interestingly, also no further metal clusters are detected to appear on the attempted platinum reduction upon irradiation with the electron beam of the TEM.

Metal clusters arranged in loosely chains and larger in size, namely of up to 5 nm diameter, are determined for carbon replicas after UV-induced reduction (Figures 3.16c

3 Photoinduced Platinum Deposition on DNA Templates

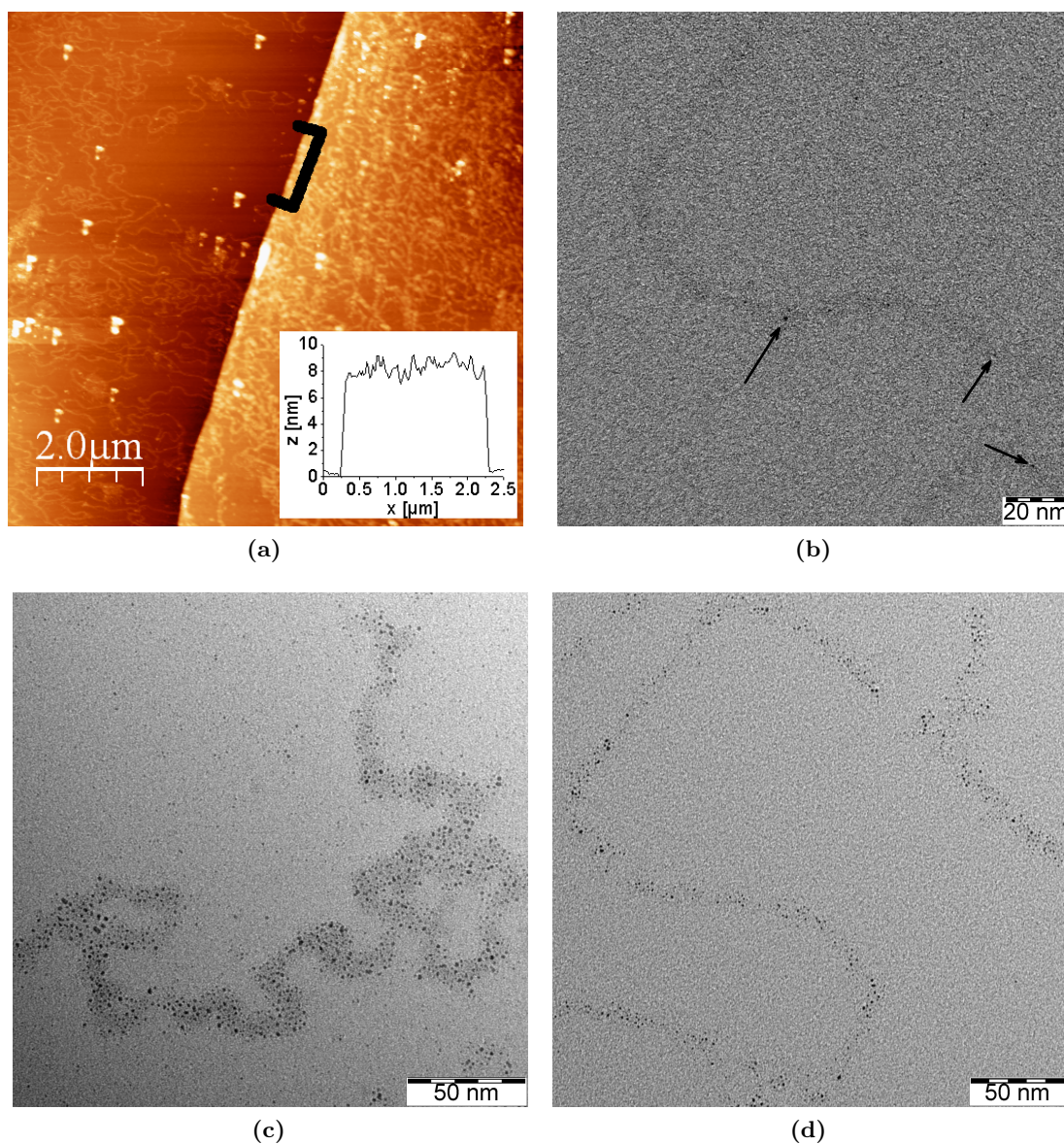


Figure 3.16: Carbon replicas of λ -DNA initially immobilized and metalized on mica. (a) AFM micrograph on mica before floating. The edge of a disrupted carbon film (right) runs through the image exposing the uncovered λ -DNA molecules on the left and allowing for the determination of the carbon film thickness of 8 nm in the height profile (inset) along the black line. z -scale: 0–15 nm. (b) TEM micrograph of a carbon replica of λ -DNA which was only activated in 10 mM $\text{Pt}(\text{NO}_3)_2$ and not reduced. (c),(d) TEM micrographs of transferred cluster chains metalized under (c) A1R1 and (d) A100R1, respectively.

and 3.16d), that is, replicas of exactly those samples which were examined under the AFM first in Section 3.1.1 (Figure 3.4). But it also has to be stated, that (i) both replicas of A1R1 and A100R1, respectively, show clusters of similar size. That is, the

3.3 Conclusion on Photoinduced DNA Metallization

assumption is not confirmed, that lower $\text{Pt}(\text{NO}_3)_2$ concentrations during activation lead to larger clusters than higher concentrations do. (ii) The loosely cluster chains do not meet the expectations from the AFM images, especially the thereby determined height of (7.2 ± 3.6) nm for A1R1 can not be explained with such a “porous” structure of much smaller clusters. An incomplete transfer of the platinum cluster chains from the mica surface to the carbon film can be excluded because no remains therefrom can be detected by AFM on the mica after the carbon layer was floated off. Only during the mechanically demanding floating and fishing procedure clusters can get lost that are not firmly tied to the carbon layer and therefore dissolve in the water reservoir. (iii) In contrast to the above investigations with direct immobilization and metallization of the DNA on the TEM grid, but in agreement with the preceding AFM investigations, only sporadically clusters appear in the background besides the chains.

In summary, the carbon replica technique turned out to be an appropriate method to relocate large features like DNA strands from a mica surface to a carbon film, but it is inefficient in transferring small discontinuous objects like the metal clusters of about 5 nm size. Thus, a confirmation of differences in cluster size depending on activation conditions failed and future efforts should strive again for the preparation of transparent mica support layers.

3.3 Conclusion on Photoinduced Platinum Deposition on DNA Immobilized on a Surface

Although the formulation of a detailed mechanism is premature at this stage, it seems reasonable to assume that DNA bases act as photosensitizers, thanks to their strong absorption in the UV. Thus, platinum ions from an aqueous $\text{Pt}(\text{NO}_3)_2$ solution bonded electrostatically to the backbone of surface-immobilized DNA in an activation step can be reduced upon irradiation with UV light of 254 nm wavelength. Initially heterogeneously formed platinum seeds at the biotemplate, then grow into larger clusters in an autocatalytic process. For the cluster height, a range between 2 and 5 nm was routinely observed, but also elevations of up to 11 nm were detected. These differences result from an involvement of the $\text{Pt}(\text{NO}_3)_2$ solution covering the sample surface during the UV exposure. Increasing its concentration from 1 to 100 mM $\text{Pt}(\text{NO}_3)_2$ leads to a solution quasi nontransparent for light of 254 nm, thus inhibiting the irradiation and photooxidation, respectively of DNA and causing homogeneous nucleation in the solution instead. However, even when low concentrations of $\text{Pt}(\text{NO}_3)_2$ are applied, TEM investigations revealed no continuous cluster chains, but gaps of 1–2 nm were observed between the platinum clusters.

3.4 Metallization of DNA Tubes

The above shown studies have used only double-stranded DNA. Such templates based on simple double-stranded DNA provide structures with limited diversity and less fine control of associations compared with the programmable superstructures described in Section 1.6.

3 Photoinduced Platinum Deposition on DNA Templates

One aim of further development of these tile and lattice structures is their use as templates on which to organize desired patterns of materials other than DNA, for example, chemical groups, nanoparticles, nanorods, carbon nanotubes, and proteins. Such DNA templates may be useful as “pinboards” for the creation of nanoelectronic circuits. However, to provide electric current transport between the elements on the scaffold, these complex DNA structures have to be metalized as well and the question arises how a metallization procedure like the above described one affects the DNA superstructure. Thus in the following, as a model system the photoinduced platinum deposition on DNA nanotubes assembled from one DNA single-strand [90] is investigated. DNA nanotubes also represent a novelty in the self-assembly of nanometer-scale electric circuits because in comparison to “floppy” dsDNA their higher stiffness promises easier handling, i.e. positioning between two specific locations. At the same time the dimensions of these nanotubes are also perfect suited for applications involving interconnection of molecular-scale devices with macroscale components fabricated by conventional photolithography.

3.4.1 Verification by Transmission Electron Microscopy

The self-assembled DNA nanotubes described here were formed by annealing a solution of single-stranded DNA [90] containing only one type of 52-nucleotide long strands (Figure 1.18c). Analogous to the metallization of double-stranded DNA, after adsorption to a substrate the DNA nanotubes were metalized using the two-step procedure consisting of 5 h activation in a 1 mM $\text{Pt}(\text{NO}_3)_2$ solution and UV light irradiation (5 min at

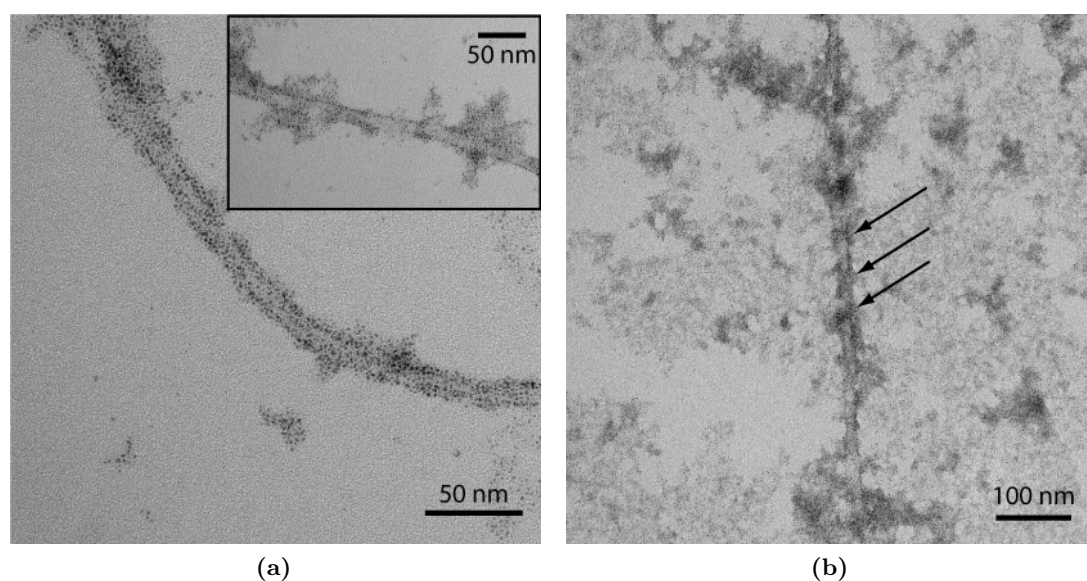


Figure 3.17: TEM micrographs of photoinduced platinum deposition on single-stranded DNA tubes. Note the partial wrapping of the tubes in (a) and the carpet-like depositions in the background of (b). The immobilized tubes had been activated for 5 h in 1 mM $\text{Pt}(\text{NO}_3)_2$ and were reduced therewith for 5 min at $10 \text{ mJ}/\text{cm}^2$.

3.4 Metallization of DNA Tubes

10 mJ/cm²). Figure 3.17a shows a TEM micrograph of a metallized nanotube in which one can see the tubular structure of the underlying template. In contrast to the cluster band on double-stranded DNA (Figure 3.13b) here the centerline of the cluster band is not winding but straight due to the increased stiffness of the tubes. Also, the cluster band is confined by a darker edge as a result of the higher amount of metal transmitted along the tube walls. With a very low background level of homogeneously nucleated platinum the metallization is restricted to the DNA structure, i.e. it is very selective and results in clusters of about 3 nm diameter, separated by gaps of similar size on a width of 15 nm and lengths of up to 20 μ m.

But many DNA tubes show accessory matter which seems to laterally grow out of the tubes (inset in Figure 3.17a) or is wrapped around the tube with a certain chirality (arrows in Figure 3.17b). Additionally, Figure 3.17b also shows areas of flat lattices, that are metallized as well. As it was shown above that the photoinduced formation of platinum clusters takes place selectively on the DNA structure, the interpretation of this data is that the nanotubes rip up or become opened into a flat lattice during the metallization, i.e. either due to the binding of the platinum species during activation or as a result of photodamage from UV irradiation.

To investigate this suspicion UV/VIS spectra were recorded during activation. These are discussed in the following.

3.4.2 UV/VIS Investigation of Metal Salt-Tube Interaction

The incubation of an annealed DNA tube solution with 1 mM aqueous Pt(NO₃)₂ was monitored by UV/VIS absorbance spectroscopy. In Figure 3.18 the time evolution of the spectrum is shown for the first 20 h after mixing. It reveals a quite different time dependence than in the case of double-stranded DNA where a steady increase in absorbance was observed. Instead, in the presence of DNA nanotubes a quite large

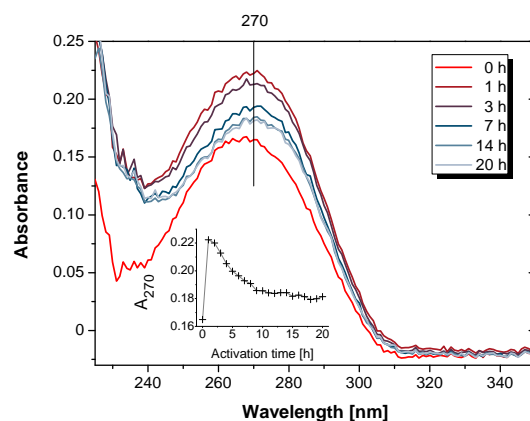


Figure 3.18: UV/VIS spectral evolution during activation of single-stranded DNA tubes with 1 mM Pt(NO₃)₂. The spectrum of the pure 1 mM Pt(NO₃)₂ solution is subtracted from the spectra of the 1 mM Pt(NO₃)₂ solution containing the tubes obtained at different times after mixing. The inset shows the time evolution of the absorbance at 270 nm.

3 Photoinduced Platinum Deposition on DNA Templates

absorbance increase at 270 nm by 34.5% is detected after the first hour of activation. But in the following 13 h the absorbance decreases again and balances at a lower level still above the original value right after mixing (compare inset in Figure 3.18) and stays constant for times larger than 14 h.

Knowing the TEM results, this spectral evolution is attributed to a detachment of single DNA strands out of the tubular assembly leading to a hyperchromic shift at 270 nm (acidic character of the solution) as some tubes denature. As each loosened segment is a palindrome, thus self-complementary, with progress in time two single-strands will reassociate with each other to form a two-stranded complex again, i.e. base stacking is partially recovered leading to a decrease in absorbance at 270 nm. If the complexes will further assemble through hybridization between their single-stranded overhangs in the resulting 2D lattices even more double-stranded structure with a regular base stacking is recovered, thus the absorbance falls further but does not reach the original level of the tube solution with the greatest extend of order. This behavior agrees well with the results of melting and renaturation studies of SOBEY *et al.* [168], who determined that assembly occurs in several hierarchical steps related to the formation of tiles, lattices and tubes, whereas melting of DNA nanotubes appears to occur in a single step.

3.5 Conclusion on Photoinduced Metallization of DNA Tubes

By TEM analysis it was shown that the photoinduced metallization of DNA tubes in principle is possible. That is, platinum clusters of 3 nm diameter are selectively formed on the complex DNA structure. However, the DNA nanotube structure denatures to a not inconsiderable extent due to interaction with the metal salt. This might be encouraged by the many open spots in the non-ligated backbone of the tubular construct. So for the metallization of DNA constructs of higher complexity than a double-strand, one starting-point for the further investigation is the use of ligated assemblies. Additionally, melting studies lead to a better understanding of the many factors that affect the assembly process or lead to a dissociation induced for instance by metal ions and complexes. In accordance to the studies of SOBEY *et al.* [168] it is suggested to perform DNA tube melting and renaturation in the presence of metal salt and to compare this curves from activated and non-activated DNA tubes. The results will not only be essential for the assembly of increasingly complex DNA nanostructures but also for their suitability for the bottom-up assembly of nano-scale electric circuits.

4 DNA Nanowire Fabrication

In the preceding two chapters at the one hand the successful bridging of electric contacts by DNA molecules was shown and on the other hand the DNA-templated photoreduction of platinum ions was reported to achieve strings of platinum clusters in a simple, rapid and effective way. The need for a combination of both techniques, that is the need for the application of the latter not only to randomly surface immobilized DNA molecules but to such molecules that were specifically integrated into electrode structures for the purpose of serving as electric conducting interconnection shall be demonstrated with an experiment.

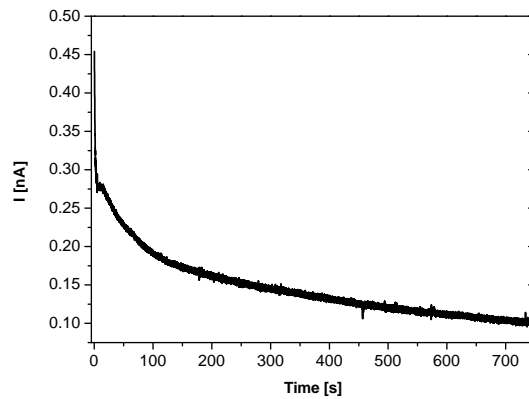


Figure 4.1: Time evolution of the electric current in a 4 μm wide finger electrode gap upon application of a 5 V voltage after the gap is bridged by about 180 DNA molecules.

The time evolution of the electric current running between two neighboring electrodes was measured after the flow mediated stretching and binding of thiol-functionalized DNA molecules in between them.¹ As shown in Figure 4.1 after capacitive contributions fade away with time the current levels out to 0.06 nA at an applied voltage of 5 V. Furthermore, it has to be considered that this is the current through a parallel connection of several DNA molecules. Staining the DNA with YOYO-1 after the electricity measurement allowed for the enumeration of the actual number of molecules N in the measured gap which equaled to 180. Thus, the resistance of a single DNA molecules can be calculated by $R_{DNA} = N \cdot R_{total} = N \cdot V/I$ and results in a value in the range of T Ω . This resistance is too high for a reasonable use as electric conducting wire and necessitates the deposition

¹With the existing experimental setup around the Source-Meter Unit (Keithley 2602), the measurement of current-voltage characteristics, i.e. the relationship between the dc current through the gap and the dc voltage across the electrodes, is not reasonable for currents on the scale of pico amperes due to the high influence of capacitive effects.

4 DNA Nanowire Fabrication

of a thin continuous metal cover along the DNA molecule for a reduction of the resistance. Thus, in this chapter first the DNA-templated photoinduced platinum reduction is utilized on DNA molecules that bridge the gaps in an interdigital electrode array after a preceding stretching step using hydrodynamic flow. It should be anticipated at this point, that the application of the reduction protocol with the parameters optimized on a mica surface (Chapter 3) onto other substrates like glass and silicon carrying the electrodes does not lead to the same optimal results, that is *conducting* DNA-templated platinum nanowires. A discussion and experiments giving hints for possible reasons for that therefore rounds of this chapter.

4.1 Photoinduced Metallization of Integrated DNA Molecules

Up to here the synthesis of platinum cluster chains along randomly adsorbed DNA molecules has been shown. But now, the DNA networks obtained by hydrodynamic flow stretching provide the basis for the metallization procedure. That is, the end of the flow-mediated stretching operation is not followed by a fluorescence staining of the integrated molecules but by the dismounting of the substrate from the flow cell, a washing step in distilled water and the application of 30 μl of $\text{Pt}(\text{NO}_3)_2$ solution for activation. Subsequent to 5 h activation time, the sample is UV exposed and finally washed. AFM imaging thereafter unveils linear chains of metal clusters oriented perpendicular to the electrode stripes (Figure 4.2a). This means, that the platinum clusters are selectively deposited on the DNA molecules which were aligned in the direction of flow across the

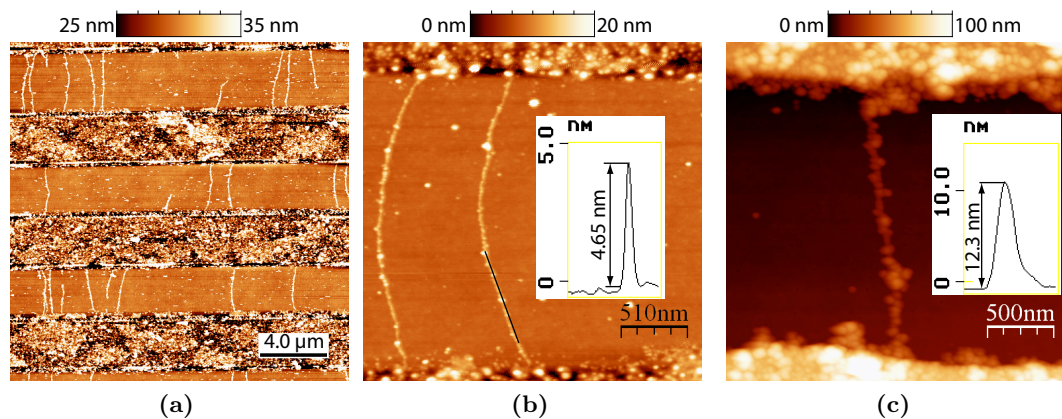


Figure 4.2: AFM images of metallized DNA networks. (a) Overview of a subarea of the electrode array. Note the bending of the molecules and the few molecules stripped off the electrodes with one of their ends. Metallization parameters were (a),(b) A1R1 with 40 min UV exposure time at 10 mJ/cm^2 and (c) three times repetition of A1R1 with 20 min UV exposure time at 10 mJ/cm^2 each. The insets show the averaged height profile of the metallized DNA molecule along the black lined section in (b) and of the whole molecule in (c).

4.2 Towards Electric Conductivity Measurements

electrodes. Also a bending of the cluster chains can be seen resulting from a shear flow emerging during dismounting of the substrate from the flow cell and nicely affirming again the strong and solely end-specific attachment of the T-DNA-T to the gold electrodes. Moreover, a DNA bridge itself rather breaks than the anchorage does as the few ruptured bridges prove. However, the actual pathway of the DNA molecules on top of the gold electrodes cannot be resolved by AFM because the roughness of the electrodes lies in the range of the molecule's height, rendering a differentiation impossible even in the phase contrast.

Concerning the achieved height of the cluster chains, it has to be stated that in general the experience in the UV-induced metallization of DNA molecules immobilized on mica can be transferred to such DNA molecules bridging gold electrodes on a glass support without difficulty, only the yield on glass is not as high as on mica (for the further discussion of this phenomenon refer to Section 4.2 below). That is, by a straightforward application of the optimized parameters, i.e. activation in a highly concentrated $\text{Pt}(\text{NO}_3)_2$ solution (to form many nucleation sites) and UV-induced reduction in a low concentrated (UV-transparent) solution with eventually extended exposure times, only nonsatisfying results are obtained (Figure 4.2b): weak cluster chains, far away from penetrable by an electric current. Therefore, the strategy of multiple repeated activation and reduction steps was pursued, thus using initially formed platinum clusters on the biomolecular template for a preferential growth in subsequent reduction steps. And indeed, following this concept cluster chains of increased height could be achieved. Figure 4.2c shows a cluster chain of 12.3 nm mean height. However, none of these promising samples was proven to possess resistances considerably below $\text{G}\Omega$. In spite of the fact that some clusters can be grown together, thus forming continuous parts of up to about 100 nm length, on a μm -length-scale the presence of one single gap with a length of smaller than 5 nm is sufficient to efface the conductivity of a single cluster chain. But, in order to apply metalized DNA for the wiring in electronic circuits, definitely a continuous metal film is required, i.e. in the following section phenomena are discussed that may influence the metallization yield and a method is applied, which is able to fill these gaps with additional metal.

4.2 Towards Electric Conductivity Measurements

4.2.1 Influence of the Substrate Surface

To elucidate the low metallization level of DNA on glass supports, for the purpose of comparison, λ -DNA was stretched by molecular combing on a silica surface and afterwards metalized thereon. With the help of a slightly acidic buffer (pH 5.0, see Appendix A.1.2) it is possible to unspecifically immobilize λ -DNA on a silica surface so that it withstands the metallization procedure, whereas native λ -DNA could never be located on an unfunctionalized cover slip after the metallization, although the cover slip material borosilicate glass is composed of about 75% silica as well. Additionally, in comparison to glass, silicon and silica surfaces, respectively, are the substrates rather oriented towards application and a transparent glass substrate was anyway needed only

4 DNA Nanowire Fabrication

for the observation of the hydrodynamic flow induced stretching procedure on the inverted microscope.

However, in such simplified experiments starting with unspecifically immobilized λ -DNA on silica substrates rather than integrated DNA networks, it is easily possible to investigate the potential influence of the underlying substrate systematically. To do so, the adsorbed λ -DNA was subjected to an A1R1 metallization with 5 h activation time and 5 min UV exposure. Indeed, in a first experiment on (100) oriented p-doped Si with an about 1.5 nm thick native silica layer and a silicon substrate covered by a thermally grown silicon dioxide layer of 1000 nm thickness differences in the resulting mean height of the platinum cluster chains were detected (Figure 4.3d): on the one hand, on both substrates the mean height is noticeable larger than on glass (compare Figure 4.2b). On

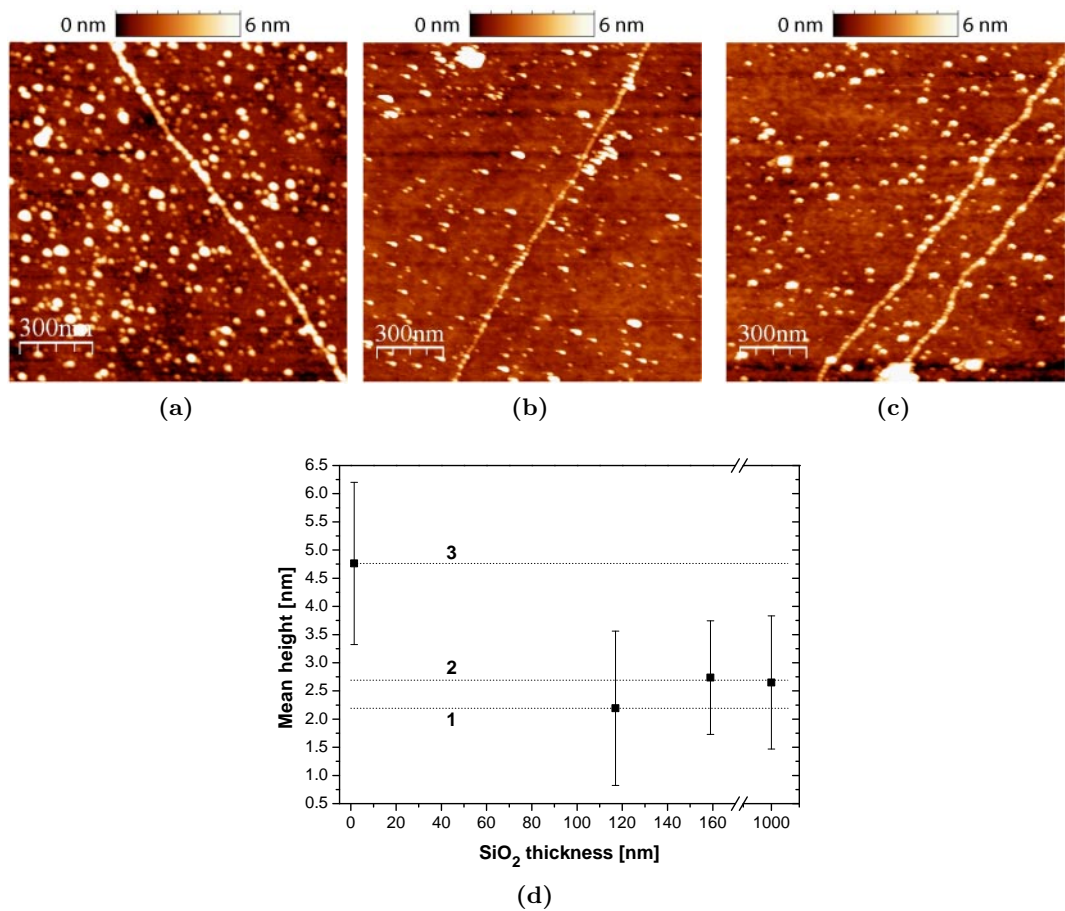


Figure 4.3: Influence of the surface silica thickness. (a)-(c) AFM images of metallized DNA immobilized on Si substrates with different thick silica surface layers: (a) native SiO₂, (b) 117 nm thermal grown SiO₂ and (c) 159 nm thermal grown SiO₂. Metallization parameters always were A1R1 with 5 min UV exposure time at 10 mJ/cm² after 5 h activation. (d) Comparison of the analyzed mean cluster chain heights in dependence on the thickness of the underlying silica layer.

4.2 Towards Electric Conductivity Measurements

the other hand, surprisingly the result is different on the two substrates, that is a mean cluster chain height of (4.76 ± 1.44) nm is achieved on native SiO_2 whereas on 1000 nm thick SiO_2 it averages to (2.65 ± 1.18) nm. For this outcome the surface reflectivity at the used wavelength of 254 nm was speculated to be responsible. Maybe a reflection of the irradiated light at the substrate surface leads to an increased amount of energy available for the photooxidation of the adsorbed DNA, whereas a substrate of high absorbance at 254 nm wavelength can not provide this “secondary” amount of energy. In other words, the question arises at which thickness of the silicon dioxide layer does the intensity of the reflected light reach a maximum and minimum, respectively due to additive or subtractive superposition of the light reflected at the surface and the light reflected at the silica-silicon interface (see inset in Figure 4.4a). This question was answered in a simulation of the reflectivity curve of a multilayer configuration using the software Winspall [169] which is based on the FRESNEL formalism. The inset of Figure 4.4a shows the multilayer system used as well as the refractive indices and extinction coefficients of the layers at 254 nm wavelength [170], the angle of incidence is 0° . The result of such a simulation is also shown in Figure 4.4a. A periodic pattern of distinct minima and maxima in the reflectivity can clearly be seen. It was calculated with transverse-magnetic polarized light, i.e. for the light source used in the experiment the absolute reflectivity values may be different, but the periodicity of the pattern remains constant. A SiO_2 thickness of 118 nm (minimum reflectivity) and 160 nm (maximum reflectivity), respectively was chosen to be produced by thermal SiO_2 growth on Si wafers² to experimentally prove a potential difference in the photoinduced metallization grade of DNA immobilized thereon.

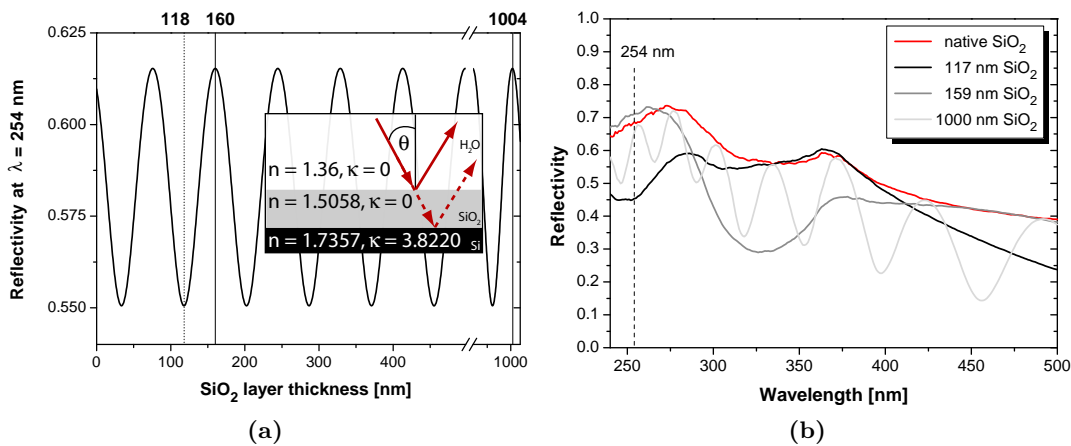


Figure 4.4: Reflectivity of a SiO_2 layer depending on its thickness. (a) Calculated reflectivity at 254 nm wavelength for a SiO_2 layer of 0–1000 nm thickness on a Si substrate and covered with water. The refractive indices n and the extinction coefficients κ used for the calculation are noted in the scheme, the angle of incidence θ is 0° . Also notice a minimal reflectivity at 118 nm SiO_2 layer thickness and a maximum for 160 nm and 1004 nm. (b) Measured reflectivity spectra of (100) Si substrates carrying differently thick layers of silica.

²With the help of René Landgraf obtained from Dr. Karola Richter, IHM, TU Dresden.

4 DNA Nanowire Fabrication

The reflectivity spectra of the fabricated substrates, whose actual SiO₂ layer thickness is 1 nm lower than calculated, were measured³ (Figure 4.4b) to experimentally confirm a difference in their reflectivity. Thereby, at 254 nm wavelength two levels appear: the reflectivities of the native SiO₂ layer (≈ 1.5 nm) as well as a 159 nm and 1000 nm thick silicon dioxide film—as simulated—are measured to lie in the same high range, that is 0.65 to 0.71. In contrast, the reflectivity of a 117 nm spanning SiO₂ layer is considerably lower with 0.45.

In the same fashion, the outcome of the photoinduced metallization of λ -DNA immobilized on these four substrates shows distinct levels. Figure 4.3d shows the mean height of the platinum cluster chains determined from AFM images on the 5×5 mm² large samples, where adsorbed and stretched λ -DNA was activated in 1 mM Pt(NO₃)₂ for 5 h and subsequently reduced by 5 min UV irradiation through that solution at 10 mJ/cm². According to the similar reflectivity, the (2.74 ± 1.00) nm mean height of a cluster chain on 159 nm thick SiO₂ is of equal value than the one at 1000 nm (level 2 in Figure 4.3d). In contrast, the averaged value at a substrate of low reflectivity, i.e. 117 nm SiO₂ thickness, lies with (2.19 ± 1.37) nm considerably below the above level. Thus, the above supposition is confirmed, i.e. at the 254 nm wavelength of interest a higher reflectivity of the substrate where the DNA is immobilized leads upon UV exposure to an enhancement of the available light energy and an augmented reduction of platinum ions along the DNA. Interestingly, a change in the amount of homogeneous nucleation can not be detected, that is the background area covered with particles is constantly 10%.

However, the large mean cluster chain height on native SiO₂ does not join the upper level 2 in Figure 4.3d, but exceeds it. The reason for this is the photo-stimulated formation of photocarriers in the semiconducting silicon during UV exposure [171]. Irradiation with UV light of 254 nm wavelength, that is a photon energy higher than the 1.1 eV bandgap of Si, leads to the creation of electron/hole pairs, whereof the electrons in the conduction band diffuse to the surface to reduce metal ions there [172]. An insulating silicon dioxide layer of about 1.5 nm thickness does not represent a tunnel barrier for these electrons. Thus, at the Si substrate with the native SiO₂ layer only, the reduction potential for platinum ions is further increased although the reflectivity is equal to a SiO₂ film of 159 nm and 1000 nm, respectively. The slightly increased amount of background nucleation of 22% supports this finding.

Nonetheless, also the metallization of DNA molecules bridging gold electrodes fabricated on a silicon substrate covered with a native oxide layer only, did not lead to an appreciable electric current conduction due to the abovementioned existence of small gaps between the platinum clusters. Therefore, in a last series of experiments it was tried to obtain electric conducting wires by a carefully performed metallization, where only the gaps of the cluster chain are filled.

³With the help of René Kullock at IAPP, TU Dresden.

4.2.2 Photochemical Tuning of Platinum Cluster Chains Using Their Surface Plasmon Resonances

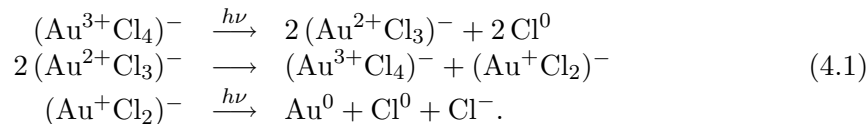
Although still discontinuous, it is believed that the up to here fabricated platinum cluster chains can serve as the base for obtaining continuous metal nanowires. Platinum clusters have already previously been used as catalysts to cover DNA with a continuous gold film [173]. In an electroless metallization gold is deposited at the platinum nucleation centers from a metastable metallization bath of KAuCl_4 [130]. Besides, the past decade has witnessed huge activities concerning the optical properties of metal nanoparticles as they play a key role in the field of nanooptics. Since metal nanoparticles can support localized surface plasmons (LSP) and in the spectral vicinity of these resonances the electric field surrounding the particle can reach very high values, they find applications for enhancing field-sensitive optical processes such as surface-enhanced Raman spectroscopy and fluorescence emission [174]. Furthermore, if two metal nanoparticles are brought close to each other (to a distance smaller than their respective diameter), their LSP modes can couple which leads to extraordinarily enhanced optical fields inside the interparticle gap [175].

These high electric fields in the vicinity of metal nanoparticles and particularly in the small gaps in-between them can be used to trigger the photochemical reduction of surrounding metal ions or complexes leading to optically controlled interparticle distance tuning and “welding” of single nanoparticles [176]. Due to the suitability of the technique for the preferential formation of metal bridges in-between metal particles before their radii actually overlap it was applied also for the synthesis of continuous wires at DNA making use of the already prepared platinum clusters. Thus, by a carefully performed metallization, where mainly the gaps of the platinum cluster chain are filled, it was thought to be possible to obtain wires with diameters in the 10-nm range.

Experimental Procedure

The synthesis of continuous wires by further metallization of Pt-DNA cluster chains was done in fruitful collaboration with Dr. Thomas Härtling at the Institut für Angewandte Photophysik, TU Dresden, who developed the experimental procedure [177], which will be described briefly in the following.

Gold is deposited at the Pt nucleation centers from a solution of tetrachloroaurate (HAuCl_4) dissolved in the immersion oil Cargille #1160 (Cargille Laboratories, USA). The photochemical reaction underlying the gold deposition process is the disproportionation of the salt complex. As a first step, the following redox reaction is induced by illuminating a HAuCl_4 solution with photons of high enough energy [178]:



4 DNA Nanowire Fabrication

This process⁴ takes place preferentially in the vicinity of seed particles, as the presence of such particles alters the reduction potential of the chemical system. The formation of new nucleation centers in the solution is therefore much more unlikely compared to the reduction of salt complexes in the vicinity of an already existing seed. Furthermore and of utmost importance for this work, in comparison to the increased reduction rate at the surface of illuminated particles, the gold complex reduction rate is even further raised in the interparticle region due to the influence of the extremely high electric fields inside the gap region (as a result of plasmonic coupling) on the metal deposition.

The realization of this process was carried out as follows (Figure 4.5): A cover glass carrying a finger electrode array with platinum metalized DNA bridges was mounted onto an inverted microscope Zeiss Axiovert 200. 532-nm focused laser beam excitation and collimated wide-field white-light detection were used to address and monitor single parts of DNA molecules. A 20- μl droplet of a 0.5 mM HAuCl_4 solution dissolved in the low-viscosity Cargille #1160 immersion oil was applied on the sample.⁵ The deposition process was initiated by exposing a single section of a Pt-DNA to the diffraction-limited

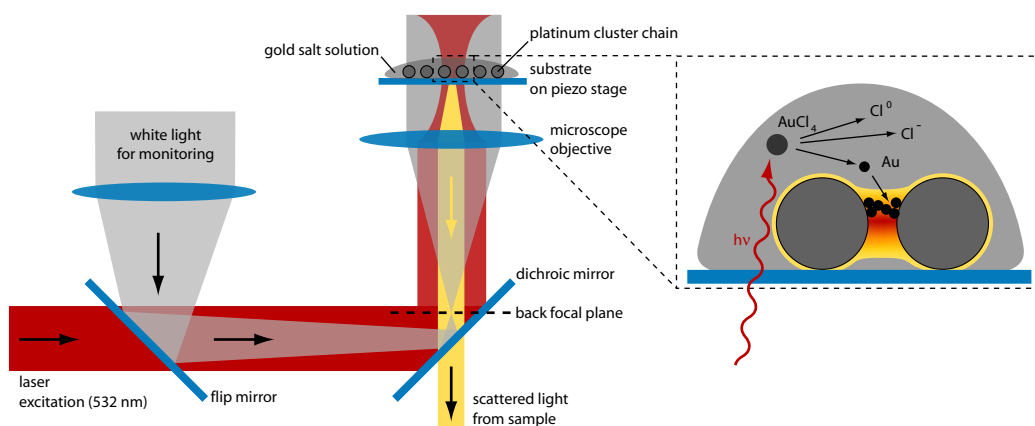


Figure 4.5: Experimental setup (adapted from [177]) for photochemical metal deposition onto individually addressed platinum cluster chains. Due to 532-nm focused laser excitation the reduction of gold salt complexes is induced preferentially in the vicinity of Pt-DNA. By white light detection the process is monitored. The zoomed region shows, that the coupling of the LSP modes leads to a high charge and thus electric field concentration around the gap so that the photochemical reduction takes preferentially place there.

⁴The chloride ions originating in the reaction are compensated by scavengers in the solution or the solvent itself.

⁵To embed the sample in a liquid with a refractive index matching the one from the objective renders possible the detection of the scattered light from the nm-sized metallic sample making use of a technique called *homogeneous immersion*. In an inverted microscope under such conditions, only very low reflection at the glass-sample oil interface occurs and the contrast between the (usually low-intensity) scattered light from the sample and the (otherwise high-intensity) reflected light is augmented. In addition to this optical effect, the plasmonic response, i.e. the scattering cross section of a metal particle is increased due to the high refractive index of the surrounding medium, further easing the detection.

4.2 Towards Electric Conductivity Measurements

532-nm laser spot (1 mW, spot diameter ≈ 220 nm). Therefore, the laser spot was moved along an electrode gap by scanning the sample, which is mounted onto a piezo-driven stage (PXY 101 CAP, piezosystem jena), through the focus until an increased scattering of the laser spot was observed indicating the encounter of a Pt cluster chain. Each chain was illuminated for a period of several minutes thereby moving the laser spot across the electrode gap following the “scattering track”, i.e. the chain. Then, the laser was blocked and the white-light beam was directed into the microscope by means of a flip mirror to *in-situ* monitor the state of the deposition. If necessary, the next laser exposure, i.e. metal deposition, followed. This procedure was iterated several times until the Au-Pt-DNA showed white-light scattering over the full length. Finally, the HAuCl_4 solution was removed from the sample in a washing step in ethanol.

Photochemical Tuning of Single Platinum Cluster Chains

With the purpose of tuning the discontinuous Pt-DNA molecules bridging the gaps in a finger electrode array into continuous, electric conducting wires, the photochemical deposition of gold onto the “prefabricated” platinum cluster chains was carried out as described in the above section. That is, the sample was exposed to the 0.5 mM HAuCl_4 -immersion oil solution, once hit, a section of the particle chain was scanned with the 532-nm focused laser beam and monitored by means of a white-light beam. The obtained bright field micrographs and AFM images of the corresponding region are shown for two chains in Figures 4.6 and 4.7. The series of images in Figure 4.6a reveals the time flow of the deposition process. Already after 3 min exposure of the central interelectrode region, a bright stripe is observable in exactly the laser scan field. Continuing the exposure in the region above and below this stripe leads to a continuously bright, tilted line indicating an enhanced amount of scattering at deposited metal. In fact, the AFM images in Figures 4.6c and 4.6d taken after the salt solution has been washed off, display a (partial) thickness augmentation to 50 nm in comparison to the original state before the gold deposition when the platinum clusters had a height of about 12 nm (Figure 4.6b). Note the course of the deposition as it follows the underlying platinum cluster chain and furthermore, is restricted thereto, thus demonstrating the specificity of the deposition. As the LSP excited in the platinum particles leads to an electric field enhancement in their gaps even in the nonresonant case [179], metal is deposited only onto an individual particle chain intentionally addressed by the laser focus. Although the laser spot of about 220 nm diameter is larger in size than the platinum particles, there is no precipitation of metal on the cover glass. Also, adjacent unexposed particles or chains show no changes (Figure 4.7b).

As a result of the exposure with a focused laser beam, the application of energy is localized leading to a quick and intense gold deposition due to the field enhancement in the vicinity of the platinum seeds. In consequence, first this entails the generation of wires with diameters considerably higher than 10 nm, typically 50 nm. In fact, this is also a consequence of the experimental execution simply because only comparatively thick chains have a scattering cross section of sufficient size ($\approx 1 \mu\text{m}$) to be observable in white light. To ensure sufficient deposition for an electric contact, the laser exposure was always

4 DNA Nanowire Fabrication

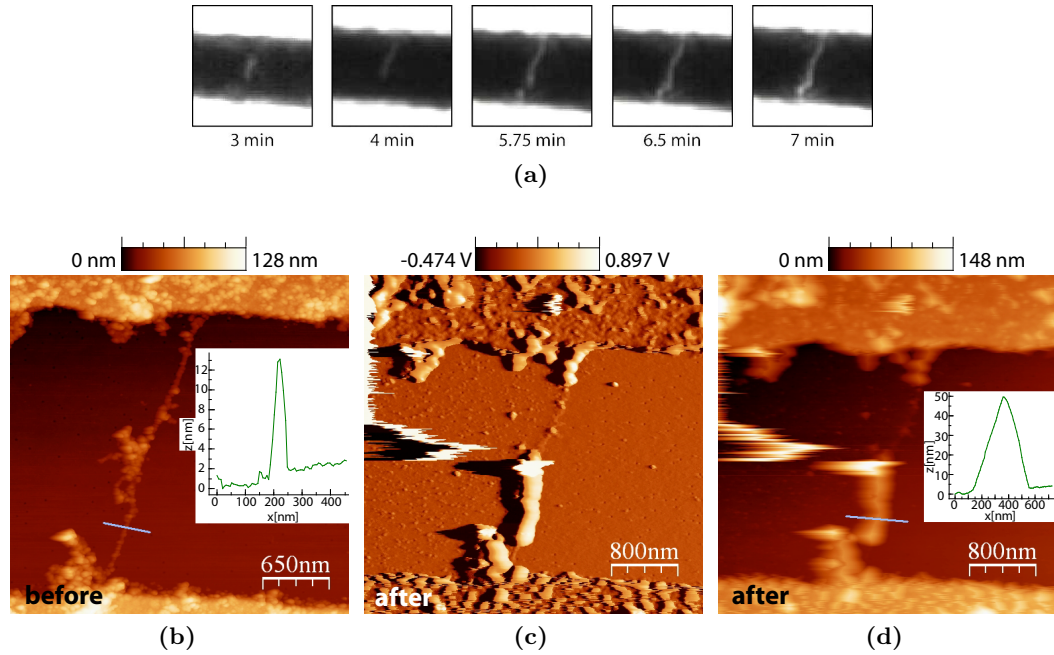


Figure 4.6: Results of photochemical gold deposition from 0.5 mM HAuCl_4 using a focused 532-nm laser beam at 1 mW power. (a) Time course of the photochemical reduction procedure. Starting at the middle section of the platinum decorated cluster chain (first 4 min), the laser was then focused to its upper end (5.75 min) and lower end (6 and 7 min), respectively. Note the course of the deposition as it follows the underlying platinum cluster chain. (b) AFM height image showing the original state of the DNA bridge after UV-induced platinum metallization. Platinum clusters are up to about 11 nm in diameter as depicted in the inset height profile. (c) AFM amplitude and (d) height image revealing the outcome of the photochemical gold deposition specifically at the platinum seeds. The about 50 nm thick gold deposition in the upper half of the chain was probably washed away leaving a gap where the underlying platinum chain becomes visible again. The streaks in the left part of images (c) and (d) are artifacts.

continued until the scattered light of the chain could be resolved. Second, the thick gold depositions apparently are easy to wash off during the removal of the oily HAuCl_4 solution at the end of the exposure procedure. The AFM images of Figure 4.6 reveal a section along the Au-Pt-DNA where the according to the bright field image (Figure 4.6a) evidently deposited gold was dissolved and the underlying platinum chain re-emerges in its original state (compare Figure 4.6b). Also with the example shown in Figure 4.7 it finally turned out to be difficult to remove the liquid without rinsing off the chain. After a first deposition step (Figure 4.7a) with successful transfer of the entire sample AFM imaging affirmed the existence of a small gap inhibiting the current conduction to the upper electrode (Figure 4.7b). This gap was effectually closed in a second deposition step (Figure 4.7b) whereupon however the whole molecule was rinsed off (Figure 4.7d). Such problems rather in the handling of the samples than in the realization of the method so far prevent the proof of the electric conductivity of the successfully prepared gold enhanced Pt-DNA bridges.

4.3 Conclusion on DNA Nanowire Fabrication

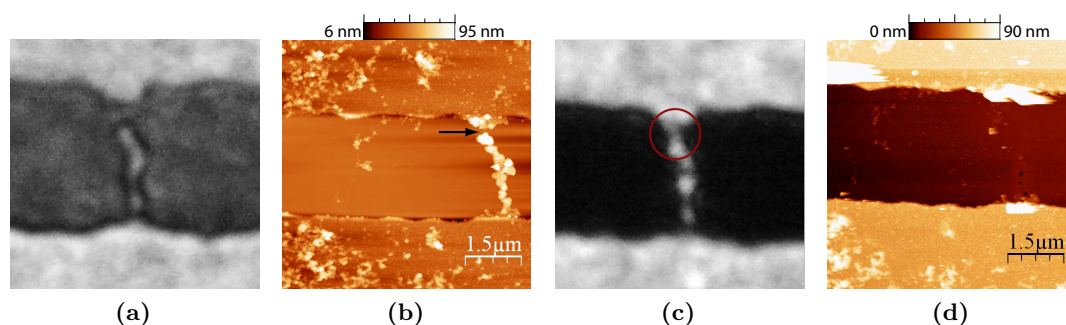


Figure 4.7: (a) Bright field micrograph and (b) AFM height image showing the successful enlargement of another Pt-DNA making use of the same parameters as in Figure 4.6. A little gap (arrow) is left at the upper electrode attachment point. The unexposed platinum cluster chain in the left half remains unaffected. (c) Bright field micrograph after the closure of this gap (red circle). (d) AFM height image revealing the absence of the chain after the washing step following the gap closure.

4.3 Conclusion on DNA Nanowire Fabrication

From the above section two conclusions can be drawn: (i) Besides the metal salt concentration applied during the activation of DNA and its photoinduced reduction, also the substrate where the DNA is immobilized plays a decisive role. The substrate's reflectivity at 254 nm wavelength and most notably its electric conductivity affect the reduction of metal ions bound to the DNA. (ii) In another photoinduced electroless deposition, gold can be deposited selectively onto the preformed, discontinuous platinum cluster chains on DNA making use of the electric field enhancement around the nanoparticles and particularly in the nanometersized gaps in-between them. Thus, the initially formed platinum clusters serve as seeds and become welded, resulting in granular wires 50 nm in diameter. However, to decrease the diameter of the fabricated wires substantially and at the same time reduce the probability of dissolution, a more sophisticated deposition and handling protocol has to be developed in an extended series of experiments. So supposably a wide-field instead of a focused excitation together with a fine tuned HAuCl_4 concentration leads to refined results. Also a reduced exposure time—probably at the expense of the *in-situ* monitoring capability of the deposited material amount—is conceivable.

However, although up to here still discontinuous metal nanowires are the outcome, it is believed that the above presented methodology can serve as the base for obtaining continuous metal nanowires. Furthermore, because of the intrinsic simplicity in using light as the key step, but without being limited thereby in resolution as the underlying biomolecule introduces the aspired spatial control, this process can most likely be extended to large-scale development, eventually leading to a very efficient molecular-photolithography process.

Summary

The forecast for electronics has vastly underestimated developments, with predictions such as “future computers will weigh no less than 1.5 tons”. Over the past twenty years, the number of transistors on a chip has risen drastically, and is still increasing. Now the biggest question is: what will take over from MOORE’s Law in about a decade? This question has been driving research far beyond the world of electronics only.

The geometry and connectivity of future electronic circuits could perhaps be controlled by DNA self-assembly, rather than by destructive lithography techniques. Such bottom-up approaches are elegant, cheap and possibly enormously powerful techniques for future mass replication, but their applicability remains limited until total control over the emerging structures in terms of wiring and interconnections can be obtained. In this framework, the aim of the present thesis was to explore techniques, how DNA can be used to build up electronic circuitry as an alternative method in electronics packaging technology. Therein, essential steps are the transformation of a naturally coiled DNA molecule into a wire-like conformation and the integration of an immense number of such molecules into microelectrode contact arrays as well as the introduction of electric conductivity by *in-situ* site-specific deposition of metal on the immobilized molecules. On the way to accomplish these steps, methods were developed, which are summarized in the following.

Single DNA molecules could be stretched between microstructured gold electrodes. A simple, but nonetheless reliable and efficient method was used to attach DNA end-specifically to the electrodes. To this end, one thiol group was incorporated at each DNA end by filling its single-stranded overhangs with the complementary bases whereas a thiol-modified form of a single base is used. The thiol group allows for a selective bonding to gold surfaces. The advantage of using thiols is the simplicity of the filling method together with the readily availability of the second binding partner—the lithographically patterned gold electrodes—without necessity of further modification.

Using this anchoring method, single-end surface-tethered DNA molecules could be stretched between two electrodes by hydrodynamic flow applied through microcapillaries in an open flow cell. The assembly is not only well controlled in respect to the specificity and stability of the DNA interconnects but also the number of integrated DNA molecules can be adjusted from single molecules to the batch-wise assembly of hundreds of interconnects. A simple experiment was performed to determine the anchoring points of the integrated DNA molecules in an inclined hydrodynamic flow and to thus give clear evidence that the molecules are solely tethered to adjacent electrodes. Despite of the outstanding success of this approach (also with regard to the subsequent metallization), it has to be stated that the interconnection of a single contact pair within a field of chemically identical and

4.3 Conclusion on DNA Nanowire Fabrication

closely neighboring contacts relies on the accuracy the hydrodynamic flow can be applied with, i.e. how much it can be confined to a single contact pair.

Therefore, in a second approach the realization of single connections in an addressable electric field-based stretching method was investigated. The hope was to establish a directed stretching mechanism localized only to that electrode pair where the electric field is applied and thus allowing for the switchable formation of interconnects in variable configurations. However, experiments showed evidence for a stretching mechanism where the main contribution to the elongation does not rely on dielectrophoresis but is provided by an electric field induced fluid flow. Although this electrothermal flow is often considered as a negative effect for dielectrophoresis applications, under the established appropriate conditions, it can turn into a useful mechanism for stretching single-end-tethered DNA molecules from a tapered electrode towards a stripe electrode. However, the construction of complex networks in terms of a “wiring diagram” could not be achieved based on this approach as a highly controlled and localized stretching is not realizable in a complete array of electrode tips. The applied electric field between the “turned on” electrodes is affected by the presence of the metallic areas of the other electrodes, so that electric field gradients and fluid flows also arise elsewhere than between the contacted electrodes, thus complicating a localized stretching at a designated position.

Furthermore, a method was developed, which accomplishes the *in-situ* growth of platinum clusters selectively at DNA molecules stretched between gold electrodes and immobilized on the substrate surface. The synthesis was done by photoinduced reduction of platinum ions, which were bound to the DNA beforehand. The DNA bases act as photosensitizers due to their strong absorption in the UV. As a result, the cluster nucleation is promoted by the DNA, i.e. it is template directed, and takes place heterogeneously at the DNA molecules. This leads to the suppression of the homogeneous cluster nucleation process in solution, if UV irradiation and photooxidation of the DNA are not inhibited by a highly concentrated and thus quasi non-UV-transparent cover of $\text{Pt}(\text{NO}_3)_2$ solution. This procedure yielded micrometer long platinum cluster chains with an average cluster diameter of 4 nm. By transmission electron microscopy single clusters were found to be partly grown together, but gaps of 1-2 nm were observed between the clusters.

On the way towards continuous and thus electric conducting wires the substrate where the DNA is immobilized was found to play a decisive role in the reduction process. Furthermore, in another photochemical metallization step, using the discontinuous platinum cluster chain as seed gold was deposited selectively thereon, thus reducing the interparticle gap space. This way wires with a diameter of 50 nm could be prepared.

Instead of rounding off the respective topics, the results of this thesis open up several paths for further scientific inquiries, both fundamental and application-oriented. The different methods, which were developed in the framework of this thesis, can be seen as steps towards a future DNA-based assembly of electronic circuits. However, the main focus of attention has to lie on the transformation of the presented techniques which are developed on the laboratory level into satisfying, industrialized processes considered to be competitive to the lithographical techniques applied in chip production which are still much more powerful. Nonetheless, because of the intrinsic simplicity

4 DNA Nanowire Fabrication

in using light as the key step, but without being limited thereby in resolution as the underlying biomolecule introduces the aspired spatial control, the presented methodology is thought to be extendable to large-scale development, eventually leading to a very efficient molecular packaging process.

Appendix

A.1 Experimental Methods

A.1.1 Integration of DNA into Microstructures

Thiolfunctionalization of λ -DNA

For thiol labeling both ends of λ -DNA its sticky ends are filled in with single nucleotides using the Klenow exo^- fragment of DNA polymerase, in which the 3' to 5' exonuclease activity has been removed, whereas a thiol-modified form of T's is employed. For two batches, two aliquots of 20 μl methyladenine-free λ -DNA (0.5 $\mu\text{g}/\mu\text{l}$) (New England Biolabs) each are linearized by heating to 65°C for 10 min. For the incorporation reaction the following reagents were added on ice to each DNA aliquot:

- 5 μl NEBuffer 2, 10 \times (New England Biolabs)
- 1 μl 10 mM dATP (Sigma Aldrich)
- 1 μl 10 mM dCTP (Sigma Aldrich)
- 1 μl 10 mM dGTP (Sigma Aldrich)
- 3 μl 100 mM S⁴TTP (tebu-bio GmbH)
- 17 μl H₂O (fill up to 50 μl total volume)
- 2 μl Klenow exo^- (5 000 U/ml, New England Biolabs)

The mixture was incubated for 25 min at 25°C, followed by 10 min enzyme deactivation at 75°C. For purification the DNA was loaded together with 450 μl PB 100, pH 7.5 (a mixture of sodium dihydrogen phosphate monohydrate and di-sodium hydrogen phosphate dihydrate, 100 mM, Merck) in a Microcon YM-100 filter (Millipore) and centrifuged at 500 g. After repetition of this step with another 450 μl PB 100, the purified T-DNA-T was recovered by inverting the filter and centrifuging at 1000 g for 4 min.

Substrate Preparation

Patterned gold surfaces were lithographically prepared on glass cover slips for use in fluorescence microscopy. Glasses of 16 mm diameter, thickness nr.1 (0.13–0.16 mm) (PLANO) were cleaned in Piranha solution (sulfuric acid (95–97 wt% in water, Merck) and hydrogen peroxid (30 wt% in water, Merck) in a ratio 3:1) for 10 min, extensively rinsed with water and blown dry. 80 μl of positive photoresist AR-P 5350 (Allresist) were spin coated (4500 rpm/s, 4500 rpm, 30 s) and baked for 5 min at 105°C on the hotplate. After rehydration of the resist for several minutes in normal atmosphere, the substrates were UV exposed ($\lambda=365$ nm) through a positive chromium mask (mask aligner MJB4, SÜSS MicroTec) using vacuum contact and 2.5 s exposure time. The subsequent development step was carried out in a petri dish with AR 500-47 developer (Allresist)

4 DNA Nanowire Fabrication

diluted 1:2 with water until no dissolving streaks of resist are visible any more (after about 30 s). The metal films were prepared by evaporating 50 nm of gold on top of a 3 nm thick chromium adhesion layer. Finally, the photoresist was lifted off in AR 300-72 remover (Allresist) with the help of ultrasound.

Substrate Cleaning

Glass cover slips with/without patterned gold surface were cleaned by immersing them for 20 s into fuming nitric acid (100%, Merck) and then for 1 min into a neutralization solution (hydrogen peroxide (30 wt% in water, Merck), ammonia solution (25 wt% in water, Merck), and deionised water in the ratio of 1:1:5). After rinsing in deionised water, the wet structures were immediately installed into the experimental setup.

Flow-Mediated Stretching of T-DNA-T in the Open Flow Cell

After cleaning, the interdigital electrode structure was immediately assembled into the home-made open flow cell and covered with 200 μl of PB 100, pH 7.5 buffer. The flow cell is mounted into an inverted optical microscope (Axiovert 200M, Carl Zeiss) equipped with an oil immersion objective (α -Planfluor 100 \times , N.A.=1.45, Carl Zeiss). Two microcapillaries (GB100F8P, Science Products GmbH) are mounted from above under an angle of about 45 $^\circ$ to accomplish fluid flow over the sample surface by means of a peristaltic pump (Watson Marlow) where they are connected to via a tubing system. In the field of view of the 10 \times objective the lower edge of each capillary is manually positioned 100 μm above the substrate surface by means of a micro-manipulation system (Luigs&Neumann) and the motorized focus drive of the microscope. Before positioning, the tubing system was completely filled with PB 100, pH 7.5 and 30 μl of T-DNA-T in PB 100 buffer, pH 7.5 are drawn up in one of the microcapillaries. Thus, after placing the microcapillaries the T-DNA-T can be flushed over the contact array. To accomplish anchoring of T-DNA-T coils with one of their thiol-functionalized ends at the gold contacts, the DNA solution was twice pumped back and forth at 0.2 rpm over the contact array for 30 s with 1 min break inbetween each flush. Then, to uncoil and stretch the molecules the flow speed was increased to 1.5 rpm for 3 min for each direction of pumping.

To verify the formation of interconnects, the bound DNA molecules were stained after the stretching procedure by addition of 10 μl 0.4 mM aqueous YOYO-1 solution (Invitrogen) to the liquid volume in the flow cell. Fluorescence microscopy images were acquired with 300 ms exposure time using a cooled, 16-bit frame-transfer CCD camera (Visitron), a 100 W mercury lamp and the Zeiss filter set nr. 09 (excitation bandpass filter: 450–490 nm, dichroic mirror: 510 nm, emission longpass filter: 515 nm).

Electric Field Induced Stretching Experiments

Experiments concerning the dielectrophoretic stretching of DNA were performed in a similar setup as in the case of hydrodynamic flow. Gold electrode structures on glass substrates were cleaned according to the protocol above and mounted into a matched microscope holder. A sealing ring (2 mm inner diameter, 3 mm outer diameter) punched

A.1 Experimental Methods

out of a 1 mm thick PDMS film (polydimethylsiloxane (SYLGARD 184 SILICONE ELASTOMER KIT, Dow Corning), monomer:cross-linking agent=9:1, curing for 4 h at 65°) was centered around the contacts of interest to confine the DNA solution there and ensure no immersion of the contacting needles into the solution. The tungsten needles (SIGNATONE SE-T, USA) are fixed in manipulators (SÜSS MicroTec PH100) which are screwed to the microscope-sided manipulation system (Luigs&Neumann) that allows for their positioning. A frequency and voltage synthesizer (Sony Tektronix AFG 320), eventually amplified (ENI Inc. Model 3100LA), provides the oscillating electric field whereas an AC potential is applied to one needle and the other one is set to ground. To be able to record the DNA behavior in time sequences of minutes length the λ -DNA or T-DNA-T was stained with YOYO-1 in a dye:base pair ratio of 1:10 and β -mercaptoethanol (Bio-Rad) was added to the solution to prevent photobleaching. A typical solution contains: 76.5 μ l TRIS buffer (1, 10 or 100 mM, Sigma), 20 μ l 14.2 M β -mercaptoethanol, 2.5 μ l DNA (0.01 μ g/ μ l) and 0.1 μ l 40 μ M YOYO-1. Thereof or of a 10-fold dilution in buffer, 10 μ l were set onto the electrodes into the enclosed reservoir. Then, the stream acquisition function of the MetaVue software (Molecular Devices) allows for the automated recording of time series with the Uniblitz shutter being permanently open and a computer controlled, variable switching of the electric field at certain points in the time series (at certain frame numbers). Care has to be taken about the readout speed of the CCD camera limiting the time resolution. Typically, for images of 512 \times 512 pixels 25 ms exposure time is the lowest limit.

A.1.2 UV-Induced Preparation of Cluster Chains Along DNA

Immobilization of DNA on Mica

λ -DNA was immobilized on mica as described by BEZANILLA *et al.* [180] by diluting the stock solution to 1 ng/ μ l in HEPES/MgCl₂ buffer (40 mM HEPES (sodium salt, Fluka), 10 mM MgCl₂ (magnesium chloride hexahydrate, Merck), pH 7.6) and placing a 10 μ l droplet onto a 5 \times 5 mm² piece of freshly cleaved mica (PELCO mica, PLANO) for 5 min to allow adsorption. Subsequently, the sample was washed by dipping into water, excess fluid was soaked up with filter paper and the metal salt solutions were applied.

Immobilization of DNA on Silicon

5 \times 5 mm² pieces of (100) silicon with silica layers of different thicknesses were cleaned according to the procedure above. In consequence, λ -DNA can be stretched on the hydrophobic surface by molecular combing. To do so, λ -DNA stock solution was diluted to 1 ng/ μ l in 10 mM PB, pH 5.0 and a 10 μ l droplet was sat on the silica surface for 30 s to allow end-specific adsorption. Finally, slowly blowing the droplet away with nitrogen resulted in stretched DNA molecules on the surface.

4 DNA Nanowire Fabrication

UV-Induced Metallization of DNA

If not otherwise stated, 15 μl of 1–100 mM aqueous $\text{Pt}(\text{NO}_3)_2$ solution (ChemPur) were placed on the mica with the previously immobilized DNA. The droplet sat there for the activation time while the substrate was stored in a high humidity environment in the dark. For a combination of different $\text{Pt}(\text{NO}_3)_2$ concentrations during activation and reduction, this initial droplet was washed away by dipping the substrate into water and a droplet of a different concentrated $\text{Pt}(\text{NO}_3)_2$ solution was immediately applied. Otherwise the sample was UV exposed with the original droplet. The cluster formation was initiated by exposing the samples to a controlled amount of ultraviolet radiation (254 nm) in a CL-1000 crosslinker (UVP) which allows to set the exposure time and the UV energy dose. Finally, the samples were dipped in water and blown dry with nitrogen.

Imaging was performed with a Nanoscope IIIa (Digital Instruments) in tapping mode in air.

US/VIS absorption spectra were recorded on a Cary 50 photospectrometer (Varian) and melting curves were studied on the same spectrometer measuring the 270 nm absorbance of the solution in a quartz cuvette (Helma) which was heated from the side by a computer controlled peltier element. The cuvette was heated from 20°C to 60°C in steps of 4°C, where the temperature was held for 5 min before the absorbance measurement was started and the next temperature elevation followed. From 60°C to 100°C the temperature step was 1°C and the hold time amounted 3 min.

UV/VIS reflectivity spectra were acquired using a Shimadzu UV-2101PC spectrometer.

A.1.3 Preparation of TEM Samples

General Protocol

If not otherwise stated, formvar/carbon films on 400 mesh gold grids (PLANO) were plasma treated for 10–20 s (air atmosphere, SPI Plasma Prep II). Directly thereafter, 7 μl of an aqueous 10 ng/ml DNA solution were applied and left for adsorption for 5 min. Excess liquid is removed by tapping the grid etch onto filter paper. For activation the grid is laid upside-down onto a 25 μl droplet of 1–100 mM $\text{Pt}(\text{NO}_3)_2$ solution deposited on a parafilm covered glass slide. For the duration of activation the glass slide is placed on a wet tissue in a petri dish which is wrapped with aluminum foil. For reduction the activated grid is gripped by a reverse action tweezer. A defined volume of 10 μl $\text{Pt}(\text{NO}_3)_2$ solution is applied and the tweezer is placed under the UV lamps in the CL-1000 crosslinker (UVP) for usually 5 min at 10 mJ/cm². Finally the grid is washed by dipping into distilled water, excess fluid is soaked away from the edge and the grid is left to dry exposed to air.

Carbon Replica Technique

Carbon replicas are made from DNA molecules which were immobilized and metallized according to the above protocol. A carbon layer was evaporated immediately after finishing the preparation on mica. That is, in a bench-top carbon rod evaporation device

A.2 Matlab Based Image Processing

(MED010, BAL-TEC) the samples were evacuated to $4.1 \cdot 10^{-6}$ mbar and a high current is run through the carbon rods to “flash” evaporate it (2s spitting). The key step to enable the carbon films to float off the mica onto a water reservoir is to score the film on one edge of the mica piece. Then the film easily comes off when the mica piece is slid into a water “cupola” (the cap of test-tube filled with distilled water) under an angle of 45° with the scored edge first. The film is finally collected from below with an uncoated 400 mesh copper grid (PLANO) which was rendered hydrophilic by dipping into acetone and drying in air just before use.

Transmission electron micrographs were obtained on a Philips CM200FEG or a Zeiss LIBRA200FEG using 200 kV acceleration voltage each.

A.2 Matlab Based Image Processing

A routine tracing the ridge of a chain-like object was implemented in Matlab with the particular goal of analyzing the height profile along the ridge. Image preprocessing, including plane subtraction and flattening, was done using WSxM freeware (www.nanotec.es). However, in a preprocessing step of the Matlab routine the background of the image, i.e. the substrate surface, is set to zero by subtracting the average height of a rectangular area, that the user defined in a region of the image where no objects of interest or other “artifacts” are present.

The actual routine is based on an AFM height image, i.e. a matrix of height values. Chain tracing is initiated by the user, who roughly predetermines the route of tracing by marking start and end point of the chain and an arbitrary number of points inbetween. Thus, a running direction is defined and more important the loss of track, i.e. the movement in circles is hindered. The algorithm then walks down the user-defined track, interpolated by a cubic spline with dynamic spacing (thin white line in Figure A.8a), searching for the points of maximum height in a certain distance normal to the walking direction (Figure A.8c). The scheme is as follows: (i) A tangent is defined by the ray connecting the current point and the next point in the spline. (ii) The height data is interpolated (Figure A.8d) every 1 nm along a segment of 20 nm length, centered on the next point and normal to the current tangent. (iii) The maximum value of all heights on the perpendicular segment is saved in the trace and becomes the new current point. This process is repeated until the end of the chain is reached. The found trace is visualized on top of the original height image (Figure A.8a) and the height profile along this trace is plotted (Figure A.8b). The mean height of the chain analyzed in this run, its standard deviation and the distances between the positions of the local maxima in the height profile are saved to be summarized in total values for that kind of sample.

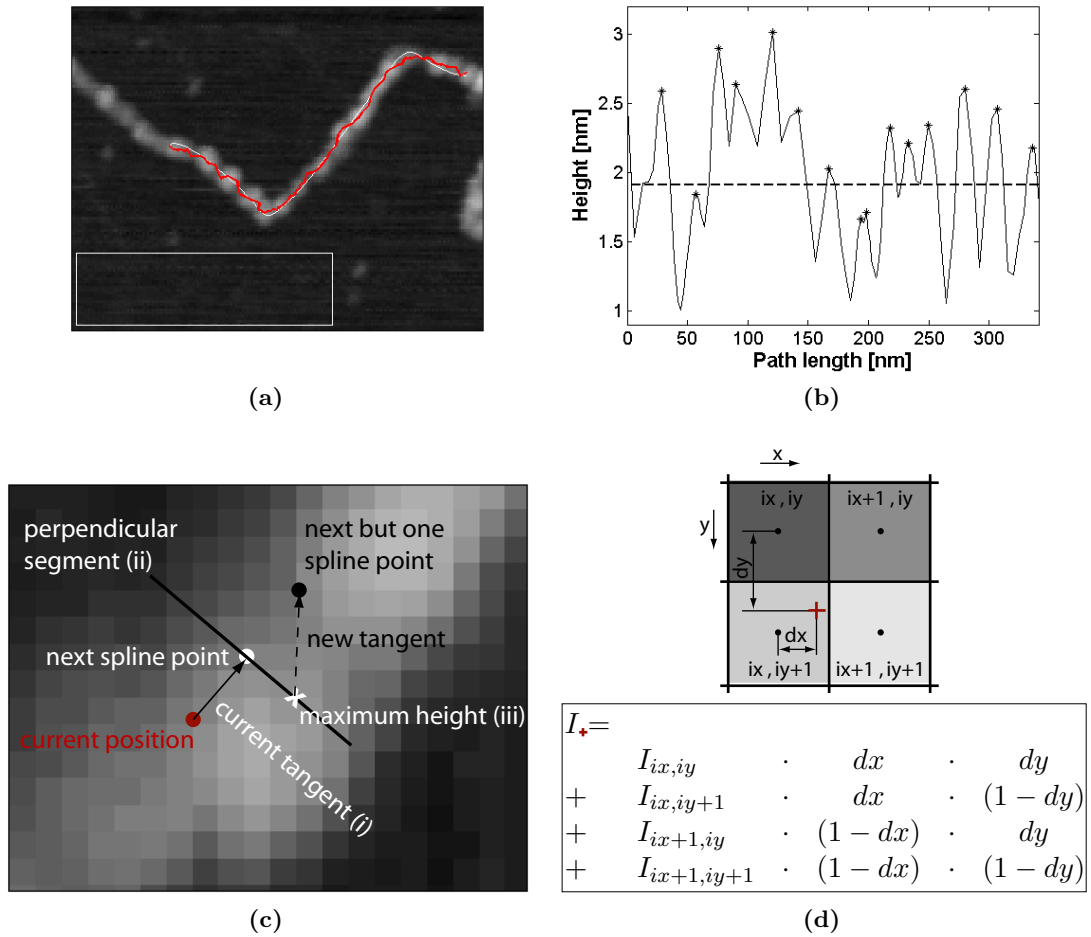


Figure A.8: DNA tracing algorithm. (a) Section of an AFM height image where the initial user-defined spline (thin white path), the calculated ridge (thick red path) and the rectangle used for background correction were superimposed. (b) Height profile (solid line), mean height (dashed line) and local maxima (stars) along the found DNA ridge, i.e. the red line in the neighboring image. (c) Scheme of the algorithm alluded to in the text. (d) Routine for interpolation of height values.

Bibliography

- [1] International technology roadmap for semiconductors - 2008 update. <http://www.itrs.net>.
- [2] H. Li, J. D. Carter and T. H. LaBean. Nanofabrication by DNA self-assembly. *Materials Today* **12** (5), 24 (2009).
- [3] C. A. Mirkin, R. L. Letsinger, R. C. Mucic and J. J. Storhoff. A DNA-based method for rationally assembling nanoparticles into macroscopic materials. *Nature* **382** (6592), 607 (1996).
- [4] W. Shenton, S. A. Davis and S. Mann. Directed self-assembly of nanoparticles into macroscopic materials using antibody-antigen recognition. *Adv. Mater.* **11** (6), 449 (1999).
- [5] C. M. Niemeyer, W. Bürger and J. Peplies. Covalent DNA-streptavidin conjugates as building blocks for novel biometallic nanostructures. *Angew. Chem. Int. Ed.* **37** (16), 2265 (1998).
- [6] M. Górzny, A. Walton, M. Wnek, P. Stockley and S. Evans. Four-probe electrical characterization of Pt-coated TMV-based nanostructures. *Nanotechnology* **19** (16), 165704 (2008).
- [7] R. Kirsch, M. Mertig, W. Pompe, R. Wahl, G. Sadowski, K. Böhm and E. Unger. Three-dimensional metallization of microtubules. *Thin Solid Films* **305** (1-2), 248 (1997).
- [8] M. Mertig, R. Kirsch, W. Pompe and H. Engelhardt. Fabrication of highly oriented nanocluster arrays by biomolecular templating. *Eur. Phys. J. D* **9** (1), 45 (1999).
- [9] N. C. Seeman. Nucleic acid junctions and lattices. *J. theor. Biol.* **99**, 237 (1982).
- [10] J. Watson and F. Crick. A structure for deoxyribose nucleic acid. *Nature* **171**, 737 (1953).
- [11] M. Wilkins, S. A.R. and H. Wilson. Molecular structure of deoxypentose nucleic acids. *Nature* **171**, 738 (1953).
- [12] R. Franklin and R. Gosling. Molecular configuration in sodium thymonucleate. *Nature* **171**, 740 (1953).
- [13] T. Zerna. *Aufbau- und Verbindungstechnik für Elektronik-Baugruppen der Höchstintegration, System integration in electronic packaging*, vol. 4. Verlag Detert (2008).

Bibliography

- [14] R. Compañó. Nanotechnology roadmap for nanoelectronics. <http://cordis.europa.eu/ist/fet/nidqf.htm> (2000).
- [15] O. Kratky and G. Porod. Röntgenuntersuchung gelöster Fadenmoleküle. *Rec. Trav. Chim.* **68**, 1106 (1949).
- [16] J. F. Marko and S. Cocco. The micromechanics of DNA. *Physics World* **16** (3), 37 (2003).
- [17] S. Smith, Y. Cui and C. Bustamante. Overstretching B-DNA: the elastic response of individual double-stranded and single-stranded DNA molecules. *Science* **271**, 795 (1996).
- [18] S. B. Smith, L. Finzi and C. Bustamante. Direct mechanical measurements of the elasticity of single DNA molecules by using magnetic beads. *Science* **258**, 1122 (1992).
- [19] M. D. Wang, H. Yin, R. Landick, J. Gelles and S. M. Block. Stretching DNA with optical tweezers. *Biophys. J.* **72**, 1335 (1997).
- [20] J. van Mameren, P. Gross, G. Farge, P. Hooijman, M. Modesti, M. Falkenberg, G. J. L. Wuite and E. J. G. Peterman. Unraveling the structure of DNA during overstretching by using multicolor, single-molecule fluorescence imaging. *PNAS* **106** (43), 18231 (2009).
- [21] P. Cluzel, A. Lebrun, C. Heller, R. Lavery, J.-L. Viovy, D. Chatenay and F. Caron. DNA: an extensible molecule. *Science* **271**, 792 (1996).
- [22] M. C. Williams, I. Rouzina and V. A. Bloomfield. Thermodynamics of DNA interactions from single molecule stretching experiments. *Acc. Chem. Res.* **35**, 159 (2002).
- [23] D. Bensimon, A. J. Simon, V. Croquette and A. Bensimon. Stretching DNA with a receding meniscus: Experiments and models. *Phys. Rev. Lett.* **74** (23), 4754 (1995).
- [24] R. Zimmermann and E. Cox. DNA stretching on functionalized gold surfaces. *Nucl. Acids Res.* **22** (3), 492 (1994).
- [25] F. Luderer and U. Walschus. *Immobilization of DNA on Chips I, Topics in Current Chemistry*, vol. 260, chap. Immobilization of Oligonucleotides for Biochemical Sensing by Self-Assembled Monolayers: Thiol-Organic Bonding on Gold and Silanization on Silica Surfaces, pages 37–56. Springer-Verlag, Berlin/Heidelberg (2005).
- [26] M. Savage, G. Mattson, S. Desai, G. Neilander, S. Morgensen and E. Conklin. *Avidin-biotin chemistry: A handbook*. Pierce Chemical Comp., Rockford, Illinois (1992).

- [27] O. H. Willemsen, M. M. Snel, A. Cambi, J. Greve, B. G. De Groot and C. G. Figdor. Biomolecular interactions measured by atomic force microscopy. *Biophys. J.* **79**, 3267 (2000).
- [28] R. Merkel, P. Nassoy, A. Leung, K. Ritchie and E. Evans. Energy landscapes of receptor-ligand bonds explored with dynamic force spectroscopy. *Nature* **397** (6714), 50 (1999).
- [29] F. Schreiber. Structure and growth of self-assembling monolayers. *Progress in Surface Science* **65**, 151 (2000).
- [30] J. Love, L. Estroff, J. Kriebel, R. Nuzzo and G. Whitesides. Self-assembled monolayers of thiolates on metals as a form of nanotechnology. *Chem. Rev.* **105** (4), 1103 (2005).
- [31] M. Grandbois, M. Beyer, M. Rief, H. Clausen-Schaumann and H. E. Gaub. How strong is a covalent bond? *Science* **283** (5408), 1727 (1999).
- [32] Z. Deng and C. Mao. DNA-templated fabrication of 1D parallel and 2D crossed metallic nanowire arrays. *Nano Lett.* **3** (11), 1545 (2003).
- [33] J. Allemand, D. Bensimon, L. Jullien, A. Bensimon and V. Croquette. pH-dependent specific binding and combing of DNA. *Biophys. J.* **73** (4), 2064 (1997).
- [34] A. Bensimon, A. Simon, A. Chiffaudel, V. Croquette, F. Heslot and D. Bensimon. Alignment and sensitive detection of DNA by a moving interface. *Science* **265** (5181), 2096 (1994).
- [35] F. Rose, P. Martin, H. Fujita and H. Kawakatsu. Adsorption and combing of DNA on HOPG surfaces of bulk crystals and nanosheets: application to the bridging of DNA between HOPG/Si heterostructures. *Nanotechnology* **17** (13), 3325 (2006).
- [36] H. Nakao, M. Gad, S. Sugiyama, K. Ohtobe and T. Ohtani. Transfer-printing of highly aligned DNA nanowires. *JACS* **125** (24), 7162 (2003).
- [37] X. Michalet, R. Ekong, F. Fougereuse, S. Rousseaux, C. Schurra, N. Hornigold, M. vanSlegtenhorst, J. Wolfe, S. Povey, J. S. Beckmann and A. Bensimon. Dynamic molecular combing: Stretching the whole human genome for high-resolution studies. *Science* **277** (5331), 1518 (1997).
- [38] Z. Gueroui, C. Place, B. Freyssingas and B. Berge. Observation by fluorescence microscopy of transcription on single combed DNA. *PNAS* **99** (9), 6005 (2002).
- [39] J. Guan and J. Lee. Generating highly ordered DNA nanostrand arrays. *PNAS* **102** (51), 18321 (2005).
- [40] P. Björk, A. Herland, I. Scheblykin and O. Inganäs. Spectroscopy of conjugated polyelectrolytes decorated on stretched aligned DNA. *Nano Lett.* **5** (10), 1948 (2005).

Bibliography

- [41] J. Zhang, M. Yufeng, S. Stachura and H. He. Assembly of highly aligned DNA strands onto Si chips. *Langmuir* **21** (9), 4180 (2005).
- [42] G. Maubach, A. Csáki, D. Born and W. Fritzsche. Controlled positioning of a DNA molecule in an electrode setup based on self-assembly and microstructuring. *Nanotechnology* **14** (5), 546 (2003).
- [43] T. T. Perkins. *Exploring Polymer Dynamics with single DNA molecules*. Ph.D. thesis, Stanford University (1997).
- [44] T. Perkins, D. Smith and S. Chu. Direct observation of tube-like motion of a single polymer chain. *Science* **264** (5160), 819 (1994).
- [45] T. Perkins, D. Smith, R. Larson and S. Chu. Stretching of a single tethered polymer in a uniform flow. *Science* **268** (5207), 83 (1995).
- [46] P. S. Doyle, B. Ladoux and J.-L. Viovy. Dynamics of a tethered polymer in shear flow. *Phys. Rev. Lett.* **84** (20), 4769 (2000).
- [47] F. Brochard-Wyart. Deformation of one tethered chain in strong flow. *Europhys. Lett.* **23** (2), 105 (1993).
- [48] F. Brochard-Wyart. Polymer chains under strong flows: Stems and flowers. *Europhys. Lett.* **30** (7), 387 (1995).
- [49] D. Wirtz. Direct measurement of the transport properties of a single DNA molecule. *Phys. Rev. Lett.* **75** (12), 2436 (1995).
- [50] M. Mertig, L. Colombi Ciacchi, A. Benke, A. Huhle, J. Opitz, R. Seidel, H. K. Schackert and W. Pompe. *Foundations of Nanoscience: Self-Assembled Architectures and Devices*, chap. DNA-based fabrication of metallic wires and networks, pages 132–145. Science Technica, Inc. (2004).
- [51] H. Yokota, J. Sunwoo, M. Sarikaya, G. van den Engh and R. Aebbersold. Spin-stretching of DNA and protein molecules for detection by fluorescence and atomic force microscopy. *Anal. Chem.* **71** (19), 4418 (1999).
- [52] W. E. Ford, O. Harnack, A. Yasuda and J. M. Wessels. Platinated DNA as precursors to templated chains of metal nanoparticles. *Adv. Mater.* **13** (23), 1793 (2001).
- [53] S. Smith and B. A.J. Electrophoretic charge density and persistence length of DNA as measured by fluorescence microscopy. *Biopolymers* **29**, 1167 (1990).
- [54] S. Ferree and H. W. Blanch. Electrokinetic stretching of tethered DNA. *Biophys. J.* **85** (4), 2539 (2003).
- [55] H. Pohl. *Dielectrophoresis: The Behavior of Neutral Matter in Nonuniform Electric Fields*. Cambridge University Press (1978).

- [56] T. B. Jones. *Electromechanics of Particles*. Cambridge University Press (1995).
- [57] S. Tsukahara, K. Yamanaka and H. Watarai. Dielectrophoretic behavior of single DNA in planar and capillary quadrupole microelectrodes. *Chem. Lett.* **3**, 250 (2001).
- [58] B. Saif, R. K. Mohr, C. J. Montrose and T. A. Litovitz. On the mechanism of dielectric relaxation in aqueous DNA solutions. *Biopolymers* **31** (10), 1171 (1991).
- [59] M. Washizu and O. Kurosawa. Electrostatic manipulation of DNA in microfabricated structures. *IEEE Transactions on Industry Applications* **26** (6), 1165 (1990).
- [60] M. Mandel. The electric polarization of rod-like, charged macromolecules. *Mol. Phys.* **4**, 792 (1981).
- [61] C. L. Asbury and G. v. d. Engh. Trapping of DNA in nonuniform oscillating electric fields. *Biophys. J.* **74** (2), 1024 (1998).
- [62] C. L. Asbury, A. H. Diercks and G. van den Engh. Trapping of DNA by dielectrophoresis. *Electrophoresis* **23** (16), 2658 (2002).
- [63] A. Castellanos, A. Ramos, A. González, N. G. Green and H. Morgan. Electrohydrodynamics and dielectrophoresis in microsystems: scaling laws. *J. Phys. D: Appl. Phys.* **36**, 2584 (2003).
- [64] D. Bakewell and H. Morgan. Dielectrophoresis of DNA: Time- and frequency-dependent collections on microelectrodes. *IEEE Transactions on Nanobioscience* **5** (2), 139 (2006).
- [65] M. Washizu, O. Kurosawa, I. Arai, S. Suzuki and N. Shimamoto. Applications of electrostatic stretch-and-positioning of DNA. *IEEE Transactions on Industry Applications* **31** (3), 447 (1995).
- [66] T. Yamamoto, O. Kurosawa, H. Kabata, N. Shimamoto and M. Washizu. Molecular surgery of DNA based on electrostatic micromanipulation. *IEEE Transactions on Industry Applications* **36** (4), 1010 (2000).
- [67] A. Ramos, H. Morgan, N. G. Green and A. Castellanos. AC electrokinetics: a review of forces in microelectrode structures. *J. Phys. D: Appl. Phys.* **31** (18), 2338 (1998).
- [68] N. G. Green, A. Ramos, A. González, A. Castellanos and H. Morgan. Electrothermally induced fluid flow on microelectrodes. *Journal of Electrostatics* **53** (2), 71 (2001).
- [69] W. Germishuizen, C. Wälti, R. Wirtz, M. Johnston, M. Pepper, A. Davies and A. Middelberg. Selective dielectrophoretic manipulation of surface-immobilized DNA molecules. *Nanotechnology* **14** (8), 896 (2003).

- [70] C. Wälti, P. Tosch, A. G. Davies, W. A. Germishuizen and C. F. Kaminski. Establishment of the AC electrokinetic elongation mechanism of DNA by three-dimensional fluorescent imaging. *Appl. Phys. Lett.* **88** (15), 153901/1 (2006).
- [71] C. Wälti, W. A. Germishuizen, P. Tosch, C. F. Kaminski and A. G. Davies. AC electrokinetic manipulation of DNA. *J. Phys. D: Appl. Phys.* **40** (1), 114 (2007).
- [72] C. Bustamante, J. F. Marko and E. D. Siggia. Entropic elasticity of λ -phage DNA. *Science* **265**, 1599 (1994).
- [73] V. Namasivayam, R. Larson, D. Burke and M. Burns. Electrostretching DNA molecules using polymer-enhanced media within microfabricated devices. *Anal. Chem.* **74** (14), 3378 (2002).
- [74] N. Green, A. Ramos and H. Morgan. AC electrokinetics: a survey of sub-micrometre particle dynamics. *J. Phys. D: Appl. Phys.* **33** (6), 632 (2000).
- [75] N. G. Green, A. Ramos, A. González, H. Morgan and A. Castellanos. Fluid flow induced by nonuniform AC electric fields in electrolytes on microelectrodes. III. observation of streamlines and numerical simulation. *Phys. Rev. E* **66** (2), 026305 (2002).
- [76] P. Garcia-Sanchez, A. Ramos, G. Green and H. Morgan. Experiments on AC electrokinetic pumping of liquids using arrays of microelectrodes. *IEEE Transactions on Dielectrics and Electrical Insulation* **13** (3), 670 (2006).
- [77] B. D. Storey, L. R. Edwards, M. S. Kilic and M. Z. Bazant. Steric effects on ac electro-osmosis in dilute electrolytes. *Phys. Rev. E* **77**, 036317 (2008).
- [78] D. Lastochkin, R. Zhou, P. Wang, Y. Ben and H. Chang. Electrokinetic micropump and micromixer design based on AC faradaic polarization. *J. Appl. Phys.* **96** (3), 1730 (2004).
- [79] V. Studer, A. Pepin, Y. Chen and A. Ajdari. An integrated AC electrokinetic pump in a microfluidic loop for fast and tunable flow control. *Analyst* **129** (10), 944 (2004).
- [80] H. Yan, S. H. Park, G. Finkelstein, J. H. Reif and T. H. LaBean. DNA-templated self-assembly of protein arrays and highly conductive nanowires. *Science* **301** (5641), 1882 (2003).
- [81] Y. He, Y. Chen, H. Liu, A. E. Ribbe and C. Mao. Self-assembly of hexagonal DNA two-dimensional (2D) arrays. *JACS* **127** (35), 12202 (2005).
- [82] Y. He, Y. Tian, A. E. Ribbe and C. Mao. Highly connected two-dimensional crystals of DNA six-point-stars. *JACS* **128** (50), 15978 (2006).
- [83] E. Winfree, F. Liu, L. A. Wenzler and N. C. Seeman. Design and self-assembly of two-dimensional DNA crystals. *Nature* **394** (6693), 539 (1998).

- [84] C. D. Mao, W. Q. Sun and N. C. Seeman. Designed two-dimensional DNA holliday junction arrays visualized by atomic force microscopy. *JACS* **121** (23), 5437 (1999).
- [85] B. Ding, R. Sha and N. C. Seeman. Pseudo-hexagonal 2D DNA crystals from double crossover cohesion. *JACS* **126** (33), 10230 (2004).
- [86] S. H. Park, R. Barish, H. Li, J. H. Reif, G. Finkelstein, H. Yan and T. H. LaBean. Three-helix bundle DNA tiles self-assemble into 2D lattice or 1D templates for silver nanowires. *Nano Lett.* **5** (4), 693 (2005).
- [87] C. Lin, Y. Liu, S. Rinker and H. Yan. DNA tile based self-assembly: Building complex nanoarchitectures. *ChemPhysChem* **7** (8), 1641 (2006).
- [88] Y. Liu, C. Lin, H. Li and H. Yan. Aptamer-directed self-assembly of protein arrays on a DNA nanostructure. *Angew. Chem. Int. Ed.* **44** (28), 4333 (2005).
- [89] D. Liu, S. H. Park, J. H. Reif and T. H. LaBean. DNA nanotubes self-assembled from triple-crossover tiles as templates for conductive nanowires. *PNAS* **101** (3), 717 (2004).
- [90] H. Liu, Y. Chen, Y. He, A. E. Ribbe and C. Mao. Approaching the limit: Can one DNA oligonucleotide assemble into large nanostructures? *Angew. Chem. Int. Ed.* **45** (12), 1942 (2006).
- [91] P. W. K. Rothmund, N. Papadakis and E. Winfree. Algorithmic self-assembly of DNA sierpinski triangles. *PLoS Biol* **2** (12), e424 (2004).
- [92] R. D. Barish, P. W. K. Rothmund and E. Winfree. Two computational primitives for algorithmic self-assembly: Copying and counting. *Nano Lett.* **5** (12), 2586 (2005).
- [93] J. Chen and N. C. Seeman. Synthesis from DNA of a molecule with the connectivity of a cube. *Nature* **350** (6319), 631 (1991).
- [94] Y. Zhang and N. C. Seeman. Construction of a DNA-truncated octahedron. *JACS* **116** (5), 1661 (1994).
- [95] Y. He, T. Ye, M. Su, C. Zhang, A. E. Ribbe, W. Jiang and C. Mao. Hierarchical self-assembly of DNA into symmetric supramolecular polyhedra. *Nature* **452** (7184), 198 (2008).
- [96] F. A. Aldaye and H. F. Sleiman. Modular access to structurally switchable 3D discrete DNA assemblies. *JACS* **129** (44), 13376 (2007).
- [97] N. C. Seeman. DNA in a material world. *Nature* **421** (6921), 427 (2003).
- [98] W. Shih, J. Quispe and G. Joyce. A 1.7-kilobase single-stranded DNA that folds into a nanoscale octahedron. *Nature* **427** (6975), 618 (2004).

Bibliography

- [99] P. W. K. Rothemund. Folding DNA to create nanoscale shapes and patterns. *Nature* **440** (7082), 297 (2006).
- [100] H. Dietz, S. M. Douglas and W. M. Shih. Folding DNA into twisted and curved nanoscale shapes. *Science* **325** (5941), 725 (2009).
- [101] E. S. Andersen, M. Dong, M. M. Nielsen, K. Jahn, R. Subramani, W. Mamdouh, M. M. Golas, B. Sander, H. Stark, C. L. P. Oliveira, J. S. Pedersen, V. Birkedal, F. Besenbacher, K. V. Gothelf and J. Kjems. Self-assembly of a nanoscale DNA box with a controllable lid. *Nature* **459** (7243), 73 (2009).
- [102] F. A. Aldaye, A. L. Palmer and H. F. Sleiman. Assembling materials with DNA as the guide. *Science* **321** (5897), 1795 (2008).
- [103] Z. Deng and C. Mao. Molecular lithography with DNA nanostructures. *Angew. Chem. Int. Ed.* **43** (31), 4068 (2004).
- [104] S. M. Douglas, H. Dietz, T. Liedl, B. Hogberg, F. Graf and W. M. Shih. Self-assembly of DNA into nanoscale three-dimensional shapes. *Nature* **459** (7245), 414 (2009).
- [105] F. A. Aldaye and H. F. Sleiman. Dynamic DNA templates for discrete gold nanoparticle assemblies: Control of geometry, modularity, write/erase and structural switching. *JACS* **129** (14), 4130 (2007).
- [106] J. Bath and A. J. Turberfield. DNA nanomachines. *Nat Nano* **2** (5), 275 (2007).
- [107] J. Sharma, R. Chhabra, A. Cheng, J. Brownell, Y. Liu and H. Yan. Control of self-assembly of DNA tubules through integration of gold nanoparticles. *Science* **323** (5910), 112 (2009).
- [108] W. Dittmer and F. Simmel. Chains of semiconductor nanoparticles templated on DNA. *Appl. Phys. Lett.* **85** (4), 633 (2004).
- [109] N. C. Seeman. Molecular craftwork with DNA. *Chem. Intell.* **1**, 38 (1995).
- [110] D. D. Eley and D. I. Spivey. Semiconductivity of organic substances. part 9.—nucleic acid in the dry state. *Trans. Faraday Soc.* **58**, 411 (1962).
- [111] B. Giese, J. Amaudrut, A.-K. Köhler, M. Spormann and S. Wessely. Direct observation of hole transfer through DNA by hopping between adenine bases and by tunnelling. *Nature* **412**, 318 (2001).
- [112] H.-W. Fink and C. Schönberger. Electrical conduction through DNA molecules. *Nature* **398** (6726), 407 (1999).
- [113] A. J. Storm, J. van Noort, S. de Vries and C. Dekker. Insulating behavior for DNA molecules between nanoelectrodes at the 100 nm length scale. *Appl. Phys. Lett.* **79** (23), 3881 (2001).

- [114] K. Tanaka and M. Shionoya. Synthesis of a novel nucleoside for alternative DNA base pairing through metal complexation. *J. Org. Chem.* **64** (14), 5002 (1999).
- [115] M. Tasaka, K. Tanaka, M. Shiro and M. Shionoya. A palladium-mediated DNA base pair of a β -c-nucleoside possessing a 2-aminophenol as the nucleobase. *Supramolecular Chemistry* **13** (6), 671 (2001).
- [116] N. Zimmermann, E. Meggers and P. G. Schultz. A novel silver(I)-mediated DNA base pair. *JACS* **124** (46), 13684 (2002).
- [117] P. Aich, L. Labiuk, Shaunivan, L. W. Tari, L. J. T. Delbaere, W. J. Roesler, K. J. Falk, R. P. Steer and J. S. Lee. M-DNA: a complex between divalent metal ions and DNA which behaves as a molecular wire. *J. Mol. Biol.* **294** (2), 477 (1999).
- [118] F. Patolsky, Y. Weizmann, O. Lioubashevski and I. Willner. Au-nanoparticle nanowires based on DNA and polylysine templates. *Angew. Chem. Int. Ed.* **41** (13), 2323 (2002).
- [119] A. Kumar, M. Pattarkine, M. Bhadbhade, A. B. Mandale, K. N. Ganesh, S. S. Datar, C. V. Dharmadhikari and M. Sastry. Linear superclusters of colloidal gold particles by electrostatic assembly on DNA templates. *Adv. Mater.* **13** (5), 341 (2001).
- [120] M. Sastry, A. Kumar, S. Datar, C. V. Dharmadhikari and K. N. Ganesh. DNA-mediated electrostatic assembly of gold nanoparticles into linear arrays by a simple drop-coating procedure. *Appl. Phys. Lett.* **78** (19), 2943 (2001).
- [121] T. Torimoto, M. Yamashita, S. Kuwabata, T. Sakata, H. Mori and H. Yoneyama. Fabrication of CdS nanoparticle chains along DNA double strands. *J. Phys. Chem. B* **103** (42), 8799 (1999).
- [122] O. Harnack, W. E. Ford, A. Yasuda and J. M. Wessels. Tris(hydroxymethyl)phosphine-capped gold particles templated by DNA as nanowire precursors. *Nano Lett.* **2** (9), 919 (2002).
- [123] C. J. Loweth, W. B. Caldwell, X. Peng, A. P. Alivisatos and P. G. Schultz. DNA-based assembly of gold nanocrystals. *Angew. Chem. Int. Ed.* **38** (12), 1808 (1999).
- [124] A. P. Alivisatos, K. P. Johnsson, X. Peng, T. E. Wilson, C. J. Loweth, M. P. Bruchez and P. G. Schultz. Organization of "nanocrystal molecules" using DNA. *Nature* **382** (6592), 609 (1996).
- [125] L. Coffey, S. Bigham and X. Li. Dictation of the shape of mesoscale semiconductor nanoparticle assemblies by plasmid DNA. *Appl. Phys. Lett.* **69** (25), 3851 (1996).
- [126] E. Braun, Y. Eichen, U. Sivan and G. Ben-Yoseph. DNA-templated assembly and electrode attachment of a conducting silver wire. *Nature* **391** (6669), 775 (1998).

Bibliography

- [127] Q. Gu, C. Cheng and D. T. Haynie. Cobalt metallization of DNA: toward magnetic nanowires. *Nanotechnology* **16** (8), 1358 (2005).
- [128] Q. Gu, H. Jin and K. Dai. Fabrication of nickel and gold nanowires by controlled electrodeposition on deoxyribonucleic acid molecules. *J. Phys. D: Appl. Phys.* **42** (1), 015303 (2009).
- [129] H. A. Becerril, P. Ludtke, B. M. Willardson and A. T. Woolley. DNA-templated nickel nanostructures and protein assemblies. *Langmuir* **22** (24), 10140 (2006).
- [130] K. Keren, M. Krueger, R. Gilad, G. Ben-Yoseph, U. Sivan and E. Braun. Sequence-specific molecular lithography on single DNA molecules. *Science* **297** (5578), 72 (2002).
- [131] S. H. Park, M. W. Prior, T. H. LaBean and G. Finkelstein. Optimized fabrication and electrical analysis of silver nanowires templated on DNA molecules. *Appl. Phys. Lett.* **89** (3), 033901 (2006).
- [132] C. F. Monson and A. T. Woolley. DNA-templated construction of copper nanowires. *Nano Lett.* **3** (3), 359 (2003).
- [133] H. Becerril, R. Stoltenberg, C. F.M. and A. Woolley. Ionic surface masking for low background in single- and double-stranded DNA-templated silver and copper nanorods. *J. Mater. Chem.* **14**, 611 (2004).
- [134] M. Mertig, L. Colombi Ciacchi, R. Seidel, W. Pompe and A. De Vita. DNA as a selective metallization template. *Nano Lett.* **2** (8), 841 (2002).
- [135] R. Seidel, M. Mertig and W. Pompe. Scanning force microscopy of DNA metallization. *Surf. Interface Anal.* **33** (2), 151 (2002).
- [136] R. Seidel, L. Colombi Ciacchi, M. Weigel, W. Pompe and M. Mertig. Synthesis of platinum cluster chains on DNA templates: Conditions for a template-controlled cluster growth. *J. Phys. Chem. B* **108** (30), 10801 (2004).
- [137] J. Richter, M. Mertig, W. Pompe and H. Vinzelberg. Low-temperature resistance of DNA-templated nanowires. *Appl. Phys. A* **74** (6), 725 (2002).
- [138] J. Richter, M. Mertig, W. Pompe, I. Monch and H. K. Schackert. Construction of highly conductive nanowires on a DNA template. *Appl. Phys. Lett.* **78** (4), 536 (2001).
- [139] Z. Hossain and F. Huq. Studies on the interaction between Ag^+ and DNA. *Journal of Inorganic Biochemistry* **91** (2), 398 (2002).
- [140] R. H. Jensen and N. Davidson. Spectrophotometric potentiometric and density gradient ultracentrifugation studies of binding of silver ion by DNA. *Biopolymers* **4** (1), 17 (1966).

- [141] L. Colombi Ciacchi, M. Mertig, R. Seidel, W. Pompe and A. De Vita. Nucleation of platinum clusters on biopolymers: a first principles study of the molecular mechanism. *Nanotechnology* **14**, 840 (2003).
- [142] A. Rakitin, P. Aich, C. Papadopoulos, Y. Kobzar, A. S. Vedeneev, J. S. Lee and J. M. Xu. Metallic conduction through engineered DNA: DNA nanoelectronic building blocks. *Phys. Rev. Lett.* **86** (16), 3670 (2001).
- [143] K. Keren, R. S. Berman and E. Braun. Patterned DNA metallization by sequence-specific localization of a reducing agent. *Nano Lett.* **4** (2), 323 (2004).
- [144] L. Berti, A. Alessandrini and P. Facci. DNA-templated photoinduced silver deposition. *JACS* **127** (32), 11216 (2005).
- [145] A. Blüher. *S-Schichtproteine als molekulare Bausteine zur Funktionalisierung mikroelektronischer Sensorstrukturen*. Ph.D. thesis, Technische Universität Dresden (2008).
- [146] H. S. Rye, S. Yue, D. E. Wemmer, M. A. Quesada, R. P. Haugland, R. A. Mathies and A. N. Glazer. Stable fluorescent complexes of double-stranded DNA with bis-intercalating asymmetric cyanine dyes: properties and applications. *Nucl. Acids Res.* **20** (11), 2803 (1992).
- [147] A. Larsson, C. Carlsson, M. Jonsson and B. Albinsson. Characterization of the binding of the fluorescent dyes YO and YOYO to DNA by polarized light spectroscopy. *JACS* **116** (19), 8459 (1994).
- [148] A. Sischka, K. Toensing, R. Eckel, S. D. Wilking, N. Sewald, R. Ros and D. Anselmetti. Molecular mechanisms and kinetics between DNA and DNA binding ligands. *Biophys. J.* **88** (1), 404 (2005).
- [149] M. Eriksson, H. J. Karlsson, G. Westman and B. Akerman. Groove-binding unsymmetrical cyanine dyes for staining of DNA: dissociation rates in free solution and electrophoresis gels. *Nucl. Acids Res.* **31** (21), 6235 (2003).
- [150] B. Akerman and E. Tuite. Single- and double-strand photocleavage of DNA by YO, YOYO and TOTO. *Nucl. Acids Res.* **24** (6), 1080 (1996).
- [151] C. Kanony, B. Åkerman and E. Tuite. Photobleaching of asymmetric cyanines used for fluorescence imaging of single DNA molecules. *JACS* **123** (33), 7985 (2001).
- [152] C. Erler and M. Mertig. Synthesis of metallic nanowire networks on DNA. *IEEE Conference Proceedings (ESTC 2008)* page 1063 (2008).
- [153] C. Erler, K. Günther and M. Mertig. Photo-induced synthesis of DNA-templated metallic nanowires and their integration into micro-fabricated contact arrays. *Appl. Surf. Science* **255**, 9647 (2009).

Bibliography

- [154] B. Lippert. From cisplatin to artificial nucleases - the role of metal ion-nucleic acid interactions in biology. *BioMetals* **5** (4), 195 (1992).
- [155] M. Watzky and R. Finke. Transition metal nanocluster formation kinetic and mechanistic studies. A new mechanism when hydrogen is the reductant: Slow, continuous nucleation and fast autocatalytic surface growth. *JACS* **119** (43), 10382 (1997).
- [156] C. Zimmer, G. Luck, H. Venner and J. Frič. Studies on the conformation of protonated DNA. *Biopolymers* **6** (4), 563 (1968).
- [157] H. Jaganathan, J. M. Kinsella and A. Ivanisevic. Circular dichroism study of the mechanism of formation of DNA templated nanowires. *ChemPhysChem* **9** (15), 2203 (2008).
- [158] Y. P. Blagoi, V. A. Sorokin, S. A. Valeyev, S. A. Khomenko and G. O. Gladchenko. Magnesium ion effect on the helix-coil transition of DNA. *Biopolymers* **17**, 1103 (1978).
- [159] N. C. Bigall, T. Härtling, M. Klose, P. Simon, L. M. Eng and A. Eychmüller. Monodisperse platinum nanospheres with adjustable diameters from 10 to 100 nm: Synthesis and distinct optical properties. *Nano Lett.* **8** (12), 4588 (2008).
- [160] J. M. Lin, H. Y. Lin, C. L. Cheng and Y. F. Chen. Giant enhancement of bandgap emission of ZnO nanorods by platinum nanoparticles. *Nanotechnology* **17** (17), 4391 (2006).
- [161] J. Petty, J. Zheng, N. Hud and R. Dickson. DNA-templated Ag nanocluster formation. *JACS* **126** (16), 5207 (2004).
- [162] C. Brack and J. D. Griffith. DNA electron microscopy. *Critical Reviews in Biochemistry and Molecular Biology* **10** (2), 113 (1981).
- [163] J. D. Griffith. *Methods in Cell Biology*, vol. 7, chap. Electron microscopic visualization of DNA in association with cellular components, page 129. Academic Press, New York (1973).
- [164] M. Nitschke, G. Schmack, A. Janke, F. Simon, D. Pleul and C. Werner. Low pressure plasma treatment of poly(3-hydroxybutyrate): Toward tailored polymer surfaces for tissue engineering scaffolds. *J Biomed Mater* **59**, 632 (2002).
- [165] M. L. Jackson. *Soil Chemical Analysis: Advanced Course*. Parallel Press Madison, Wisconsin, rev. 2nd edn. (2005).
- [166] K. Novoselov, D. Jiang, F. Schedin, T. Booth, V. Khotkevich, S. Morozov and A. Geim. Two-dimensional atomic crystals. *PNAS* **102** (30), 10451 (2005).

- [167] T. Koller, J. M. Sogo and H. Bujard. An electron microscopic method for studying nucleic acid-protein complexes. visualization of RNA polymerase bound to the DNA of bacteriophages t7 and t3. *Biopolymers* **13** (5), 995 (1974).
- [168] T. L. Sobey, S. Renner and F. C. Simmel. Assembly and melting of DNA nanotubes from single-sequence tiles. *J. Phys.: Condens. Matter* **21** (3), 034112 (9pp) (2009).
- [169] J. Worm. Winspall-Programm zur Simulation von Plasmonen, version 3.02. <http://www.mpip-mainz.mpg.de/knoll/soft/> (2009). Max Planck Institute for Polymer Research, Mainz.
- [170] <http://refractiveindex.info/> (2009).
- [171] J. Wen, K.-J. Jin, M. He, H. Lu, F. Yang and G. Yang. The substrate thickness dependence of the photovoltage in $\text{LaAlO}_{3-\delta}$ /Si heterostructures. *Appl. Phys. Lett.* **94**, 061118 (2009).
- [172] T. Okamoto and I. Yamaguchi. Photocatalytic deposition of a gold nanoparticle onto the top of a SiN cantilever tip. *Journal of Microscopy* **202** (1), 100 (2001).
- [173] R. Seidel. *Methods for the development of a DNA based nanoelectronics*. Ph.D. thesis, Technische Universität Dresden (2003).
- [174] T. Härtling, P. Reichenbach and L. M. Eng. Near-field coupling of a single fluorescent molecule and a spherical gold nanoparticle. *Opt. Express* **15** (20), 12806 (2007).
- [175] M. Käll, H. Xu and P. Johansson. Field enhancement and molecular response in surface-enhanced Raman scattering and fluorescence spectroscopy. *J. Raman. Spec.* **36**, 510 (2005).
- [176] T. Härtling, Y. Alaverdyan, A. Hille, M. T. Wenzel, M. Käll and L. M. Eng. Optically controlled interparticle distance tuning and welding of single gold nanoparticle pairs by photochemical metal deposition. *Opt. Express* **16**, 12362 (2008).
- [177] T. Härtling. *Photochemical tuning of surface plasmon resonances in metal nanoparticles*. Ph.D. thesis, Technische Universität Dresden (2009).
- [178] K. Kurihara, J. Kizling, P. Stenius and J. H. Fendler. Laser and pulse radiolytically induced colloidal gold formation in water and in water-in-oil microemulsions. *JACS* **105** (9), 2574 (1983).
- [179] J. Renger. *Excitation, interaction, and scattering of localized and propagating surface polaritons*. Ph.D. thesis, Technische Universität Dresden (2006).
- [180] M. Bezanilla, S. Manne, E. Daniel, Y. Lyubchenko and H. Hansma. Adsorption of DNA to mica, silylated mica, and minerals: Characterization by atomic force microscopy. *Langmuir* **11**, 655 (1995).

Bibliography

- [181] C. Erler and M. Mertig. Incorporation of DNA networks into micro electrode structures. *J. Vac. Sci. Technol. B* **27**, 939 (2009).
- [182] J. Gulbins and C. Kahrmann. *Mut zur Typographie: Ein Kurs für Desktop-Publishing*. X.media.press. Springer Berlin/Heidelberg (2000).

Own Publications

Publications related to the subject of this thesis:

- [181] C. Erler and M. Mertig. Incorporation of DNA networks into micro electrode structures. *J. Vac. Sci. Technol. B* **27**, 939 (2009).
- [153] C. Erler, K. Günther and M. Mertig. Photo-induced synthesis of DNA-templated metallic nanowires and their integration into micro-fabricated contact arrays. *Appl. Surf. Science* **255**, 9647 (2009).
- [152] C. Erler and M. Mertig. Synthesis of metallic nanowire networks on DNA. *IEEE Conference Proceedings (ESTC 2008)*, 1063 (2008).

Other publications:

A. Haußmann, P. Milde, C. Erler and L. M. Eng. Ferroelectric lithography: bottom-up assembly and electrical performance of a single metallic nanowire. *Nano Lett.* **9**, 763 (2009).

M. Nirschl, A. Blüher, C. Erler, B. Katzschner, I. Vikholm-Lundin, S. Auer, J. Vörös, W. Pompe, M. Schreiter and M. Mertig. Film bulk acoustic resonators for DNA and protein detection and investigation of in vitro bacterial S-layer formation. *Sensors and Actuators A* **156**, 180 (2009).

H. Ehrlich, D. Janussen, P. Simon, V. V. Bazhenov, N. P. Shapkin, C. Erler, M. Mertig, R. Born, S. Heinemann, T. Hanke, H. Worch and J.N. Vournakis. Nanostructural organization of naturally occurring composites. Part II: Silica-chitin-based biocomposites. *Journal of Nanomaterials* (2008).

Acknowledgement

I wish to thank all the people who supported me during my work on this thesis.

First of all I want to thank Michael Mertig who as my advisor always found a way to motivate and guide me through the ups and downs of this work. His lab has been a stimulating and challenging environment.

I wish to thank my referees, Professor Wolfgang Pompe and Professor Gerald Gerlach for evaluating my work.

Thanks are also given to all the three hitherto mentioned persons for my admittance to the DFG funded Graduiertenkolleg “Nano- und Biotechniken für das Packaging elektronischer Systeme”. Besides the funding, I enjoyed the collaborative work, many hours of discussion as well as the ease with which we worked together. The latter especially holds true for Thomas Härtling, René Landgraf, René Kullock, Alexander Haußmann, Mathias Lakatos, Marco Schossig and Tobias Schuster who all helped providing this and that, performing measurements or served as a “telephone joker” to answer a question.

Special thanks also go to Professor Hannes Lichte, who arouse my interest for transmission electron microscopy with his special lab. At the same time thanks are given to his members of staff. Thank you for passing a huge part of scientific experience to me and sharing the passion for science at a special place. I thank Daniel Wolf and Petr Formanek whom I also had the pleasure to work with and learn from during hours at the TEM lab. In this context, I also wish to thank Ute Trommer and Sylvia Mühe for spontaneous carbon evaporations.

Furthermore, I thank all the members of the BNS group for the enjoyable working atmosphere, technical help and fruitful scientific and non-scientific chats. In particular, I would like to thank my “Frauenzimmer” for sharing weal and woe in a scientist’s everyday life.

I thank all the “HIWI” and diploma students who supported me during the work, namely Andreas Klinton, Anja Henning, Maria Stammwitz and Kathia Lorena Jimenez Monroy.

Last but not least, my special thanks go to Roman Schuster, not only for the “L^AT_EXnical” and hopefully “typographically noiseless”⁶ realization of this thesis, but also for his understanding for an extensive job-related dedication (I know, I was (too) late often.). The latter also applies for my family, to whom my thanks go for their perpetual support.

⁶ „Gute Typografie macht keine Geräusche beim Lesen“ (Otl Aicher, german designer [182])

Statement of Authorship – Erklärung

Hiermit versichere ich, dass ich die vorliegende Arbeit ohne unzulässige Hilfe Dritter und Benutzung anderer als der angegebenen Hilfsmittel angefertigt habe; die aus fremden Quellen direkt oder indirekt übernommenen Gedanken sind als solche kenntlich gemacht.

Bei der Auswahl und Auswertung des Materials sowie bei der Herstellung des Manuskriptes habe ich Unterstützung von PD Dr. rer. nat. et Ing. habil. Michael Mertig erhalten.

Weitere Personen waren an der geistigen Herstellung der vorliegenden Arbeit nicht beteiligt. Insbesondere habe ich nicht die Hilfe eines kommerziellen Promotionsberaters in Anspruch genommen. Dritte haben von mir keine geldwerten Leistungen für Arbeiten erhalten, die in Zusammenhang mit dem Inhalt der vorgelegten Dissertation stehen.

Die Arbeit wurde bisher weder im Inland noch im Ausland in gleicher oder ähnlicher Form einer anderen Prüfungsbehörde vorgelegt und ist auch noch nicht veröffentlicht worden.

Die Promotionsordnung der Fakultät Maschinenwesen der Technischen Universität Dresden vom 1. Juli 2001 erkenne ich an.

Dresden, 11. 01. 2010

Christiane Erler